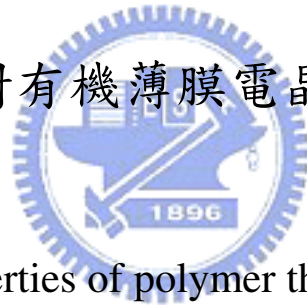


國立交通大學

電子工程學系 電子研究所

博士論文

大氣電漿技術對有機薄膜電晶體特性改善之研究



Enhancing the properties of polymer thin-film transistors using a
novel atmospheric-pressure plasma technology

研究生：林志祥

指導教授：張國明 教授

中華民國 九十七 年 七 月

大氣電漿技術對有機薄膜電晶體特性改善之研究

Enhancing the properties of polymer thin-film transistors using a
novel atmospheric-pressure plasma technology

研究生：林志祥

Student : Chih-Hsiang Lin

指導教授：張國明

Advisor : Kow-Ming Chang



A Dissertation

Submitted to Department of Electronics Engineering and
Institute of Electronics

College of Electrical and Computer Engineering

National Chiao Tung University

in partial Fulfillment of the Requirements

for the Degree of

Doctor of Philosophy

in

Electronics Engineering

July 2008

Hsinchu, Taiwan, Republic of China

中華民國 九十七 年 七 月

大氣電漿技術對有機薄膜電晶體特性改善之研究

研究生：林志祥

指導教授：張國明 博士

國立交通大學 電子工程學系 電子研究所博士班

摘要

透過旋轉塗佈的方式沉積可溶性共軛高分子，對於製作大面積且低成本的有機薄膜電晶體元件有很大的應用潛力。由於有機薄膜電晶體的效能與半導體及介電層的界面有很大的關係，所以此篇論文的研究目的是藉由控制半導體與介電層之間的界面化學特性，來改善以聚(3-烷基噻吩)作為半導體層的有機薄膜電晶體之特性。因為二氧化矽作為介電層已行之有年，材料特性較易掌控且界面改質容易，因此我們選擇熱氧化方式沉積二氧化矽作為我們的介電層，而由於高規則度聚(3-烷基噻吩)具有較高的結晶排列性，使薄膜電晶體元件能獲得較佳的電子遷移率，所以在此作為我們元件的半導體層。利用六甲基二矽氮烷對二氧化矽絕緣層進行表面處理，已證實對聚(3-烷基噻吩)薄膜電晶體的特性有明顯的改善，而本論文則透過常壓式電漿製程將六甲基二矽氮烷沉積於聚(3-烷基噻吩)與二氧化矽絕緣層間的界面，並探討此種表面處理製程對有機薄膜電晶體效能的影響。常壓電漿系統是一種可以將製程溫度操控於 120 度以下的低溫，並可工作於一般

大氣壓力之下。利用常壓式電漿製程進行表面處理後，有機薄膜電晶體元件的臨界電壓可被降至-10 伏特以內，載子遷移率也比沒經表面處理的元件提昇 15 倍以上，約為 $0.02-0.03 \text{ cm}^2/\text{Vs}$ ，其效果甚至比透過旋塗式或蒸鍍等表面改質方法還好。本論文已證實常壓式電漿系統，確實是一種低溫且高效率的有機薄膜電晶體元件界面改質製程。



Enhancing the properties of polymer thin-film transistors using a novel atmospheric-pressure plasma technology

Student : Chih-Hsiang Lin

Advisor : Dr. Kow-Ming Chang

Department of Electronics Engineering and Institute of Electronics
National Chiao Tung University

Abstract

Organic thin film transistors made by spin-coating from solution-processable conjugated polymers have potential advantages in fabricating low-cost devices with large areas. Since OTFT performance depends strongly on the interface between the semiconductor and the dielectric layer, this study attempts to demonstrate that the characteristics of P3HT-based OTFT are improved by controlling the chemistry of the dielectric/polymer interface. Thermal SiO₂ is adopted as the dielectric because of its well-characterized properties and ease of chemical modification. Regioregular P3HT (of which HT linkages represent more than 98.5% of the linkages) is utilized as the active layer, so it exhibits better ordering and crystallinity in the solid state, and substantially improved electroconductivities. The field-effect mobility was markedly improved by modifying the surface of SiO₂ with using a hexamethyldisilazane (HMDS) self-assembled monolayer. Before the active layer was deposited, the surface of SiO₂ was modified using atmospheric-pressure plasma technique (APPT). APPT is a new process that can be implemented at atmospheric pressure and at low temperature. The steps of APPT are performed below 120°C and at atmospheric

pressure, so the approach is very suited to use on a plastic substrate. After the SiO_2 surface has been modified by the APPT process with hexamethyldisilazane (HMDS), it exhibits typical I-V characteristics of TFTs. Calculations reveal that its field effect mobility can reach 0.02-0.03 cm^2/Vs , which is about 15 times that before the modification, and the threshold voltage is below -10V. The performance is even better than that obtained following the usual surface treatment of the SiO_2 surface by spin-coating or evaporation. This work suggests an interesting direction for preparing high-performance OTFTs with high efficiency and low-temperature surface treatment by APPT.



誌 謝

本論文能夠順利完成首先要感謝指導教授張國明老師，由於老師的悉心教導下，學習研究方法並完成論文，以及在生活上的關懷與照顧，使我獲益良多，且倍感溫馨。在此對老師的指導及鼓勵致上誠摯的敬意及謝忱。

其次要感謝工業技術研究院的大力栽培，使我在工作之餘可以再進修，以提昇個人學識與專業領域。感謝我的主管林正良組長與高信敬經理，不時地給予勉勵及支持，使我在工作及學業上能夠兼顧，並相輔相成。同時感謝親愛的同事們，因為有你們，使我在工作、學業及生活上不斷的學習成長。

在交通大學學習過程中，感謝實驗室學長及學弟們的幫忙，特別是黃士軒的幫助，使論文能順利完成。

最後，感謝我的父母、家人的無怨無悔照顧生活中的所有起居，若沒有你們的全力支持與鼓勵，將無法順利完成此論文，願將所有的成就與你們共享。

Contents

Abstract (in Chinese).....	i
Abstract (in English).....	iii
Acknowledgment.....	v
Contents.....	vi
Table Captions.....	ix
Figure Captions.....	xi

Chapter 1 Introduction

1.1 General background and motivation.....	1
1.2 Organic conjugated materials for OTFT.....	3
1.3 Thesis organization.....	5



Chapter 2 Property of P3HT and Spin-Coating Technique

2.1 Introduction of P3HT.....	11
2-1-1 The molecular structure of P3HT.....	11
2.1.2 Conduction mechanism.....	12
2.2 Solution processed deposition.....	16
2.2.1 Methods of OTFT fabricates.....	16
2.2.2 The motivation of spincoating.....	16
2.2.3 Effect of polymer morphology and solvents.....	17
2.3 Contact resistance of P3HT OTFT.....	18
2.4 Operation of organic thin filmtransistors.....	19

Chapter 3 Surface Treatment by Atmospheric-Pressure Plasma Technology for

Electrical Properties of OTFT.....	30
3.1 Modification of oxide surface.....	30
3.2 Introduction of APPT.....	31
3.2.1 Introduction of plasma.....	31
3.2.2 Applications of APPT.....	32
3.2.3 Plasma surface modification.....	34
3.3 Fabrication of OTFT.....	36
3.4 Determination of threshold voltage and mobility.....	38
3.5 Results and discussions.....	39
3.5.1 The influence of spin speed for OTFT.....	39
3.5.2 Electrical properties of APP surface treatment.....	40
3.5.3 The other methods of HMDS-treated SiO ₂	42
Chapter 4 Surface Treatment by Atmospheric-Pressure Plasma Technology for P3HT Alignment.....	83
4.1 Introduction of P3HT alignment.....	83
4.2 The methods to provide P3HT alignment.....	84
4.2.1 Crystallization behavior of P3HT.....	84
4.2.2 XRD and UV-vis for highly oriented crystals of P3HT.....	85
4.3 Hysteresis.....	87
4.4 Anomalous leakage current.....	89
Chapter 5 Conclusions and Future Work.....	104
5.1 Conclusions.....	104
5.2 Future work.....	106

5.2.1 In-situ passivation layer for protecting the P3HT film.....106
5.2.2 Novel method for depositing P3HT thin films.....106
5.2.3 Thermal stability of P3HT OTFT.....107
5.2.4 New gate insulator materials for P3HT OTFT.....107
Reference.....108



Table Captions

Chapter 1

Table 1-1 The differences of TFT and OTFT materials and processes.....	6
Table 1-2 Carrier mobility of inorganic and organic materials	6
Table 1-3 Highest field-effect mobility(μ) values measured from OTFT as reported in the literature annually from 1986 through 2000.....	8
Table 1-4 The chemical structures and reported mobilities of representative classes of organic materials compared to those of inorganic silicon materials.....	9



Chapter 2

Table 2-1 Field-effect mobility and ON/OFF ratio of samples prepared from different solvents and process condition.....	25
---	----

Chapter 3

Table 3-1 The types of atmospheric pressure plasma.....	45
Table 3-2 Threshold voltage, saturation mobility, and on/off ratio at different spin-speed.....	53
Table 3-3 Electrical parameters of the OTFTs in this study.....	62
Table 3-4 Comparison of contact angle and surface roughness with different scanning times by APPT.....	63
Table 3-5 The different methods of surface treatment.....	74

Chapter 4

Table 4-1: T_m and ΔH of P3HT in Run 1 and Run 2 with difference pre-heating temperature.....	95
--	----



Figure Captions

Chapter 1

Fig. 1-1 Semilogarithmic plot of the highest field-effect mobility.....7

Fig. 1-2 The chemical structures of P3HT and BBL (Polymer).....10

Fig. 1-3 The chemical structures of pentacene and oligothiophenes.....10

Chapter 2

Fig. 2-1 The structure of the polymer chain of P3HT.....21

Fig. 2-2 Two different orientations of ordered P3HT

(a) Edge-on orientation, (b) Face-on orientation.....22

Fig. 2-3 A polaron in polythiophene. Top: Change in the chemical structure.

Bottom: Corresponding energy diagram.....23

Fig. 2-4 (a) Charge carrier transport in conjugated polymers,

(b) Charge transport mechanisms in solid.....24

Fig. 2-5 Schematic of operation of organic thin film transistor, showing a lightly doped semiconductor: (a) No-bias, (b) Depletion mode, (c)

Accumulation mode, (d) Non-uniform charge density, (e) Pinch-off of

channel, (f) and (g) Growth of the depletion zone.....29

Chapter 3

Fig. 3-1 (a) The structure of APPT, (b) The diagram of plasma surface Treatment.....	46
Fig.3-2 (a) APP system of ITRI, (b) APP systems show the cold temperature.....	47
Fig. 3-3 Two basic structures of OTFT.....	48
Fig. 3-4 Process flow of top-contact OTFT.....	49
Fig. 3-5 I_D-V_G for different spin-speed (a) 800 rpm, (b) 1500 rpm, (c) 2000 rpm (All are no treatment) OTFT with $W/L = 2000 \text{ um}/500 \text{ um}$	51
Fig. 3-6 I_D-V_D for different spin-speed (a) 800 rpm, (b) 1500 rpm, (c) 2000 rpm (All are no treatment) OTFT with $W/L = 2000 \text{ um}/500 \text{ um}$	52
Fig. 3-7 SEM photo: cross-section view of test sample (upper layer is P3HT) made at spin-speed (a) 800 rpm, (b) 1500 rpm, (c) 2000 rpm.....	55
Fig. 3-8 Surface treatment of APPT HMDS 1 for OTFT (a) I_D-V_G curve, (b) I_D-V_D curve ($W/L = 2000 \text{ um}/500 \text{ um}$).....	56
Fig. 3-9 Surface treatment of APPT HMDS 2 for OTFT (a) I_D-V_G curve, (b) I_D-V_D curve ($W/L = 2000 \text{ um}/500 \text{ um}$).....	57
Fig. 3-10 Surface treatment of APPT HMDS 4 for OTFT (a) I_D-V_G curve, (b) I_D-V_D curve ($W/L = 2000 \text{ um}/500 \text{ um}$).....	58
Fig.3-11 Surface treatment of APPT HMDS 8 for OTFT (a) I_D-V_G curve, (b) I_D-V_D curve ($W/L = 2000 \text{ um}/500 \text{ um}$).....	59
Fig. 3-12 The comparison of (a), (b) I_D-V_G and (c), (d) I_D-V_D with different	

scanning times by APPT.....	61
Fig. 3-13 Comparison of threshold voltage and saturation mobility with different scanning times by APPT.....	62
Fig. 3-14 Contact angle vs. different scanning times by APPT.....	63
Fig. 3-15 Contact angle vs. exposure time for dielectric layer with different scanning times by APPT.....	64
Fig. 3-16 Comparison of contact angle and surface roughness with different scanning times by APPT.....	64
Fig. 3-17 Comparison of surface roughness and mobility with different scanning times by APPT.....	65
Fig. 3-18 Contact angle of (a) No treatment ($<10^\circ$), (b) APP 1(68.9°), (c) APP 2 (76.3°), (d) APP 4 (90.5°), (e) APP 8 (90.9°).....	68
Fig. 3-19 AFM photographs of (a) No treatment, (b) APP 1, (c) APP 2, (d) APP 4, (e) APP 8.....	71
Fig. 3-20 (a) I_D - V_G curve, (b) I_D - V_D curve with spin-coating HMDS for OTFT.....	72
Fig. 3-21 (a) I_D - V_G curve, (b) I_D - V_D curve with evaporated HMDS for OTFT.....	73
Fig. 3-22 Comparison of threshold voltage and saturation mobility with different methods of surface treatment.....	75
Fig. 3-23 Contact angle of (a) spin-coating HMDS (65.49°), (b) Evaporated HMDS (75.28°).....	76
Fig. 3-24 AFM photography of (a) Spin-coating, (b) Evaporated.....	77
Fig. 3-25 The comparison of (a), (b) I_D - V_G and (c), (d) I_D - V_D with different methods of surface treatment.....	79
Fig. 3-26 Comparison of contact angle and surface roughness with different	

methods of surface treatment.....	80
Fig. 3-27 Comparison of surface roughness and mobility with different methods of surface treatment.....	80
Fig. 3-28 Comparison of contact angle and mobility with different methods of surface treatment and different scanning times by APPT.....	81
Fig. 3-29 Comparison of contact angle and roughness with different methods of surface treatment and different scanning times by APPT.....	81
Fig. 3-30 Comparison of roughness and mobility with different methods of surface treatment and different scanning times by APPT.....	82

Chapter 4

Fig. 4-1 The molecular structure of P3HTs for High RR.....	90
Fig. 4-2 TGA thermograph of P3HT. 5 % weight loss is about 500°C	91
Fig. 4-3 DSC thermograph of P3HT was pre-heating at the temperature of 70°C for 3 min.....	91
Fig. 4-4 DSC thermograph of P3HT was pre-heating at the temperature of 90°C for 3 min.....	92
Fig. 4-5 DSC thermograph of P3HT was pre-heating at the temperature of 110°C for 3 min.....	92
Fig. 4-6 DSC thermograph of P3HT was pre-heating at the temperature of 130°C for 3 min.....	93
Fig. 4-7 DSC thermograph of P3HT was pre-heating at the temperature of 150°C for 3 min.....	93
Fig. 4-8 T _m and ΔH of P3HT in Run 1 with difference	

pre-heating temperature.....	94
Fig. 4-9 T _m and ΔH of P3HT in Run 2 with difference pre-heating temperature.....	94
Fig. 4-10 X-ray analysis of deposition of P3HT on SiO ₂ dielectric layer with various surface treatments.....	96
Fig. 4-11 UV-vis absorption spectra of P3HT films that are deposited on SiO ₂ dielectric layers following various surface treatments, normalized to the maxima of the spectra.....	97
Fig. 4-12 A typical hysteresis curve.....	98
Fig. 4-13 Hysteresis of P3HT OTFTs with no surface treatment.....	99
Fig. 4-14 Hysteresis of P3HT OTFTs with spin-coating surface treatment.....	99
Fig. 4-15 Hysteresis of P3HT OTFTs with evaporation surface treatment.....	100
Fig. 4-16 Hysteresis of P3HT OTFTs with APP 1 surface treatment.....	100
Fig. 4-17 Hysteresis of P3HT OTFTs with APP 2 surface treatment.....	101
Fig. 4-18 Hysteresis of P3HT OTFTs with APP 4 surface treatment.....	101
Fig. 4-19 Hysteresis of P3HT OTFTs with APP 8 surface treatment.....	102
Fig. 4-20 I _D versus V _G for various surface treatment processes and the gate leakage currents in V _G approaches 0 V.....	103
Fig. 4-21 I _D versus V _G for different numbers of APP scans and the gate leakage currents in V _G approaches 0 V.....	103

Chapter 1

Introduction

1.1 General background and motivation

Over the last few decades, Today's microelectronics is based on the use of highly pure and high performance semiconductors like Si, Ge, GaAs, InP, etc. These materials can provide carrier mobility (μ) in the order $10^3 \text{ cm}^2/\text{Vs}$ at room temperature, offer long lifetime, can be precisely doped and patterned with accuracy better than 100 nm. In this way, they profit at best of the device speed and manufacture complex systems on chip that are capable to receive, memorize, elaborate and transmit enormous quantity of information, making possible like PCs, mobile phones and almost every commercial products around our daily life.

Organic thin-film transistors (OTFT) using organic semiconductors have attracted a great deal of interest for use in lightweight, low-cost, large-area and flexible electronic products such as flat-panel displays, sensors, smart cards, and radio-frequency identification (RFID) tags. OTFT are more compatible with polymeric substrates than conventional silicon-based transistors because they can be fabricated with a low-temperature process. Therefore, OTFT on polymeric substrates have been developed to construct organic integrated circuits [1,2,3], electric papers, active-matrix liquid crystal displays (AMLCDs) [4,5], and active matrix organic electroluminescent displays [6]. The differences of TFT and OTFT materials and processes are shown in Table 1-1.

Organic thin-film transistors (OTFT) based on conjugated polymers, oligomers, or other molecules have been envisioned as a viable alternative to more traditional, mainstream thin-film transistors (TFT) based on inorganic materials. Because of the relatively low mobility of the organic semiconductor layers, OTFT can't rival the performance of field-effect transistors based on single-crystalline inorganic semiconductors, such as Si, Ge, GaAs, InP, which have charge carrier mobility about three orders of magnitude higher, such as Table 1-2 [7].

The performance of OTFT has steadily improved in the last two decades as a result of the development of new organic semiconductors, the optimization of deposition conditions and gate dielectric surface treatments [8,9,10,11]. We presented a semilogarithmic plot of the highest yearly reported field-effect mobility value measured from thin-film transistors based on specific organic semiconductors, beginning in 1986. An update of that plot is shown in Figure 1-1, which is based on Table 1-3.

Solution-processable conjugated polymers are among the most promising candidates for a cheap electronic and optoelectronic technology on plastic substrates. The technology that is believed to have the potential to produce the highest impact on manufacturing costs is the use of soluble organic semiconductor, both polymers and oligomers, combined with large area coating employed in OTFT is the fact that can be deposited using very low cost procedures such as spin-coating. This is the case of soluble polymers such as regioregular polythiophenes we used in experiments. Spin-coating procedures are also thermally compatible with plastic substrates, because they are carried out at the room temperature.

Therefore, here we employ the poly-3-hexylthiophene (P3HT), solution

processable conjugated materials, as active layers in OTFT. Atmospheric-pressure plasma technology (APPT) will be adopted to treat the surface of dielectric of OTFT and discuss the influence.

1.2 Organic conjugated materials for OTFT

Depending on the molecular weight, organic conjugated materials used in OTFTs can be sorted into polymers and small molecules [12]. Table 1-4 shows the chemical structures and reported mobilities of representative classes of organic materials compared to those of inorganic silicon materials.

A. Polymers

Conjugated polymers present the advantage of being amenable to specific deposition techniques that have been developed for conventional polymers. Their main drawback is that their performance is still lower than that of small molecules. Two polymers share the majority of the papers dealing with polymer-based OTFTs : Poly(3-hexyl thiophene) (P3HT) for p-type and Poly(benzobisimidazobenzophenanthroline) (BBL) for n-type. The chemical structures of P3HT and BBL are shown in Fig. 1-2. We are mainly deal with the latter, which offers the highest mobility.

After the pioneering work by Sirringhaus [13], it is now well established that the performance of polymer OTFTs crucially depends on the chemical and structural ordering of the polymer. High order first depends on the regioregularity of the polymer, the percentage of regioregular head-to-tail attachment of the alkyl side chains to the beta position of the thiophene rings. However, high regioregularity is not enough. The work by the Cambridge group

showed that two orientations could be found in P3HT films, one with the polymer chains flat on the surface, and the other one with the chains edge on. Highest mobility was $0.1 \text{ cm}^2/\text{Vs}$, and the on/off ratio greater than 10^6 .

B. Small Molecules

Encouraging performance has been reported with small molecules, which currently offers higher mobility than hydrogenated amorphous silicon. However, high performance requires high ordering, particularly in the vicinity of the insulator-semiconductor interface, a constraint that may be difficult to fulfill when specific deposition methods are used. At present, practically all devices made of small molecules use pentacene or oligothiophenes and their derivatives (Fig. 1-3). Highest mobility now reaches $6 \text{ cm}^2/\text{Vs}$ for pentacene and 1 for sexithiophenes [14].

The solubility of organic semiconductors is vital for their use in low-cost electronic devices since the desired processing techniques include solution-based methods like spin coating, dip coating, or printing techniques. However, practically all the small molecules used in OTFTs are insoluble, and need to undergo vapor deposition to form thin films. Solution processing has been reported with oligothiophenes end-substituted with alkyl groups [15,16], but these compounds require high temperatures of both the solvent and the substrate. An alternative strategy consists of using a soluble precursor that would convert into the desired molecule through a thermal post-processing step. This strategy has been used with polymers such as polyacetylene and poly-*p*-phenylene-vinylene, and more recently, to pentacene. Mobility ranging from 0.3 to $0.9 \text{ cm}^2/\text{Vs}$ has been measured on OTFTs using the soluble precursor technique.

1.3 Thesis organization

In chapter 1, we describe our background and motivation of our study.

In chapter 2, we will introduce the characteristic of P3HT and methods for OTFT fabrication.

In chapter 3, we adopt a new process, APPT, which can be operated under low temperature and atmospheric ambient. And APPT will make use of modify surface of dielectric layer SiO_2 for our experiment. In addition, the other methods of HMDS surface treatment will also be utilized in our experiment. Finally, we compare the various methods of surface treatment and discuss the results.

In chapter 4, we used DSC, XRD and UV-vis to demonstrate that high mobility requires an ordered structure. And we also explain that the phenomenon of the hysteresis behavior and the anomalous leakage current of OTFT device.

In chapter 5, we will describe the conclusions and the future works.

Table 1-1: The differences of TFT and OTFT materials and processes.

	Materials	Processes	Process temperature	Cost
TFT	Amorphous、Poly-Silicon	Like semiconductor process	High (200~400°C)	High
OTFT	Small Molecular、Polymer、Complex	Printing process	Low (< 100°C)	Low

Table 1-2: Carrier mobility of inorganic and organic materials.

	Material	Mobility(μp)
Inorganic Semiconductor	Ge	1900 ($\text{cm}^2\text{v}^{-1}\text{s}^{-1}$)
	Si	450 ($\text{cm}^2\text{v}^{-1}\text{s}^{-1}$)
	GaAs	400 ($\text{cm}^2\text{v}^{-1}\text{s}^{-1}$)
	InP	150 ($\text{cm}^2\text{v}^{-1}\text{s}^{-1}$)
Organic Semiconductor	Polyacetylene	0.0001 ($\text{cm}^2\text{v}^{-1}\text{s}^{-1}$)
	α -W-hexathiophene	0.03 ($\text{cm}^2\text{v}^{-1}\text{s}^{-1}$)
	C 60	0.3 ($\text{cm}^2\text{v}^{-1}\text{s}^{-1}$)
	Pentacene	1.5 ($\text{cm}^2\text{v}^{-1}\text{s}^{-1}$)

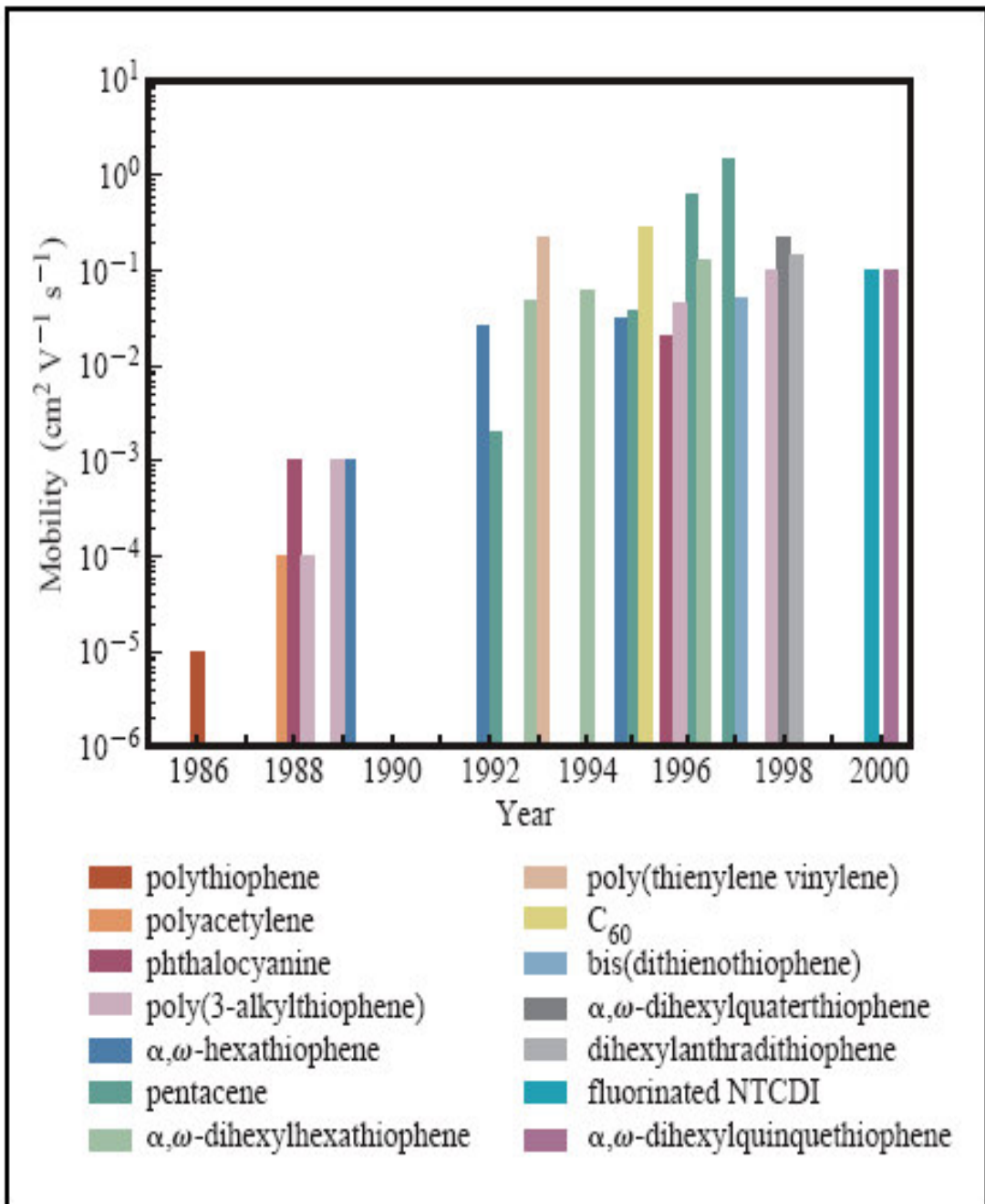


Figure 1-1: Semilogarithmic plot of the highest field-effect mobility (μ) Reported for OTFT fabricated from the most promising polymeric and oligomeric semiconductors versus year from 1986 to 2000 [17].

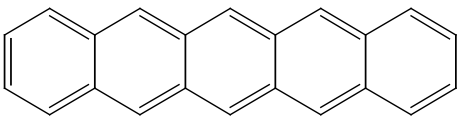
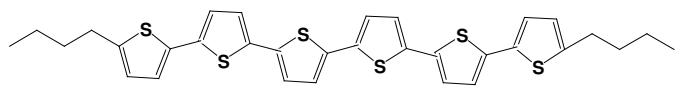
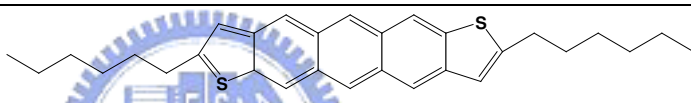
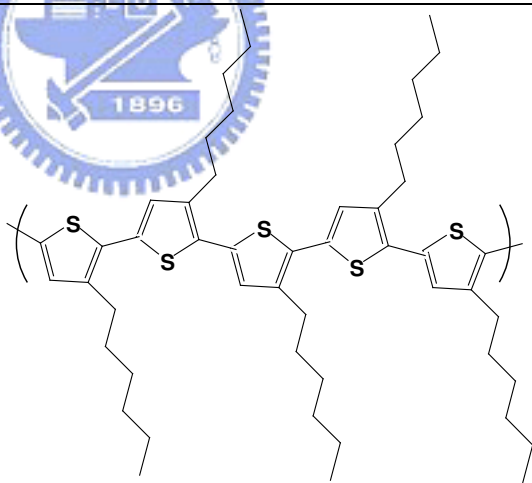
Table 1-3: Highest field-effect mobility(μ) values measured from OTFT as reported in the literature annually from 1986 through 2000 [17].

<i>Year</i>	<i>Mobility</i> ($\text{cm}^2 \text{V}^{-1} \text{s}^{-1}$)	<i>Material (deposition method)</i> (v) = vacuum deposition (s) = from solution	$I_{\text{on}}/I_{\text{off}}^*$	<i>W/L</i>	<i>Reference</i>
1983	Minimal, not reported (NR)	Polyacetylene (s) (demonstration of field effect in an OTFT)	NR	200	[16]
1986	10^{-5}	Polythiophene (s)	10^3	NR	[17]
1988	10^{-4}	Polyacetylene (s)	10^5	750	[18]
	10^{-3}	Phthalocyanine (v)	NR	3	[19]
	10^{-4}	Poly(3-hexylthiophene) (s)	NR	NR	[20]
1989	10^{-3}	Poly(3-alkylthiophene) (s)	NR	NR	[21]
	10^{-3}	α - ω -hexathiophene (v)	NR	NR	[22]
1992	0.027	α - ω -hexathiophene (v)	NR	100	[23]
	2×10^{-3}	Pentacene (v)	NR	NR	ibid.
1993	0.05	α - ω -di-hexyl-hexathiophene (v)	NR	100–200	[24]
	0.22 [†]	Polythiénylenevinylene (s)	NR	1000	[25]
1994	0.06	α - ω -dihexyl-hexathiophene (v)	NR	50	[26]
1995	0.03	α - ω -hexathiophene (v)	$>10^6$	21	[27]
	0.038	Pentacene (v)	140	1000	[28]
	0.3	C_{60} (v)	NR	25	[29]
1996	0.02	Phthalocyanine (v)	2×10^5	NR	[30]
	0.045	Poly(3-hexylthiophene) (s)	340	20.8	[31]
	0.13	α - ω -dihexyl-hexathiophene (v)	$>10^4$	7.3	[15]
	0.62	Pentacene (v)	10^8	11	[32]
1997	1.5	Pentacene (v)	10^8	2.5	[33]
	0.05	Bis(dithienothiophene) (v)	10^8	500	[34]
1998	0.1	Poly(3-hexylthiophene) (s)	$>10^6$	20	[35]
	0.23	α - ω -dihexyl-quaterthiophene (v)	NR	1.5	[36]
	0.15	Dihexyl-anthradithiophene	NR	1.5	[37]
2000	0.1	n-decapentafluoroheptyl-methyl- naphthalene-1,4,5,8-tetracarboxylic diimide (v)	10^5	1.5	[38]
	0.1	α - ω -dihexyl-quinquethiophene (s)	NR	NR	[38]

*Values for $I_{\text{on}}/I_{\text{off}}$ correspond to different gate voltage ranges and thus are not readily comparable to one another. The reader is encouraged to read the details of the experiments in the cited references.

†This result has not yet been reproduced.

Table1-4: The chemical structures and reported mobilities of representative classes of organic materials compared to those of inorganic silicon materials.

Semiconductor	Representative chemical structure	Mobility (cm ² /Vs)
Silicon	Silicon crystal	300-900
	Polysilicon	50-100
	Amorphous silicon	~1
Pentacene		~1
Dihexyl-sexithiophene		10 ⁻¹
Dihexylanthra-dithiophene		10 ⁻¹
Regioregular Poly(3-hexyl thiophene)		10 ⁻¹
Organic-inorganic hybrid	Phenethylamine-tin iodide	~1

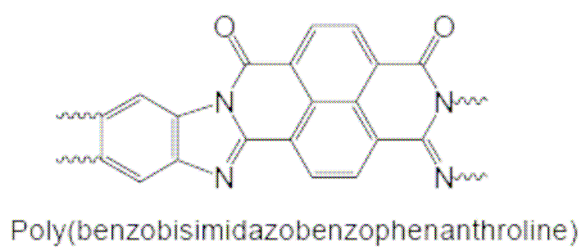
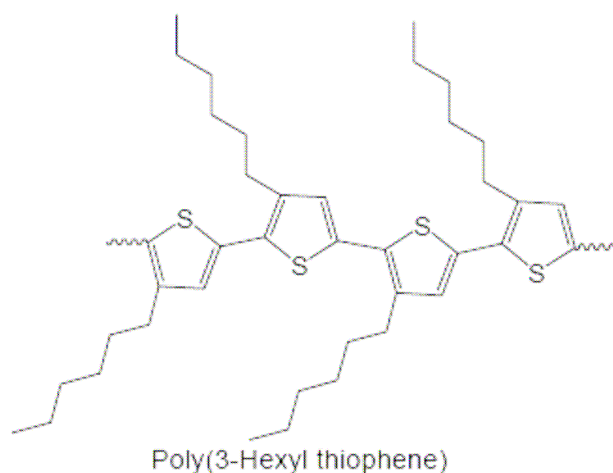


Figure 1-2: The chemical structures of P3HT and BBL (Polymer).

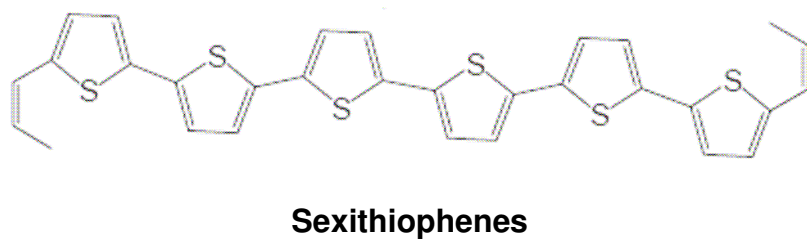
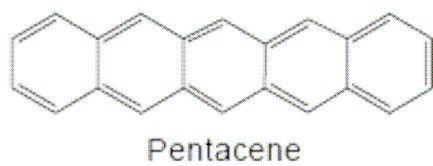


Figure 1-3: The chemical structures of pentacene and oligothiophenes (Small molecules).

Chapter 2

Property of P3HT and Spin-Coating Technique

2.1 Introduction of P3HT

2.1.1 The molecular structure of P3HT

The field-effect mobility of P(3-hexylthiophene) P3HT is strongly influenced by the structure of the polymer chain and the direction of intermolecular π - π stacking. The structure of the polymer chain of P3HT is shown in Fig. 2-1. The 3-alkylsubstituents can be incorporated into a polymer chain with two different regioregularities: head to tail (HT) and head to head (HH) [18,19].

R represents the alkyl side chain (C_6H_{13} for P3HT), which allows P3HT to be dissolved in 1 like chloroform. This solution processability enables simple film deposition. A regiorandom P3HT consists of both HH and HT 3-hexylthiophene in a random pattern while a regioregular has only one kind of 3-hexylthiophene, either HH and HT. This type of order is known as regioregularity and has been shown to give much higher field-effect mobility values over regiorandom material [20]. In our experiments, regioregular P3HT (HT regioregularity of 98.5%) and high grade solvent, chloroform, were purchased from Aldrich Chemical Company. A dramatic increase in mobility was observed relative to regiorandom poly-3-alkylthiophenes [21] when regioregular P3HT consisting of 98.5% head to tail (HT) linkages, so we did not perform further purification to these chemicals in our experiments. After being

deposited on the substrate, P3HT backbones may form two different morphologies, edge-on or face-on of lamella structure as shown in Fig. 2-2. The higher mobility is given by edge-on structure since the carriers can move more efficiently through intra-chain transport along the direction of π - π stacking. Two different methods are applied to deposit the P3HT film, one is spin-coating and while the other is dip-casting. The mobility of dip-coated films is usually higher than that of the spin-coating that's maybe due to the evaporation rate of solvents. Lower evaporation rate results in a slower crystal growth with better ordered polymer structure [22,23]. In spite of that method provide the higher field effect mobility, the dip-coating method can not be applied for coverage of a large area. Therefore, in all of our experiments, we used spin-coating technique as a key process of organic layer deposition.

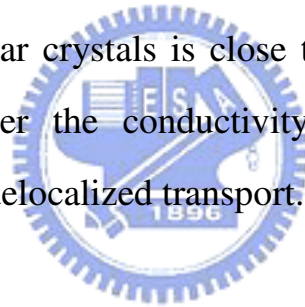
2.1.2 Conduction mechanism

Compared to the tremendous progress that the field of organic thin-film transistors has known during the past years, the theory of charge transport has hardly evolved. Basically, one can distinguish several families of charge transport models.

A. Hopping [24]

This family pertains to disordered materials, such as polymers. In metals and conventional semiconductors, charge transport occurs in delocalized states, and is limited by the scattering of the carriers, mainly on phonons, that is, thermally induced lattice deformations. Such a model is no longer valid in low conductivity materials such as amorphous or organic semiconductors, where a

simple estimate shows that the mean free path of carriers would become lower than the mean atomic distance. In these materials, transport occurs by hopping of charges between localized states. A main difference between the delocalized and localized transport is that, in the former, the transport is limited by phonon scattering, whereas in the latter, it is phonon assisted. Accordingly, the charge mobility decreases with temperature in conventional semiconductors, the reverse being true in most organic materials. Several models have been developed to rationalize the hopping transport. In most cases, the temperature dependence of the mobility follows a law of the form $\mu = \mu_0 \exp[-(T_0/T)^{1/\alpha}]$, where α is an integer ranging from 1 to 4. The boundary between the localized and delocalized processes is usually taken at a mobility between 0.1 and 1 cm²/Vs. The mobility in highly ordered molecular crystals is close to that limit, so that there is still controversy as to whether the conductivity in these materials should be described by localized or delocalized transport.



B. The Small Polaron [24]

Localization in conjugated organic materials occurs via the formation of polarons. A polaron results from the deformation of the conjugated chain under the action of the charge. In other words, in a conjugated molecule, a charge is self-trapped by the deformation it induces in the chain. This mechanism of self-trapping is often described through the creation of localized states in the gap between the valence and the conduction bands, as shown in Fig. 2-3 in the case of polythiophene [25]. The existence of such levels in doped conjugated polymers and oligomers has indeed been identified by UV-visible spectroscopy. A useful model to describe the charge transport in organic materials is that of the small polaron, developed by Holstein [26].

C. Multiple Trapping and Release (MTR)

In the multiple trapping and release model [27], a narrow delocalized band is associated with a high concentration of localized levels that act as traps. During their transit through the delocalized levels, the charge carriers interact with the localized levels through trapping and thermal release. The following assumptions are usually made: First, the carriers arriving at a trap are instantaneously trapped with a probability close to one. Second, the release of trapped carriers is controlled by a thermally activated process. The resulting drift mobility μ_D is related to the mobility μ_0 in the delocalized band by an expression of the form in Equation:

$$\mu_D = \mu_0 \alpha \exp(-Et/kT)$$

In the case of a single trapping level, Et corresponds to the distance between the trap level and the delocalized band edge, and α is the ratio of the effective density of states at the delocalized band edge to the concentration of traps. In the case of energy-distributed trap, effective values of Nt and α have to be calculated. The MTR model is currently the one most widely used to account for charge transport in amorphous silicon.

The weak intermolecular interaction forces in organic semiconductors, most usually van der Waals interactions with energies smaller than 10 Kcal mol⁻¹, may be responsible for such small carriers mobility. In contrast, in inorganic semiconductors such as Si and Ge, the atoms are tied together with very strong covalent bonds, which for the case of Si have energies as high as 76 Kcal mol⁻¹. In these semiconductors, charge carrier flows like highly delocalized plane

waves in the wide bands and have very high mobility. On the other hand, inorganic semiconductors usually have high order lattice structures and there are fewer traps than organic ones. This is another reason to explain the poor electrical characteristics of organic electronics.

However, for conjugated organic materials, the polymer chains are weakly bound by van der Waals force. These polymer typically have narrow energy bands, highest occupied molecular orbit(HOMO) and lowest occupied molecular orbit(LUMO), which can easily be disrupted by disorder. Due to disorder structures, band transport is not applicable to organic semiconductors; in which carrier transport take place by hopping [23] between localized state like Fig. 2-4. Transport from one molecular to another is much more difficult due to a small energetic coupling between molecules held by weak van der Waals force of ~ 10 Kcal mol⁻¹. Another characteristic of organic material is that most polymers conduct one kind of carrier only, either electron or hole (P3HT is p-type that majority carriers are holes). Because of the nature of large band gap(e.g. Eg of P3HT = 2.2 eV), the active layer cannot be inverted by thermal energy at room temperature(i.e. slow generation rate of inversion layer). Therefore, OTFTs operate in the accumulation mode at it's ON state and depletion at it's OFF state.

P3HT are semi-crystalline in nature, and their conduction mechanism is complex. The crystalline portion can conduct through intra-chain and inter-chain transport, whereas the amorphous portion conducts current through hopping processes.

2.2 Solution processed deposition

2.2.1 Methods of OTFT fabrication

There are four methods to form organic semiconductor film: (1) Solution-processed deposition, (2) Electro-polymerization, (3) Vacuum evaporation, (4) Langmuir-Blodgett Technique [28]. Recently, many researchers extensively use solution-processed deposition to fabricate organic semiconductor film. For solution-deposited organic semiconductor film, one kind of the organic semiconductor material such as poly (3-hexylthiophene) is dissolved in solvent such as chloroform. In our experiment, we use P3HT as the semiconductor because P3HT has many potential advantages for use the semiconductor layer in field-effect transistors. (1) P3HT is a well-known polymer as an organic semiconductor and has shown the effect mobility from 10^{-4} cm²/Vs in 1988 to 0.2 cm²/Vs in 2003 [13,29]. (2) P3HT has high solvent selectiveness, can dissolve in toluene, xylene, chloroform and so on. (3) P3HT is solution processed, therefore can be processed by spin-coating .

2.2.2 The motive of spin-coating

The organic semiconductors that exhibit the best mobility, ON/OFF current ratio, uniformity over large areas, and devices reproducibility have been deposited by vacuum sublimation. However the need for expensive vacuum chambers and lengthy pump-down cycles is unavoidable. Since the organic semiconductors have the relatively low mobility of organic semiconductors as described in chapter 1, OTFT cannot rival the performance of based on single

crystalline inorganic semiconductors, such as Si, Ge, and GaAs. However, the unique processing characteristics and demonstrated performance of OTFT suggest that they can be competitive candidates for existing or novel thin film transistor applications requiring large area coverage, structural flexibility, low temperature processing, and especially low cost. Some recent efforts in the field have focused on processes for solution deposition of small molecule [30] and polymers, as well as integration of these processes with other non-lithographic device fabrication technique [31]. To realize truly the advantages (i.e., processability and low cost) of organic materials in device applications, liquid phase processing technique by spin-coating is strongly desired. In all of our experiments, we used spin-coating technique as a key process of organic layer fabrication.



2.2.3 Effect of polymer morphology and solvents

The molecular structure of the P3HT greatly influences the charge carrier mobility and related current-voltage (I-V) characteristics of OTFT. A comparison study of P3AT (A = hexyl, octyl, dodecyl, hexadecyl) with side chains ranging from butyl to decyl showed that field-effect mobility decreases with increasing chain length [32].

Under different processing conditions, the field effect mobility of OTFT is highly anisotropic. For example, Karl et al [33] observed that the field effect mobility was highly anisotropic, with the larger mobility along the direction in which the polymer chain axis aligned.

The molecular structure obtained by using spin-coating films is usually lower than that of the cast films [18]. This is perhaps because in the cast films,

the rate of solvent evaporation is slower and has slower crystal growth, and hence better ordering, and large grain size.

The choice of solvents and polymers has a very significant impact on the electrical characteristics of OTFT. In a recent publication, Bao et al [16]. Observed that when chloroform was used as a solvent to make poly-(3-hexylthiophene)-based transistors, the field-effect mobility was $0.1 \text{ cm}^2\text{Vs}^{-1}$. However when Tetra hydrofuran (THF) was used as the solvent, the value of field-effect mobility is only $0.0006 \text{ cm}^2\text{Vs}^{-1}$. Table 2-1 shows the performance of various devices made from casting poly(3-hexylthiophene) films using different solvents with different process conditions [16].

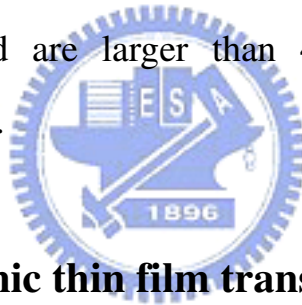
Sirringhaus et al, [20] observed that the mobility could differ by a factor of 100 depending on the direction of π - π stacking in which efficient inter-chain transport is happened . The polymer solution we used is regioregular P3HT in chloroform with high purity. From Table 2-1, the mobility is typically in the range 10^{-3} which matches the result obtained in our experiment. In chapter 4, we will discuss the relation between the orientation of P3HT and carrier mobility.

2.3 Contact resistance of P3HT OTFT

There are many parameters will impact the performance of OTFT. The contact resistance between the source/drain electrodes and the organic semiconductor is an important one of them [34,35,36]. The contact resistance between the source/drain electrodes and the semiconductor becomes increasingly important to device performance. The contact resistance dominates the overall device resistance.

Material of source/drain electrodes and the structure both affect the contact

characteristics between the source/drain electrode and the organic semiconductors. Unlike the FET of single-crystalline silicon, polycrystalline silicon, or hydrogenated amorphous silicon, the P3HT material cannot be optimized easily by semiconductor doping or silicide formation. Such properties of organic semiconductors deteriorate the performance of devices; moreover, the chemical compound always increase the contact resistance between the source/drain electrode and the organic semiconductor [37,38]. It is a straightforward method to find a suitable electrode material which forms ohmic contact with the organic active layer and thus to improve the performance of OTFT. P3HT can form an ohmic contact with material for its work function larger than 4.5eV because the work function of P3HT is 4.5eV. Work functions of all materials we used are larger than 4.5eV; they include Ni(4.5eV), Pt(5.29eV), and Cr(4.5eV).



2.4 Operation of organic thin film transistors

Refer to [39], the operation of the P3HT which bases on OTFT is described below. Organic thin-film transistors are opposed to the usual inversion mode operation of silicon MOSFETs and primarily operated as a P-type accumulation-mode enhancement type transistor. There are four basic modes which will be described later.

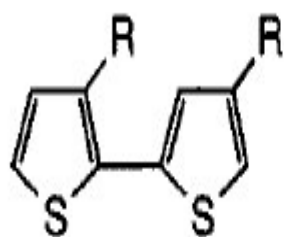
Mode (I): When zero bias is applied to three electrodes of OTFT. The schematic diagram is shown in Fig. 2-5(a), it is called cut-off. If applied a small drain bias, V_d , and the source-current, I_{ds} , will be small and ohmic.

Mode (II): When a positive bias applied, the bend bending will occur in the interface between dielectric layer and semiconductor layer. Negative charges

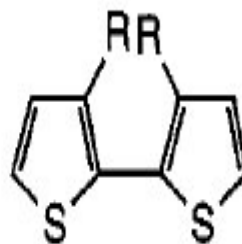
will locate at interface and form the depletion region. The schematic diagram is shown in Fig. 2-5(b). The channel resistance is so large that the current will be smaller than that of mode (I). Because of the large band gap, inversion layer cannot be observed in the organic thin-film transistor.

Mode (III): When gate bias is negative, the schematic diagram is shown in Fig. 2-5(c), the voltage is dropped over the insulator and over the semiconductor near the interface between dielectric layer and semiconductor layer. More positive charges will be accumulated in the accumulate region. When a small bias is applied to drain, the source-drain current will be larger than that of Mode (I), the schematic diagram is shown in Fig. 2-5(d).

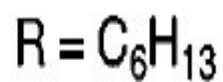
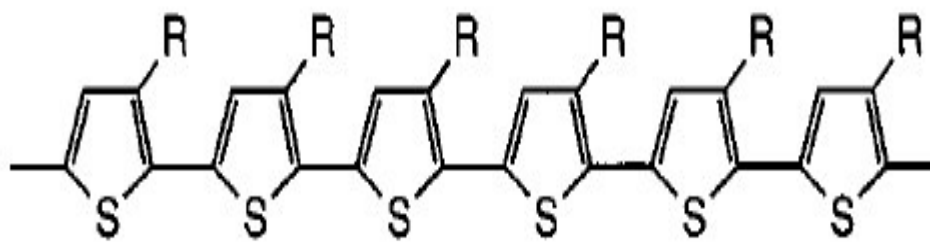
Mode (IV): When drain voltage is negative enough that the voltage difference of gate and drain, V_{gd} , which is lower than V_{th} (<0), therefore, the depletion region will form near drain and pitch-off (Fig. 2-5(e)). If drain voltage is more negative, the depletion region will grow and approach source. The schematic diagram is shown in Fig. 2-5(f), (g).



head-to-tail
(HT)

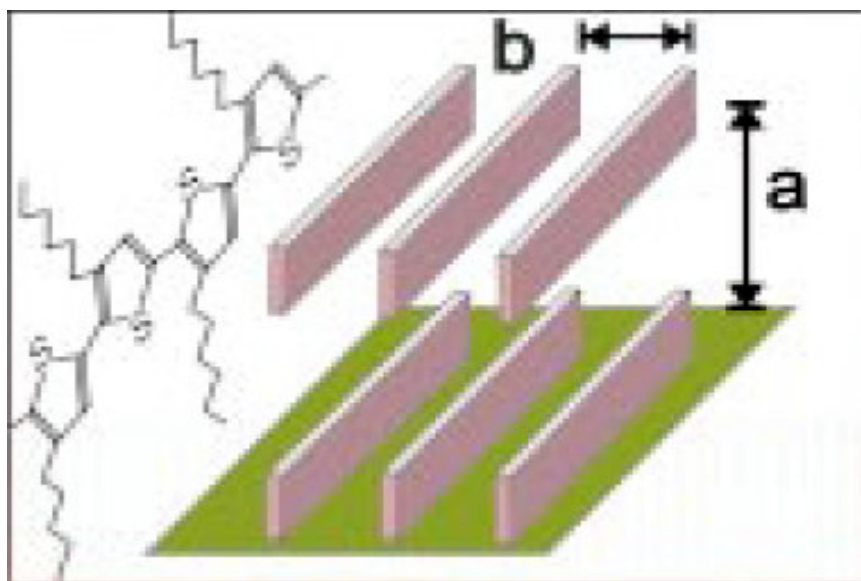


head-to-head
(HH)

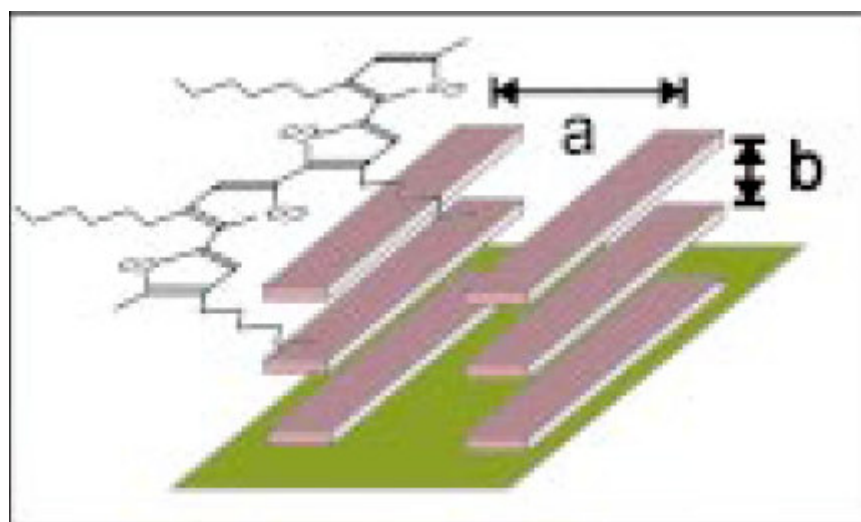


regioregular poly(3-hexylthiophene)
(P3HT)

Figure 2-1: The structure of the polymer chain of P3HT.



(a)



(b)

Figure 2-2: Two different orientations of ordered P3HT (a) Edge-on orientation, (b) Face-on orientation.

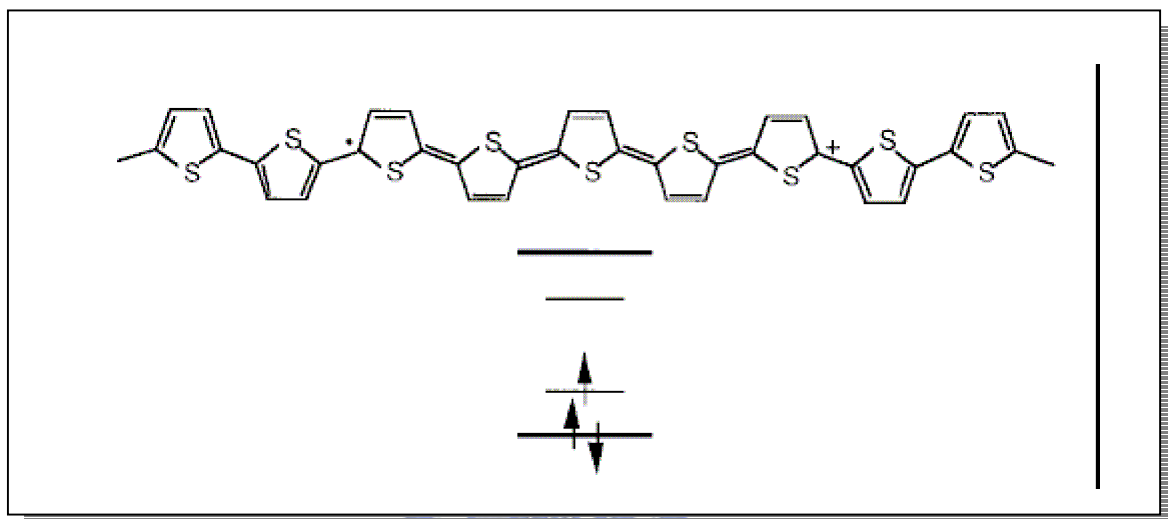
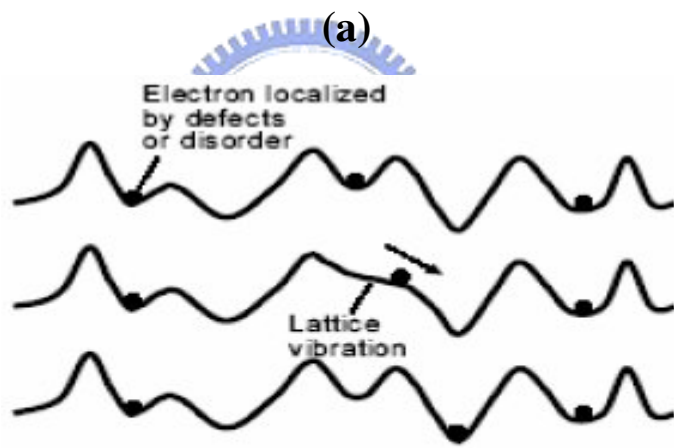
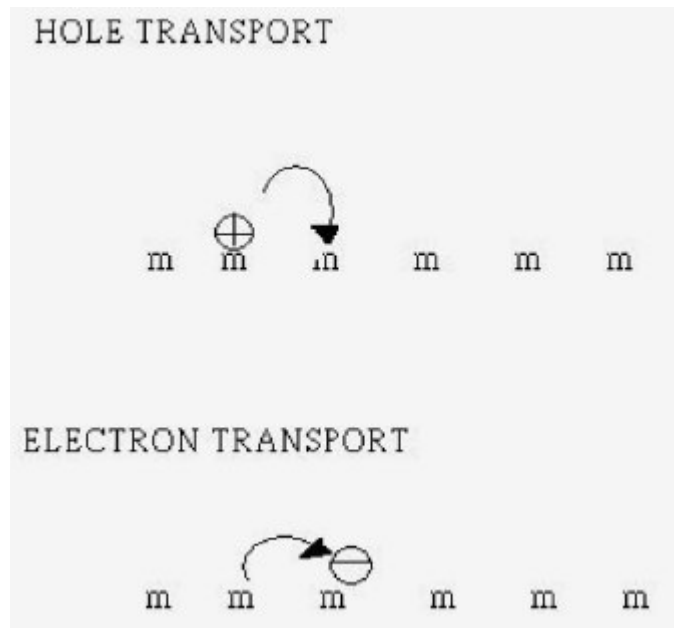


Figure 2-3: A polaron in polythiophene. Top: Change in the chemical structure. Bottom: Corresponding energy diagram.



Hopping transport

(b)

Figure 2-4: (a) Charge carrier transport in conjugated polymers,
 (b) Charge transport mechanisms in solid.

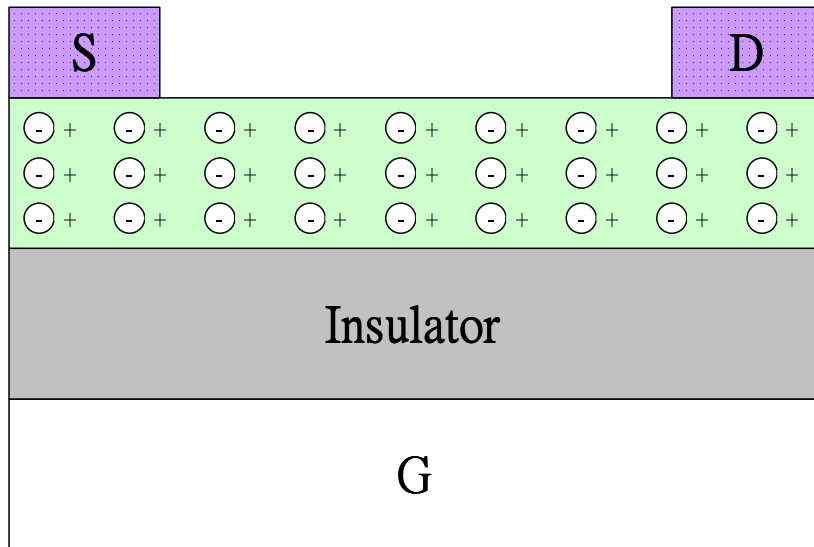
Table 2-1: Field-effect mobility and ON/OFF ratio of samples prepared from different solvents and process condition [16]. Condition 1, casting , vacuum pumped for 24 h; condition 2, spin-coated; condition 3, treated with NH₃ for 10 h; condition 4, heated to 100 °C under N₂ for 5 min; condition 5, heated to 150 °C under N₂ for 35 min.

Entry	Solvent	Condition	Mobility (cm ² /V s) ^a	On/off ratio ^b
1	THF	1	6.2×10 ⁻⁴	10
2	<i>p</i> -xylene	1	1.9×10 ⁻³	40
3		2	1.9×10 ⁻⁵	2
4	Toluene	1	3.6×10 ⁻³	10
5		2	3.2×10 ⁻³	25
6	Chlorobenzene	1	4.7×10 ⁻³	10
7		entry 6 condition 3	4.7×10 ⁻³	80
8		2	6.9×10 ⁻⁴	72
9	1,1,2,2-tetrachloroethylene	1	6.8×10 ⁻³	35
10	1,1,2,2-tetrachloroethane	1	2.4×10 ⁻²	6
11		entry 10 condition 4	1.4×10 ⁻²	35
12		entry 11 condition 5	3.3×10 ⁻³	15
13	Chloroform	2	9.2×10 ⁻³	80
14		1	4.5×10 ⁻²	340
15		entry 14 condition 3	2.1×10 ⁻²	9000

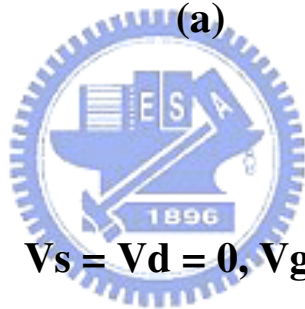
^aField-effect mobility for the accumulation-mode operation.

^bOn/off ratio is calculated for enhancement-mode operation only, and it is ten times higher for enhancement-depletion operation.

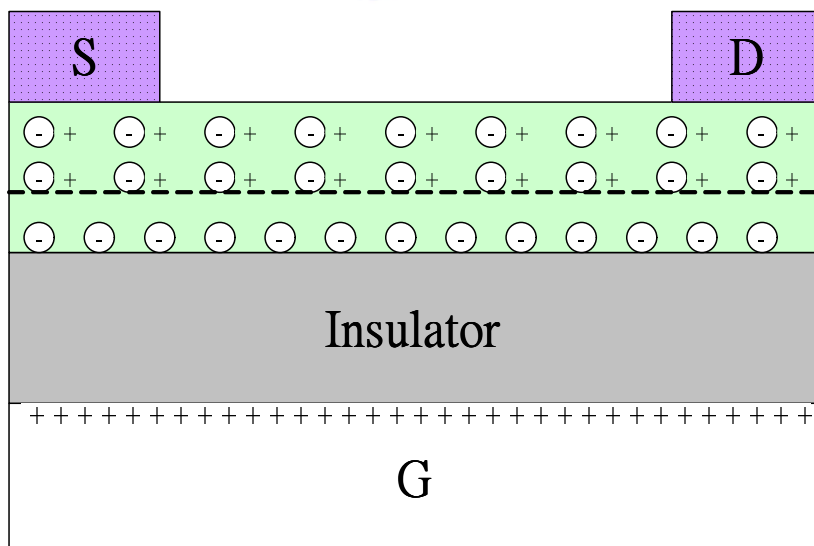
$$V_g = V_s = V_d = 0$$



(a)

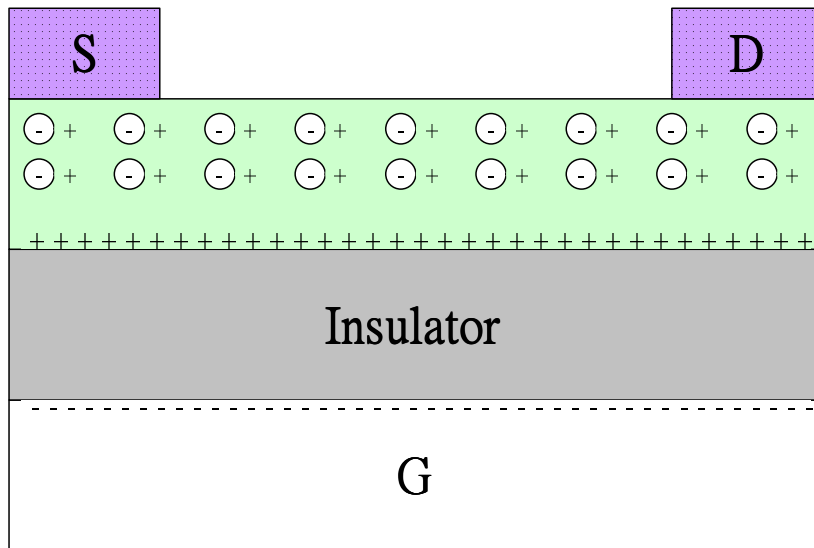


$$V_s = V_d = 0, V_g > 0$$

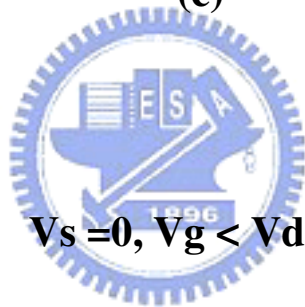


(b)

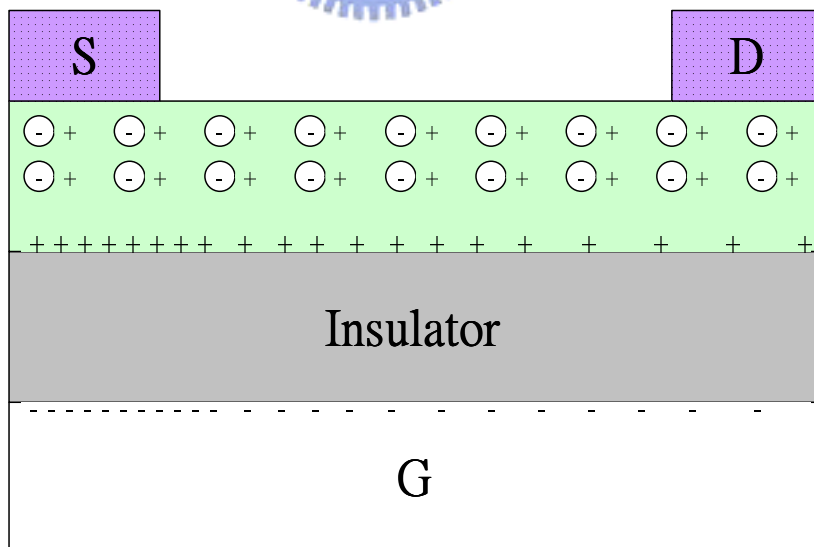
$$V_s = V_d = 0, V_g < 0$$



(c)

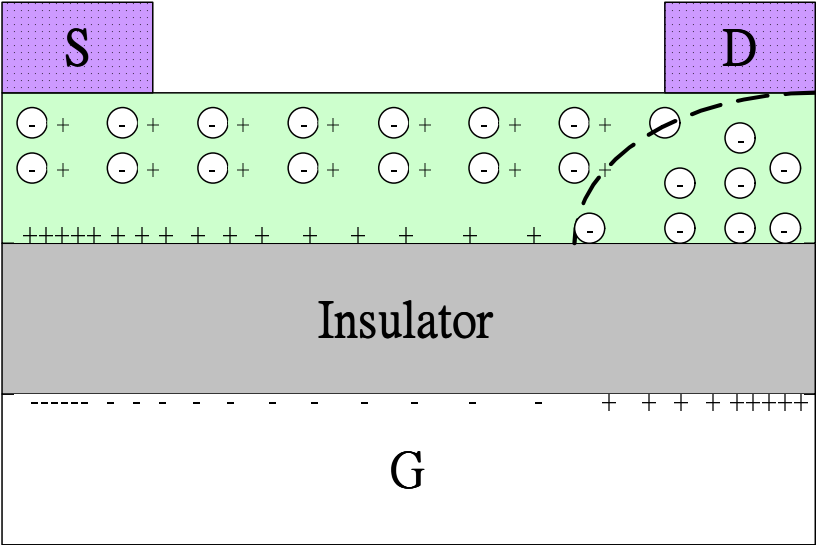


$$V_s = 0, V_g < V_d < 0$$



(d)

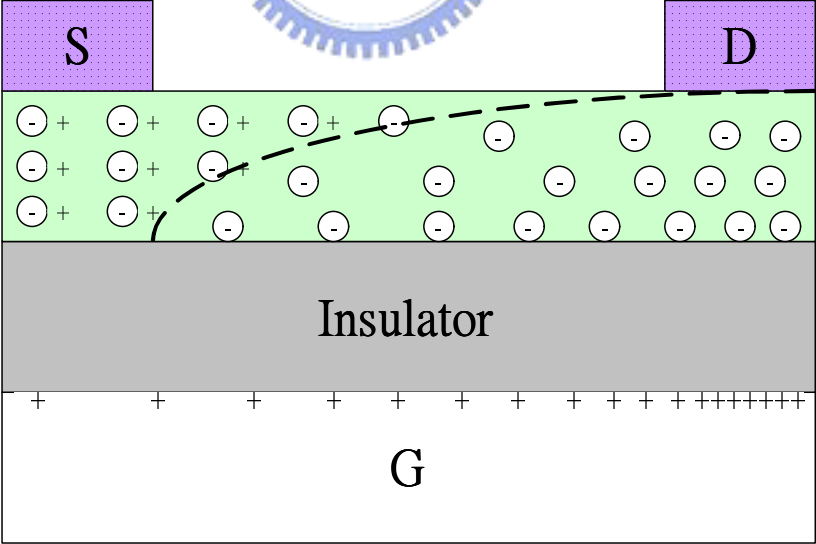
$V_s = 0, V_d < V_g < 0$



(e)

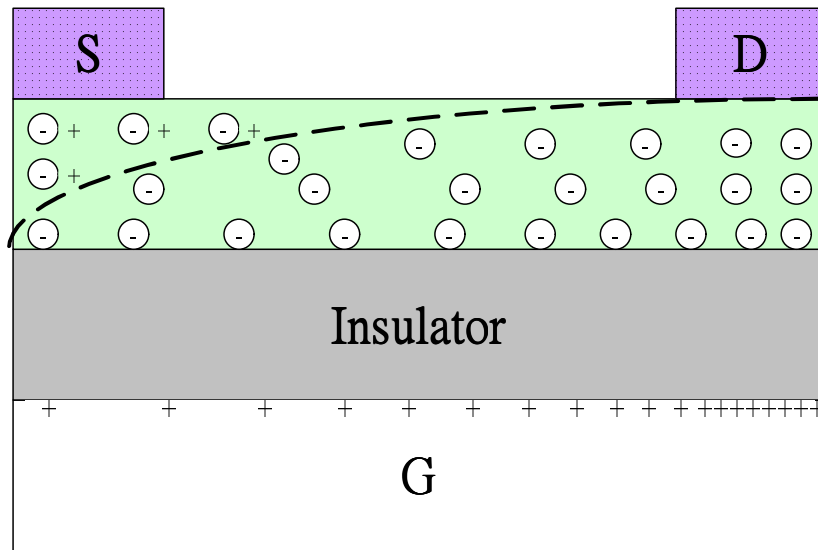


$V_s = V_g = 0, V_d < 0$



(f)

$$V_s = V_g = 0, V_d \ll 0$$



(g)

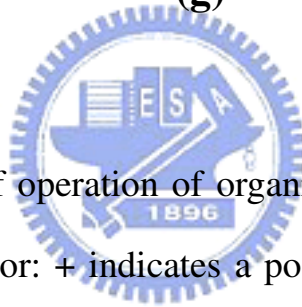


Figure 2-5: Schematic of operation of organic thin film transistor, showing a lightly doped semiconductor: + indicates a positive charge in semiconductor; - indicates a negatively charge in semiconductor. (a) No-bias, (b) Depletion mode, (c) Accumulation mode, (d) Non-uniform charge density, (e) Pinch-off of channel, (f) and (g) Growth of the depletion zone

Chapter 3

Surface Treatment by Atmospheric-Pressure

Plasma Technology for Electrical Properties of OTFT

3.1 Modification of oxide surface

The interface between an organic material and dielectric layer is a critical factor for device performance. This is because the surface of the dielectric strongly influences the quality of the dielectric/channel interface and the crystalline organic channel. The quality of the interface and the organic channel, as well as the electrical properties of the gate dielectric itself, play a major role in determining the device performance of an OTFT [40,41,42]. Although several methods have been recently proposed to improve the condition of the interface states, only a few have been proved to be reliable and robust. One of the proposed methods is the use of a self-assembly monolayer (SAM), such as octadecyltrichlorosilane (OTS) [43] and hexamethyldisilazane (HMDS) [44], have been extensively studied. A dielectric surface treatment with OTS is found to improve the mobility of OTFTs.

Another dielectric surface treatment technique is O_2 plasma cleaning and subsequent HMDS deposition on dielectrics [44]. A problem owing to O_2 plasma cleaning, which is applied to remove residues generated from previous photolithography processes, was found to be the generation of a large number of trap states during the cleaning process by assisting OH termination at the SiO_2 surface [45]. Although a HMDS layer subsequently applied is expected to reduce the number of traps and act as a SAM, the time-consuming wet processes

used to apply a SAM on the interface are unreliable and can cause other undesirable contaminations of the device.

Surface treatments using an ion beam have been widely studied in other research fields. It is well known that ion implantation techniques can change the surface conditions or thin-film properties [46]. In the LCD fabrication process, for example, Ar ion beam treatment has been considered as a viable option as a surface treatment method to replace conventional contact-based treatment such as rubbing [47]. One of the advantages of Ar ion beam treatment is that because argon is an inert gas, it can clean the surface effectively without affecting the chemical structure of the dielectric layer.

3.2 Introduction of APPT



3.2.1 Introduction of plasma

Plasma can be defined as a partially or wholly ionized gas with a roughly equal number of positively and negatively charged particles. Some scientists have dubbed plasma the "fourth state of matter" because while plasma is neither gas nor liquid, its properties are similar to those of both gases and liquids.

There are two types of plasma - high temperature and low temperature. A good example of naturally occurring high temperature plasma is lightning. This type of plasma can be artificially generated using a high voltage, high temperature arc, which is the basis for the corona discharge process and for the plasma torch used to vaporize and redeposit metals. Low temperature plasmas, used in surface modification and organic cleaning, are ionized gases generated at pressures between 0.1 and 2 torr. These types of plasmas work within a vacuum

chamber where atmospheric gases have been evacuated typically below 0.1 torr. Low pressure allows for a relatively long free path of accelerated electrons and ions. Since the ions and neutral particles are at or near ambient temperatures and the long free path of electrons, which are at high temperature or electron volt levels, have relatively few collisions with molecules at this pressure the reaction remains at low temperature.

3.2.2 Applications of APPT

Plasma processes allow realizing a multitude of surface modifications. However, since these processes usually operate under vacuum, this makes them unsuitable for many industrial applications e.g. for large-area low price products. Therefore this has been occupied for several years with developing atmospheric pressure plasma processes for surface coating and treatment. Table 3-1 shows the type of atmospheric pressure plasma.

Atmospheric pressure plasma is particularly suited for the large-area surface treatment of flat substrates (Fig. 3-1). This forms between two electrodes on application of an alternating current if at least one dielectric barrier or insulator obstructs the current. Gases are activated in these micro discharges by electronic excitation, ionization and dissociation to form very chemically reactive species. Thus the average gas temperature in the discharge gap rises only a few degrees Kelvin. Since the discharge in effect remains "cold" even temperature-sensitive substrates can be treated. Despite the filamentation of the discharges, with appropriate process control it is normal to achieve a very uniform surface treatment.

Atmospheric pressure plasma-processes are used extensively in industry for

the activation of surfaces, the generation of ozone and for the electrical charging of particles. These processes are additionally used for cleaning, coating and functionalizing a variety of surfaces. Often ultra-thin coatings are deposited, which impart the desired properties to the surface. Examples of this are very thin Si-oxide coatings on steel which then enable corrosion protection properties to be conferred e.g. by phosphatization, or the placing of epoxide groups onto the surface, which are required e.g. in biotechnology. APP can also be successfully applied to the fine cleaning of steel surfaces, since organic contaminants are removed in the plasma.

The atmospheric-pressure plasma technology (APPT) is useful for treating and modifying the surface properties of organic and inorganic materials. The APPT apparatus does not require any vacuum systems, produces high density plasma, and provides treatment of various substrates at low temperatures while operating open to the atmosphere. The plasma system has used for a wide variety of applications including treatment of polymer films, paper, wood, and foils; plasma grafting and plasma polymerization; ash various materials in the microelectronics industry; barrier layer deposition for the packaging industry; and sterilizing biologically contaminated materials. For polymer films, the technique offers the following advantages:

- Uniform treatment and No backside treatment.
- Improved surface energy with concomitant improved wettability, printability, and adhesion
- No additional vacuum system and low cost
- Continuous fabrication available and high speed for production

- High plasma density

As shown in Fig. 3-2(a), we exhibited the atmospheric-pressure plasma system which was used in our experiment, and also showed the cold temperature atmospheric-pressure plasma systems in Fig. 3-2(b).

3.2.3 Plasma surface modification

Fig. 3-2 shows the mechanisms of plasma surface modification, glow discharge plasma is created by evacuating a reaction chamber and then refilling it with a low-pressure gas. The gas is then energized by one of the following types of energy: radio frequency, microwaves, and alternating or direct current. The energetic species in gas plasma include ions, electrons, radicals, metastables, and photons in the short-wave ultraviolet (UV) range. Surfaces in contact with the gas plasma are bombarded by these energetic species and their energy is transferred from the plasma to the solid. These energy transfers are dissipated within the solid by a variety of chemical and physical processes to result in a unique type of surface modification that reacts with surfaces in depths from several hundred angstroms to 10 μ m without changing the bulk properties of the material.

A wide variety of parameters can greatly affect the physical characteristics of plasma and subsequently affect the surface chemistry obtained by plasma modification. Processing parameters, such as gas types, treatment power, treatment time and operating pressure, can be varied by the user; however system parameters, such as electrode location, reactor design, gas inlets and vacuum are set by the design of the plasma equipment. This broad range of

parameters offers greater control over the plasma process than that offered by most high-energy radiation processes.

Plasma treatment is aiming for various goals as for example:

- Improved adhesion
- Removal of the "water skin"
- Activation of the substrate surface
- Modification of the substrate surface
- Cleaning of substrate surfaces

Since the organic film of OTFT is fabricated on to the dielectric layer under the influence of the physical and chemical interactions between organic and dielectric layer, the OTFT performance strongly depends on the semiconductor/dielectric interface. The purpose of this work is to show the improvement of OTFT performance by controlling the surface treatments of dielectric/polymer interface. The surface properties such as frictional or abrasion, permeability, insulating properties, wettability and chemical reactivity are strongly dependent on a molecular aggregation state of the surface [48,49]. Therefore, the control of a molecular aggregation state in the film is important to construct a highly functionalized surface. One of the most effective ways of studying surface properties is contact angle measurement. The contact angle is the angle between the tangent to the drop's profile and the tangent to the surface at the interaction of the vapor, the liquid, and the solid. The contact angle is an index of the wettability of the solid surface. A low contact angle between solid surface water-drop indicates that the surface is hydrophilic and has a high surface energy. On the contrary, a high contact angle means that the surface is hydrophobic and has a low surface energy. The surface free energy was

traditionally quantified by contact angle measurements [50,51].

In our work, we investigated the electrical properties of the OTFT which surface treatment by APPT. Hexamethyldisilane ((CH₃)₃-Si-O-Si-(CH₃)₃) (HMDS) have already been widely used for oxide-based dielectric [52]. Oxide surfaces were treated with hexamethyldilazane to improve the adhesion between polymer chain and oxide surfaces. Modification of the substrate surface prior to deposition of regioregular P3HT has also been found to influence film morphology. For example, treatment of SiO₂ with hexamethyldilazane (HMDS) or an alkyltrichlorosilane replaces the hydroxyl groups at the SiO₂ surface with methyl or alkyl groups. The apolar nature of these groups apparently attracts the hexyl side chains of P3HT, favoring lamellae with an edge-on orientation [23]. According to [23], the mobility of OTFT with an edge-on orientation P3HT film is higher than the one with a face-on orientation.

And so HMDS would be adopted in our experiment. We will discuss and analyze the effects of APPT surface treatments latter, and find the optimum parameters in our experiments.

3.3 Fabrication of OTFT

There are two kinds of basic structures which are adopted generally, bottom-contact (BC) and top-contact (TC) were shown in Fig. 3-3. Top-contact device is favorable compared to deposition onto prefabricated source and drain electrodes bottom-contact device, yielding mobilities that are typically larger by a factor of 2 [53,54].

First, an n-type bare silicon wafer was cleaned by the standard RCA cleaning process. After that, phosphorous atoms were diffused into an n-type

silicon wafer by POCl_3 to form a common gate electrode. We used dilute to remove SiO_2 after diffusing. Before the insulating layer of silicon dioxide was deposited, the n+ silicon wafer must be cleaned by the standard RCA cleaning again. An insulating layer of silicon dioxide was grown by thermal oxidation 5hr at 1000°C . The thickness of silicon dioxide was 2000Å measured by n&k system. The wafers were taken to remove silicon dioxide of backside, and gate dielectric layer was formed. The “top-contact” OTFT structures were treated by different surface treatments before deposition of the P3HT active layer. The surface treatments were to control chemical and physical characteristics of surface by different ways. In our experiments, we adopted three methods of surface treatments and compared the difference of them.

(1) Hexamethyldisilane (HMDS) was deposited by spin-coating at 800 rpm for 3 sec as step one, 2000 rpm for 35 sec as step two, and baking at 150°C for 30 min.

(2) Evaporated HMDS at 150°C

(3) Atmospheric pressure plasma technology (APPT) was operated at 50W of plasma power, 0.1 sccm of He-gas flow, below 120°C , and various scanning times which are one, two, four, and eight times.

After finishing surface treatments, active layer P3HT was spun-coated at 1500 rpm 35sec and baked 130°C for 3 min on hot plate. The P3HT (with head-to-tail linkages greater than 98.5 %) and the high purity solvent (chloroform) used in this study were obtained from the Aldrich Chemical Company. The solutions of P3HT in chloroform were made with weight concentration of 0.3 %, and filtered through a $0.2\ \mu\text{m}$ pore-size PTFE filter. Finally, deposition of S/D contacts was formed by sputter system, Ion Tech Microvac 450CB, and

patterned through the shadow mask. The thickness of Pt contacts was 600Å. W (2000 μm) is the channel width, L (500μm) is the channel length. The process flow is shown in Fig. 3-4.

3.4 Determination of threshold voltage and mobility

The linear regime field effect mobility can be obtained by the calculation described below. At low V_D , I_D increases linearly with V_D (linear regime) and is approximately determined by the following equation:

$$I_D = \frac{W\mu_n C_{ox}}{2L} [2(V_G + V_T)V_D - V_D^2] \quad (3-1)$$

where L is the channel length, W is the channel width, C_{ox} is the capacitance per unit area of the insulating layer, V_T is the threshold voltage, and μ is the field effect mobility, which can be calculated in the linear regime from the transconductance,

$$G_m = \frac{\partial I_D}{\partial V_G} = \frac{Z}{L} \mu_n C_{ox} V_D \quad (3-2)$$

by plotting I_D versus V_G at a constant low V_D , with $-V_D \ll -(V_G - V_T)$, and equating the value of the slope of this plot to G_m , then find $G_{m,max}$ which can gain the value of threshold voltage (V_T) and linear mobility. For the known values included C_{ox} , V_T , and W/L , the value of saturation mobility can be obtained from equation (3-3)

$$I_D(sat) = \frac{W\mu_n C_{ox}}{2L} (V_G + V_T)^2 \quad (3-3)$$

3.5 Results and discussions

3.5.1 The influence of spin speed for OTFT

In our experiment, we try to test the different spin-speed of active layer P3HT and discuss their influence. There are three different spin-speed which 800, 1500, and 2000 rpm are used in our experiment. The other detail process will be not repeated in this section. The electrical characteristics of OTFT were measured immediately in atmospheric ambient by using an HP4156 semiconductor parameter analyzer. A typical plot of drain current I_D versus gate voltage V_G at various drain voltage V_D with the different spin-speed shown in Fig. 3-5. Gate voltage V_G was swept from 0 volt to -40 volt, and drain voltage V_D was -10 volt as a step volt from -20 volt to -50 volt over all our measurements. The plot will show absolute values of X-axis and Y-axis.

From the data of I_D - V_G , the values were taken into Eq. (3-1) ~ (3.3). The threshold voltage and mobility in the saturation region would be calculated. All values are shown in Table 3-2. In Table 3-2, threshold voltage increase with increasing spin-speed. But the field-effect mobility is not with increasing spin-speed, 1500 rpm has the largest field-effect mobility. This result may be due to the different evaporation rate of the chloroform. Additionally, the film thickness measured by SEM is shown in Fig. 3-7. It shows that thickness is 61nm, 49nm, and 24nm for 800 rpm, 1500 rpm, and 2000 rpm respectively. Different thickness of active layer P3HT results various electrical performance.

To summarize these electrical characteristics, we would adopt 1500 rpm as our optimal parameter. Plot of drain current I_D versus gate voltage V_D at various drain voltage V_G is also shown in Fig. 3-6 with the different spin-speed.

3.5.2 Electrical properties of APP surface treatment

Here we focus on the influence of APPT under different conditions which have different scanning times of APPT. They are one, two, four, eight scanning times respectively. We define that one time as APP 1, two times as APP 2 and so on. An absence of treatment is denoted APP 0.

As shown from Fig. 3-8 to Fig. 3-11, plot of drain current I_D versus gate voltage V_G at various drain voltage V_D and drain current I_D versus gate voltage V_D at various drain voltage V_G with different scanning times. In all figures of APP 0 to APP 8, we can observe that APP 4 has best electrical characteristic about I_D - V_G and I_D - V_D . Additionally, we plotted the comparison of I_D - V_G and I_D - V_D in the same figure due to observe clearly, they were shown in Fig. 3-12. The magnitude of saturation current at the same operated voltage shows that APP 4 > APP 8 > APP 2 > APP 1 > APP 0. Furthermore, threshold voltage and mobility would be calculated by Eq. (3-1) ~ (3-3). Arrangement of threshold voltage and mobility is shown in Table 3-3 (labeled as APP 0, APP 1, APP 2, APP 4, and APP 8) and Fig. 3-13. In Fig. 3-13, when dielectric layer was modified by the APP, it is clear that the threshold voltage reduction. This can prove that the dielectric layer / semiconductor interface really have improved. As for the device without surface treatment, the mobility in the saturation region and the threshold voltage of the OTFT are $1.9 \times 10^{-3} \text{ cm}^2/\text{Vs}$ and -21.7V , respectively. On the other hand, the values of field-induced current at the same gate voltage for

APP 4 has almost ten times higher than without treatment, as shown in Table 3-3 and Fig. 3-13. After surface treatment, threshold voltage reduce down to -8.3V and field-effect mobility ($\mu_{\text{sat}} = 2.6 \times 10^{-2} \text{cm}^2/\text{Vs}$) which is 15-fold improvement over the mobility on bare silicon oxide.

In order to further analyze the phenomenon about surface treatment of APPT, we used atomic force microscope (AFM) to observe the surface morphology. Contact angle was measured to judge the surface state. The contact angle and surface roughness of SiO_2 with different scanning times of APPT, as shown in Table 3-4. The bare SiO_2 surface is hydrophilic (contact angle $< 10^\circ$). After surface treatment of APPT, the surface of SiO_2 approach hydrophobic state. With increasing times of surface treatment, contact angle will present an increasing trend. When scanning times are more than four times, the increasing trend of contact angle will be flattened gradually, as shown in Fig. 3-14. In addition, Fig. 3-15 shows the trend of contact angle with increasing exposure time after surface treatment of APPT. It is found that the contact angle is not changed significantly for longer exposure time. It also reveals good stability for HMDS after APPT surface treatment. In the AFM photographs, the rms values of surface roughness increases with increasing scanning times of APPT. (Fig. 3-16) The rms value of surface roughness changes from 4.32 nm for APP 1 to 10.42 nm for APP 8. The surface roughness will become smooth after spin-coating P3HT, as shown in Table 3-4.

In general, most inorganic oxide surface including SiO_2 shows hydrophilic state while most of organic semiconductor (P3HT in this case) shows hydrophobic states. This mismatch has bad influence on crystalline formation of organic semiconductor fabricated on oxide substrates [55]. After surface

treatment of APPT, surface of SiO_2 becomes more hydrophobic, makes less dipolar and increases adhesion of organic semiconductor on substrate, which minimizes traps at the interface between insulator and organic semiconductor for better carries transportation. So it could affect good influence for increment of crystallinity and also increase field-effect mobility. We will further prove that in chapter 4. After surface treatment of APPT, surface of SiO_2 becomes more hydrophobic (increment of contact angle), as shown in Fig. 3-14. It obtains the improvement of field-effect mobility in our experiment. We observe the contact angle of APP 4 and APP 8 which are similar, but field-effect mobility of APP 8 is somewhat decay compared with APP 4. It is speculated that APP 8 is too rough to cause scattering effect [56]. In general, the surface roughness of the gate dielectric is an important parameter that influences the device performance and morphology of the deposited organic semiconductor film. Increased roughness leads to valleys in the channel region; these valleys can act as carrier traps and scattering sites. And a high surface roughness of the gate dielectric inhibits the growth of large and uniform crystal domains, and also affects the nucleation density of polycrystalline materials. Fig. 3-17 shows the comparison of surface roughness and mobility with different scanning times by APPT.

Detail photographs of contact angle and AFM under different conditions, as shown in Fig. 3-18 and Fig. 3-19.

3.5.3 The other methods of HMDS-treated SiO_2

As mentioned in previous section, we only emphasized on surface treatment of APPT. Here, we provide the other two methods of surface treatment which were spin-coating HMDS and evaporated HMDS. Many researches about

spin-coating HMDS could be refer to [55,57]. We will compare the difference about the three methods, and discuss the relationship of them. As shown in Fig. 3-20 and Fig. 3-21, plot of drain current I_D versus gate voltage V_G at various drain voltage V_D and drain current I_D versus gate voltage V_D at various drain voltage V_G . Fig. 3-20 shows the relationship of I-V about spin-coating HMDS, and Fig. 3-21 shows the relationship of I-V about evaporated HMDS. The same calculation for threshold voltage and mobility in saturation region is listed in Table 3-5 (labeled as No treatment, Spin-coating, Evaporation, and APP 4).

Additional measured values such as contact angle and surface roughness are also shown in Table 3-5. The two methods have obvious improvement in our experiment. The mobility in the saturation region was 4-fold for spin-coating HMDS ($\mu_{\text{sat}} = 7.8 \times 10^{-3} \text{ cm}^2/\text{Vs}$) and 11-fold for evaporated HMDS ($\mu_{\text{sat}} = 2.2 \times 10^{-2} \text{ cm}^2/\text{Vs}$) higher than no treatment ($\mu_{\text{sat}} = 1.9 \times 10^{-3} \text{ cm}^2/\text{Vs}$). In Table 3-5, for HMDS-treated SiO_2 has larger contact angle certainly, hence HMDS play an important role in the interface between SiO_2 and P3HT. Threshold voltage also decreases after HMDS-treated SiO_2 referred to [55]. Comparison of field-effect mobility and threshold voltage is shown in Fig. 3-22. The plot of measured contact angle for spin-coating and evaporation is shown Fig. 3-23, and Fig. 3-24 shows the AFM photography. Surface of SiO_2 remains smooth after spin-coating and evaporated HMDS. Comparison of I_D - V_G and I_D - V_D is shown in Fig. 3-25. The magnitude of saturation current at the same operated voltage shows that APP4 > Evaporation > Spin-coating > No treatment. So APPT is still better than the other methods of HMDS-treated SiO_2 in our experiment. This may be since the APP uses chemical bonds to stack material on the SiO_2 surface, the structure of the HMDS film becomes denser, so it becomes more hydrophobic at the same deposited thickness [58], improving the performance of the OTFTs. However,

APP treatment increases the roughness of the surface, increasing the scattering effect [56]. Therefore, although its contact angle is 15° higher than that obtained by evaporation, the mobility of the carrier is about 18.2% higher (Fig. 3-26 and Fig. 3-27).

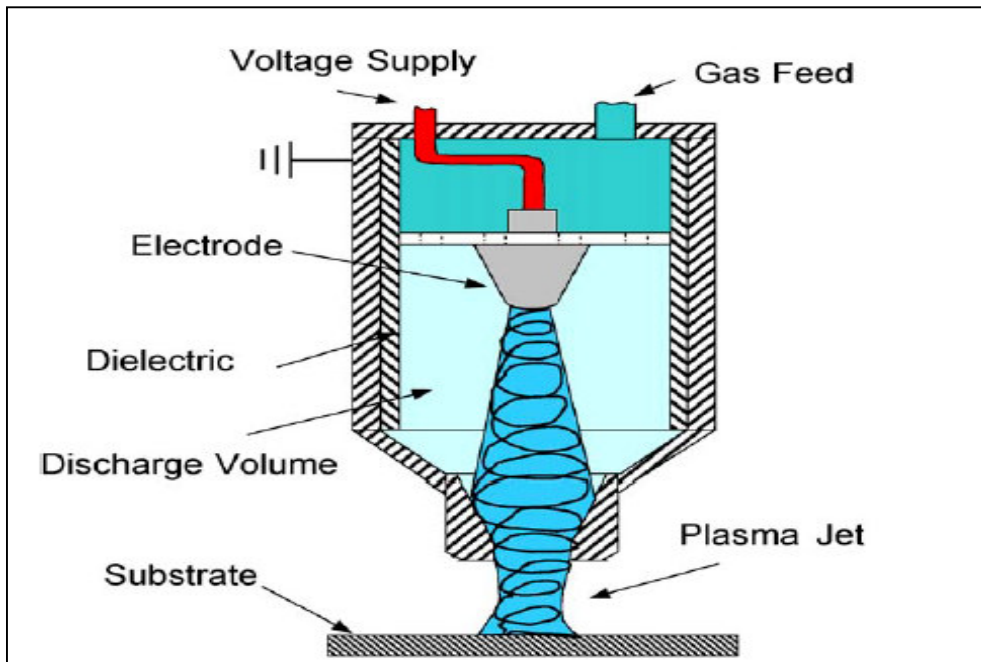
As mentioned above, there are two major factors to improve the interface of dielectric, one is “hydrophobic” and the other is “surface roughness”. Comparison of contact angle *vs.* mobility, contact angle *vs.* roughness, and roughness *vs.* mobility with different methods of surface treatment and different scanning times by APPT are shown in Fig. 3-28 ~ Fig. 3-30. But why these factors will affect the electrical properties of OTFTs. We speculate that the P3HT molecular chain exhibits a better lattice arrangement. And we will discuss this speculation in the next chapter.



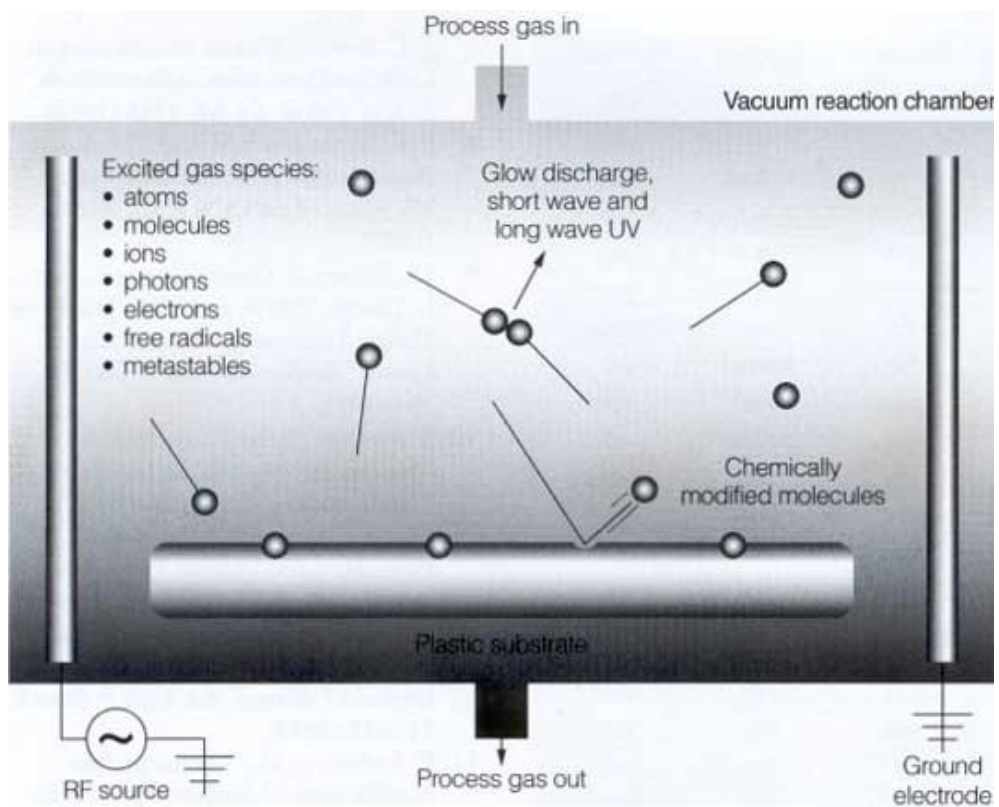
Table 3-1: The types of atmospheric pressure plasma.

	Type	Frequency	Breakdown voltage (Kv)	Plasma Density
A P P	Corona	20-40 kHz	10-50	$10^9 - 10^{13}$
	DBD (APGD)	20-30 kHz	5-25	$10^{12} - 10^{15}$
	Plasma Jet	50Hz~13.56 MHz	5-10	$10^{11} - 10^{12}$
	Plasma torch	13.56 MHz	10-50	$10^{16} - 10^{19}$



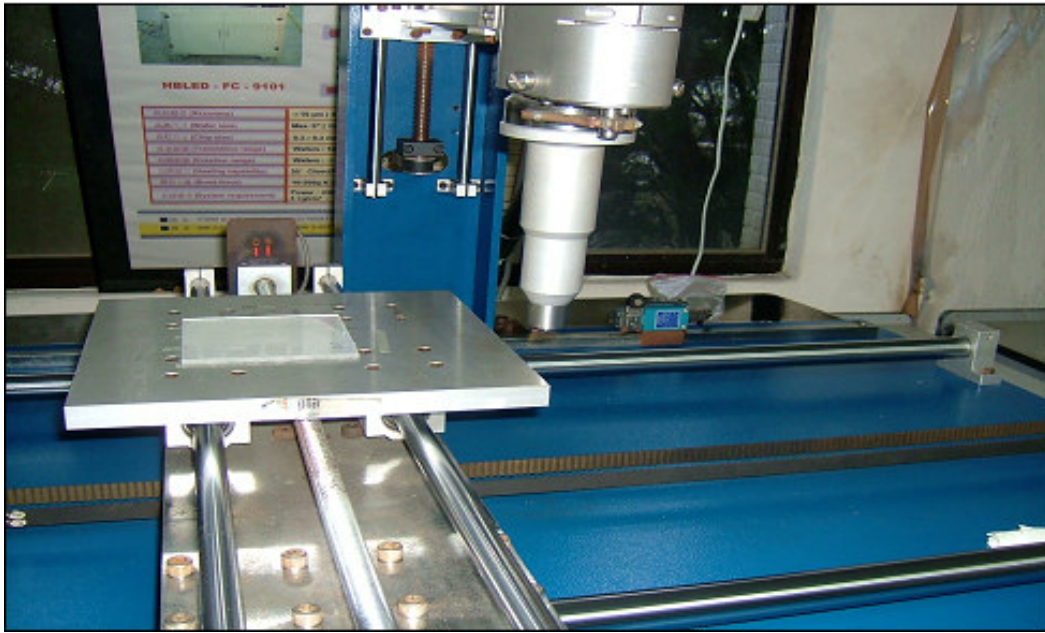


(a)



(b)

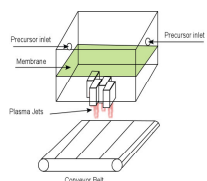
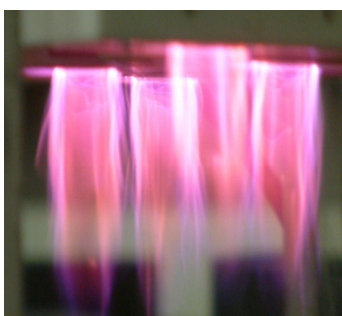
Figure 3-1: (a) The structure of APPT, (b) The diagram of plasma surface treatment.



(a)



Multiple Plasma Jet System

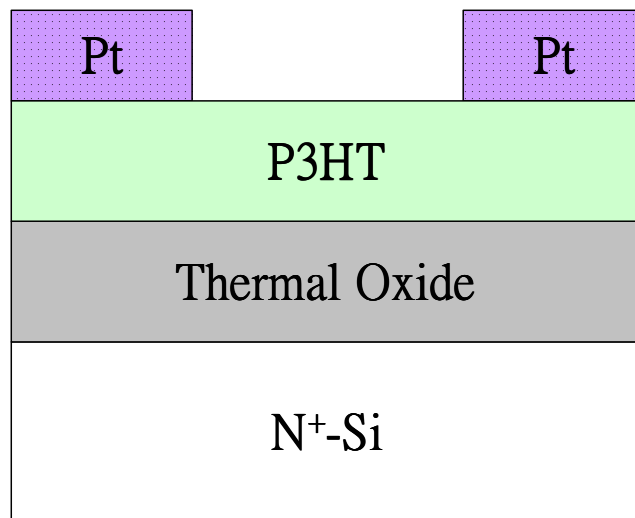
- Scale-up of single jet for 3-D atmospheric coating



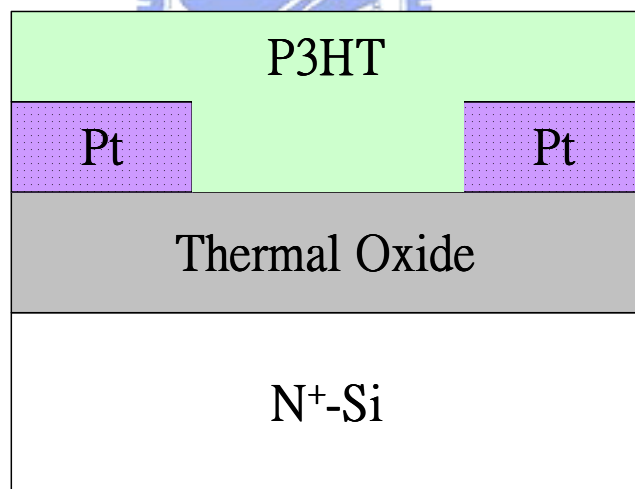
Handheld Plasma Applicator

(b)

Figure 3-2: (a) APP system of ITRI, (b) APP systems show the cold temperature.



TC



BC

Figure 3-3: Two basic structures of OTFT.

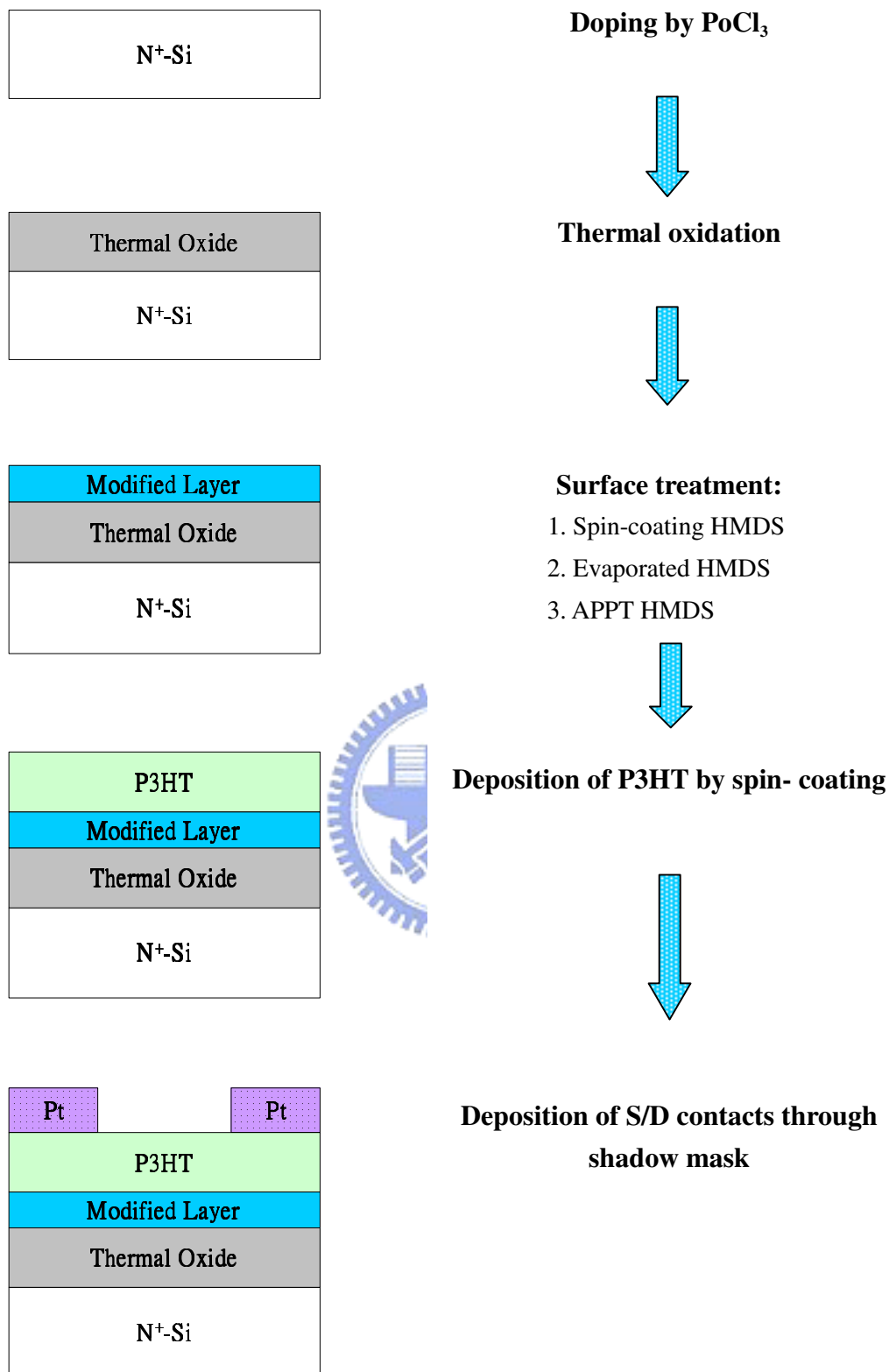
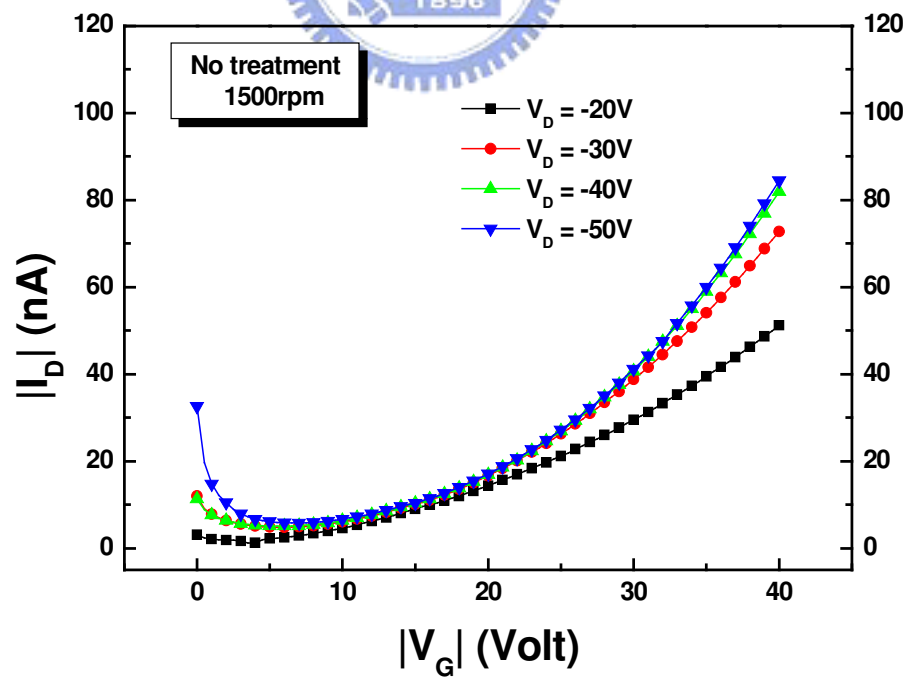
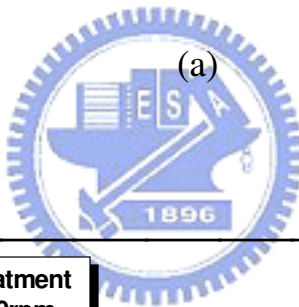
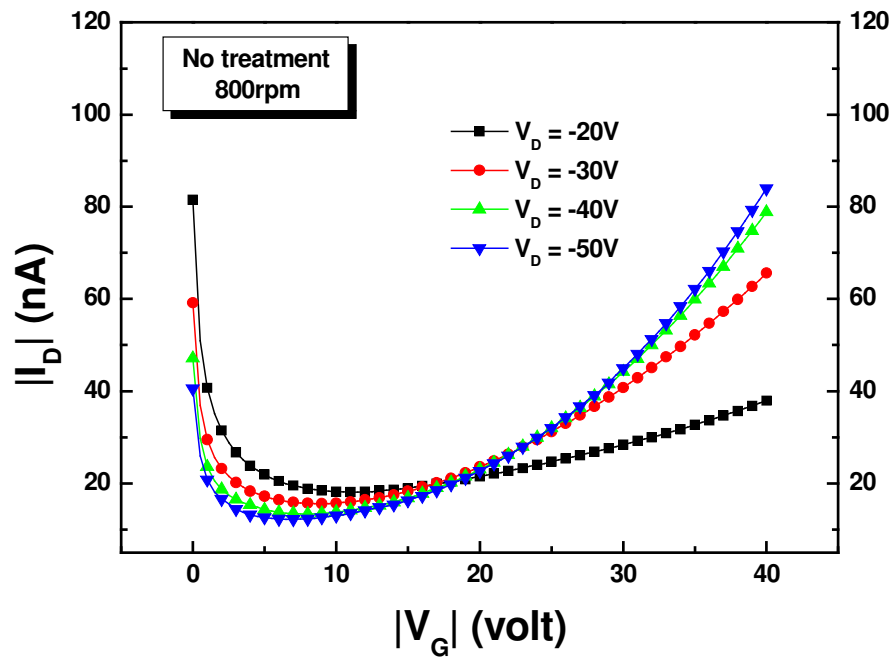


Figure 3-4: Process flow of top-contact OTFT.



(b)

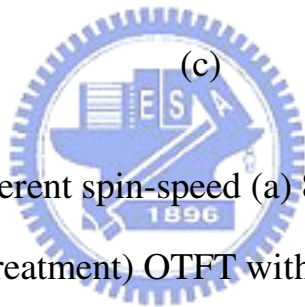
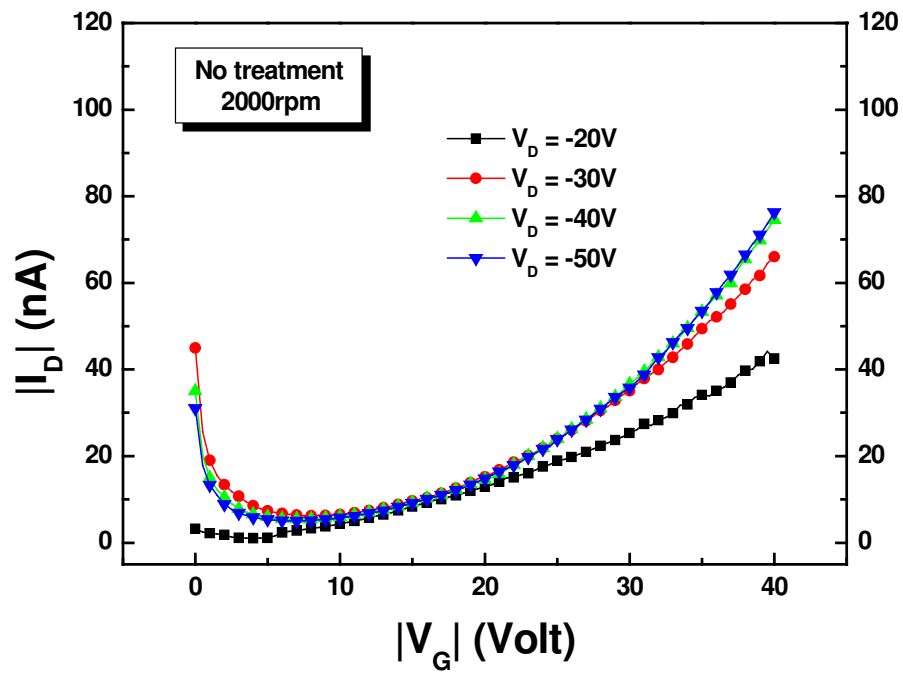
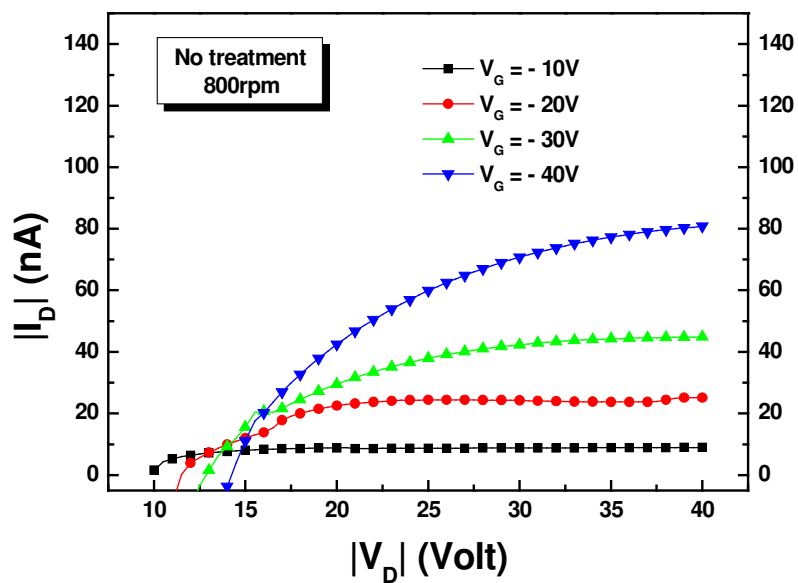
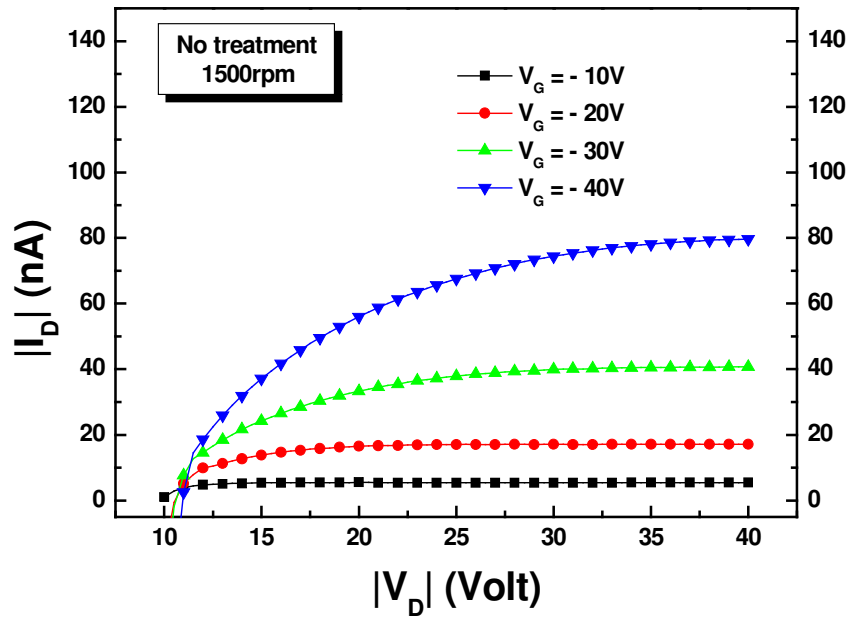


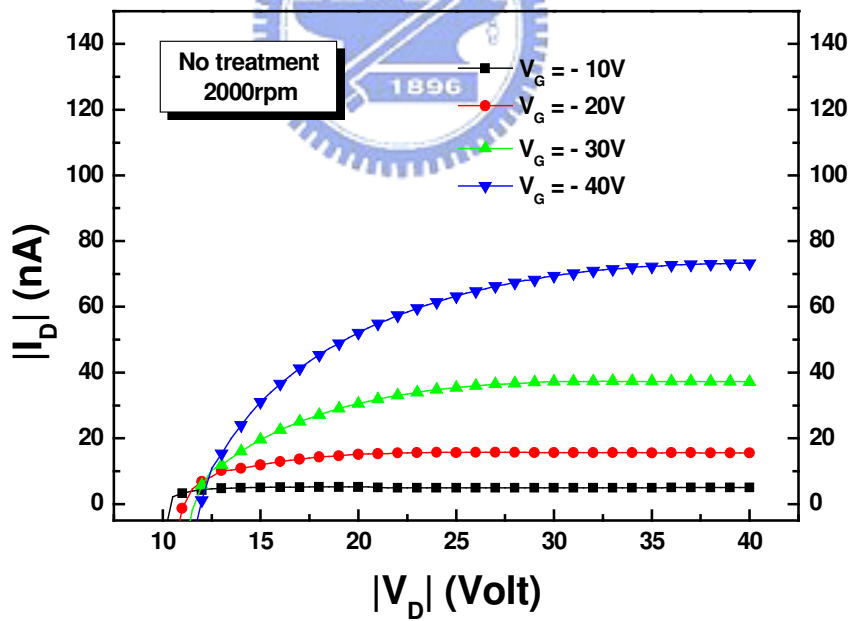
Figure 3-5: I_D - V_G for different spin-speed (a) 800 rpm, (b) 1500 rpm, (c) 2000 rpm. (All are no treatment) OTFT with $W/L = 2000 \text{ um}/500 \text{ um}$.



(a)



(b)

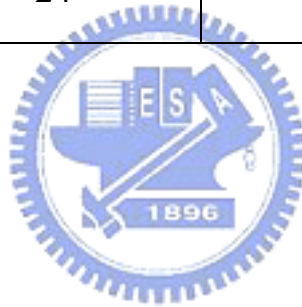


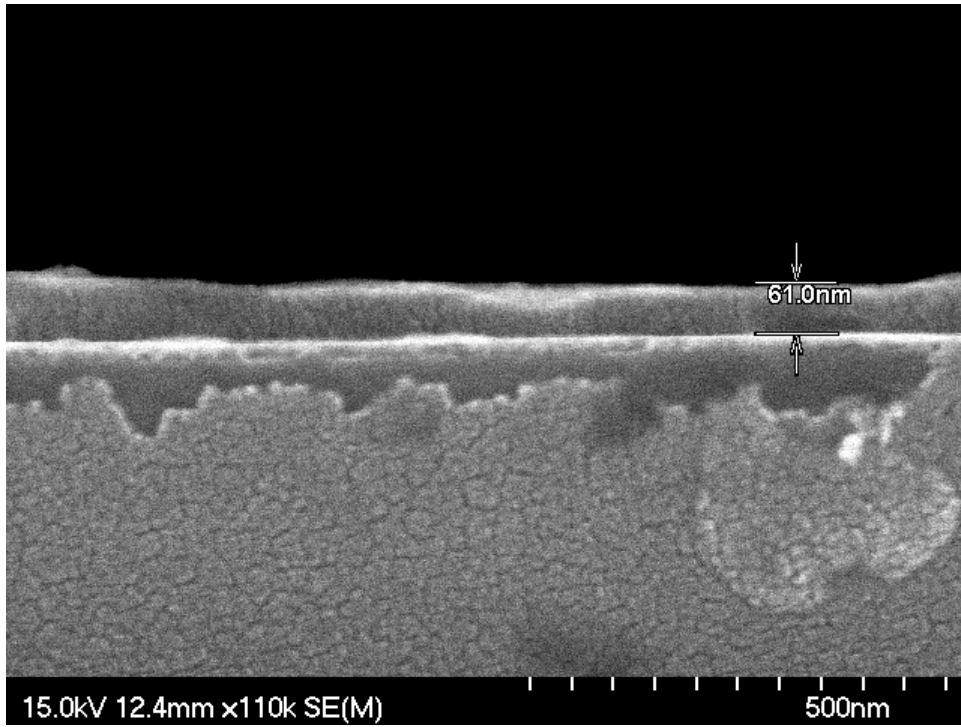
(c)

Figure 3-6: I_D - V_D for different spin-speed (a) 800 rpm, (b) 1500 rpm, (c) 2000 rpm. (All are no treatment) OTFT with $W/L = 2000 \text{ um}/500 \text{ um}$.

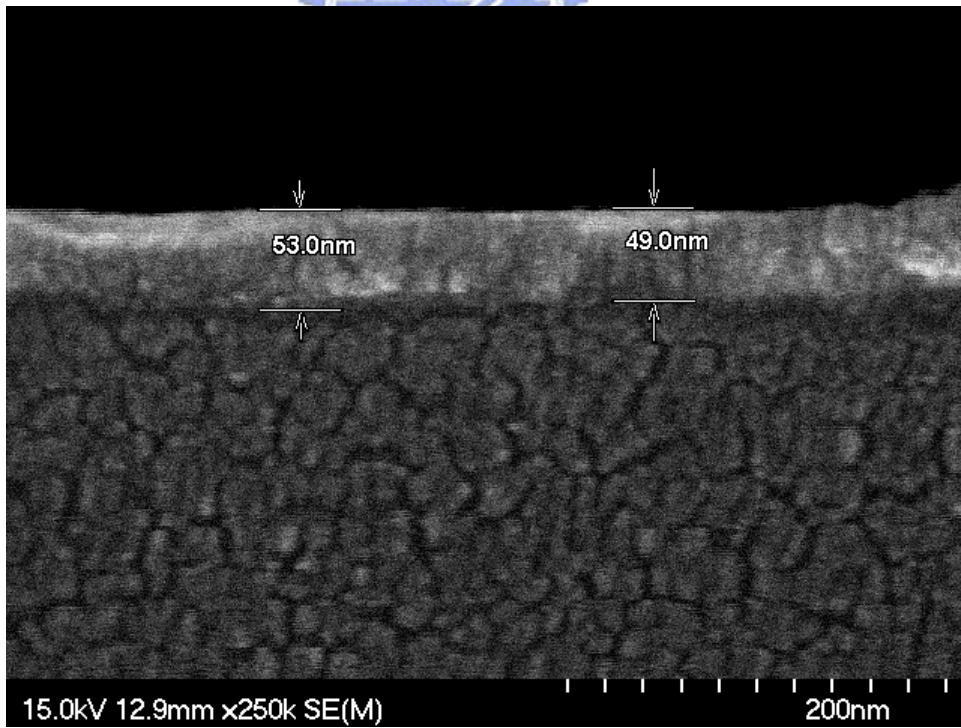
Table 3-2: Threshold voltage, saturation mobility, and on/off ratio at different spin-speed. (Surface no treatment)

Spin-speed (rpm)	Thickness (nm)	V_{th} (Volt)	u_{sat} (cm^2/Vs)
800	61	-16.97	1.518×10^{-3}
1500	49	-21.7	1.870×10^{-3}
2000	24	-25.64	7.690×10^{-4}

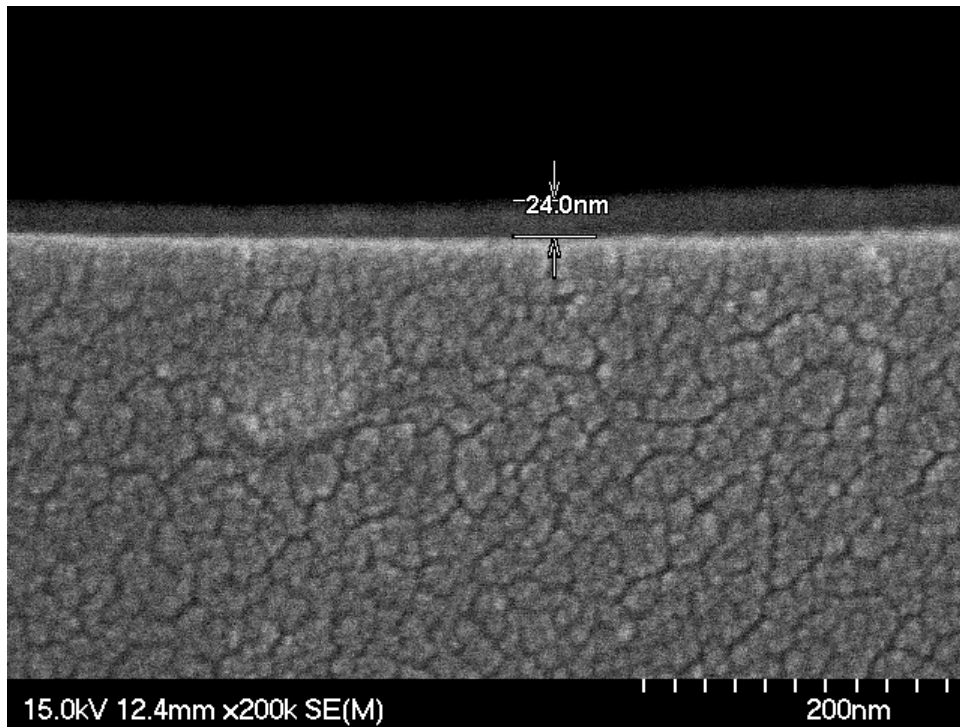




(a)

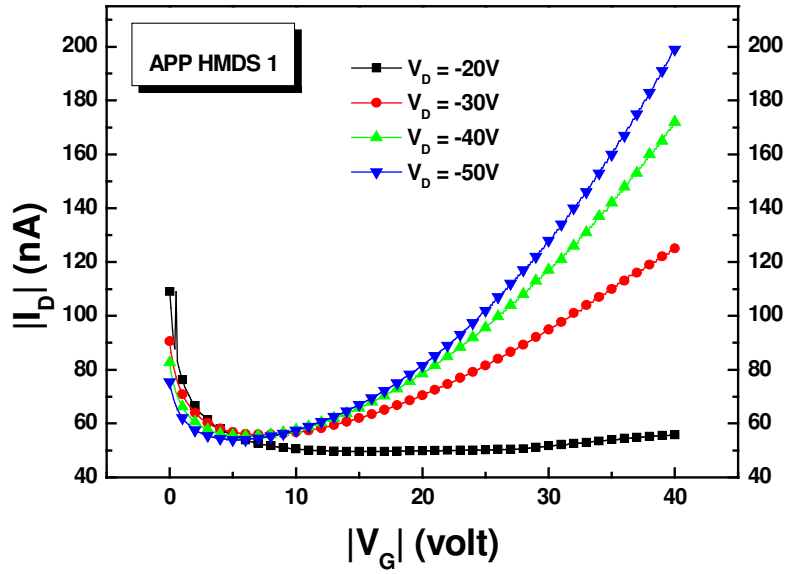


(b)

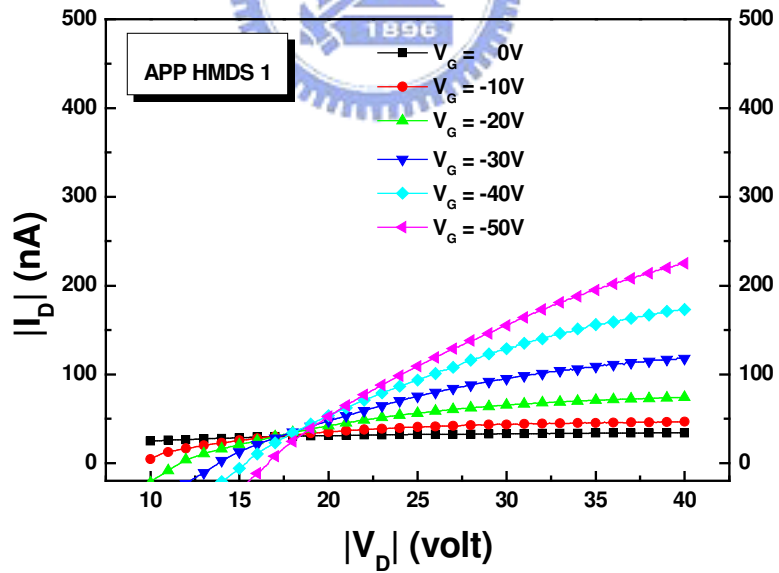


(c)

Figure 3-7: SEM photo: cross-section view of test sample (upper layer is P3HT) made at spin-speed (a) 800 rpm, (b) 1500 rpm, (c) 2000 rpm.

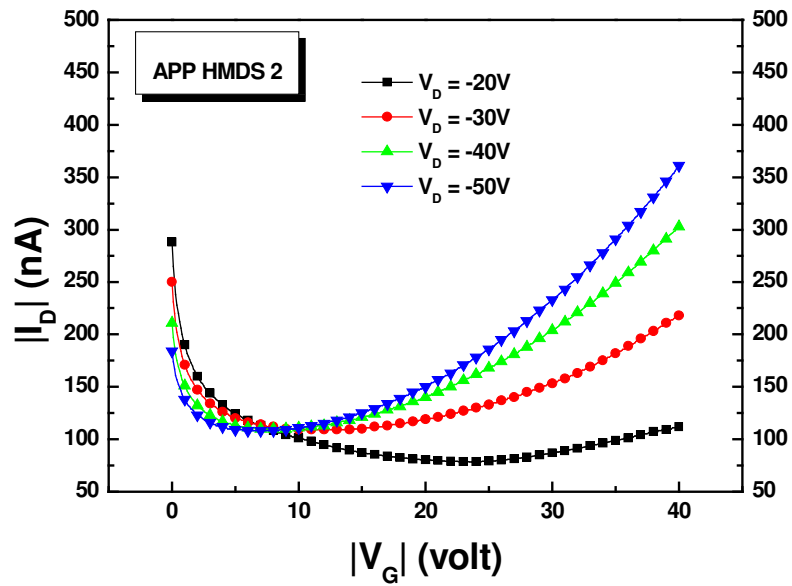


(a)

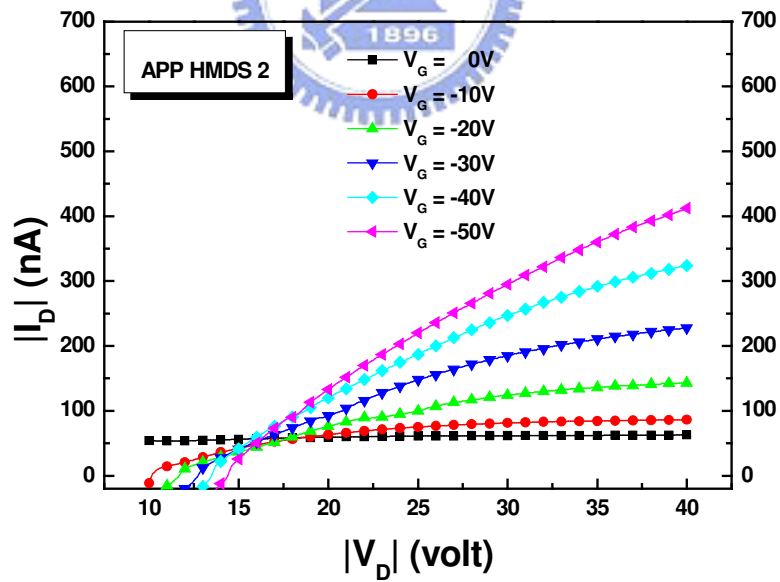


(b)

Figure 3-8: Surface treatment of APPT HMDS 1 for OTFT (a) I_D - V_G curve, (b) I_D - V_D curve ($W/L = 2000 \text{ um}/500 \text{ um}$)

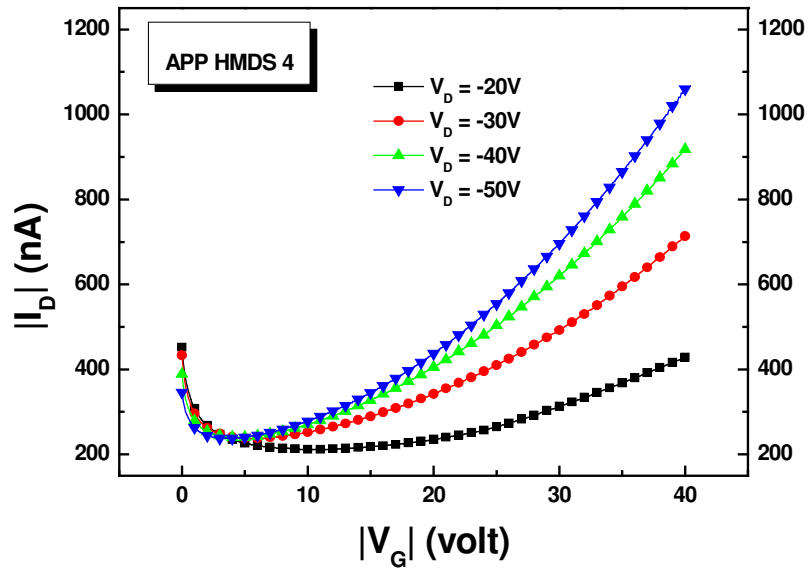


(a)

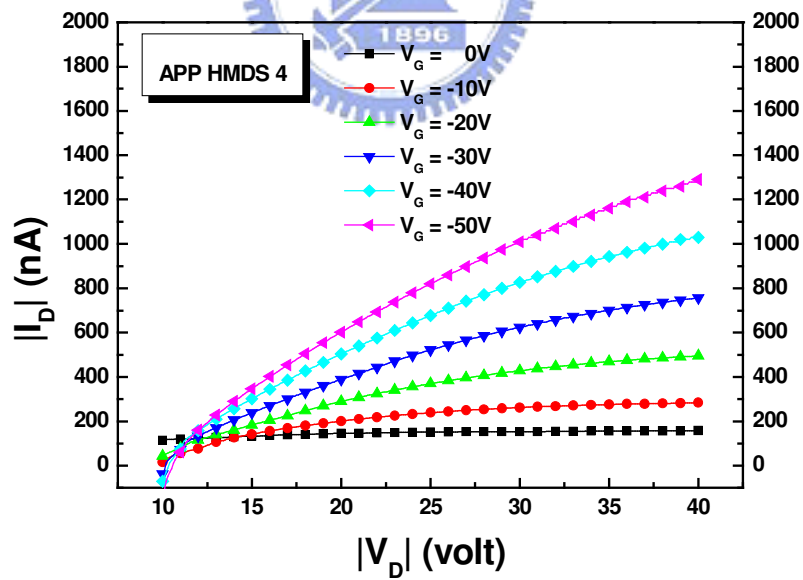


(b)

Figure 3-9: Surface treatment of APPT HMDS 2 for OTFT (a) I_D - V_G curve, (b) I_D - V_D curve ($W/L = 2000 \text{ um}/500 \text{ um}$)

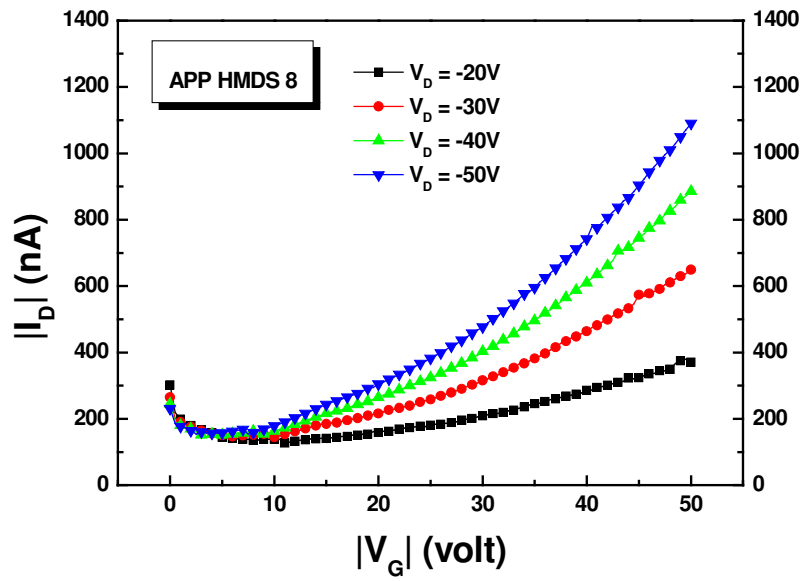


(a)

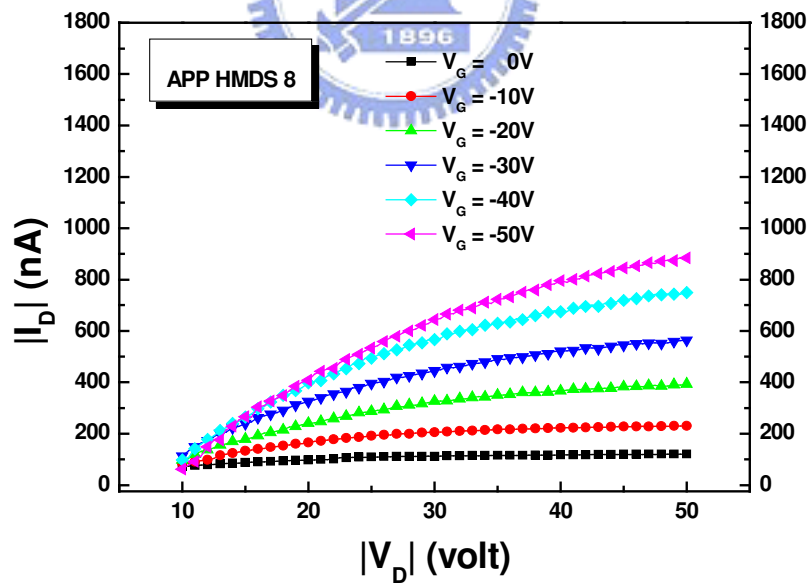


(b)

Figure 3-10: Surface treatment of APPT HMDS 4 for OTFT (a) I_D - V_G curve, (b) I_D - V_D curve ($W/L = 2000 \text{ um}/500 \text{ um}$)

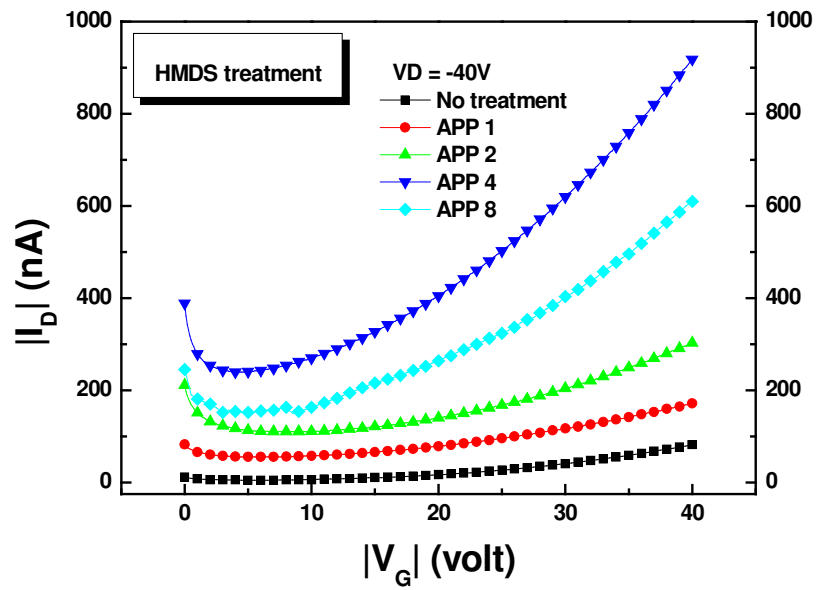


(a)

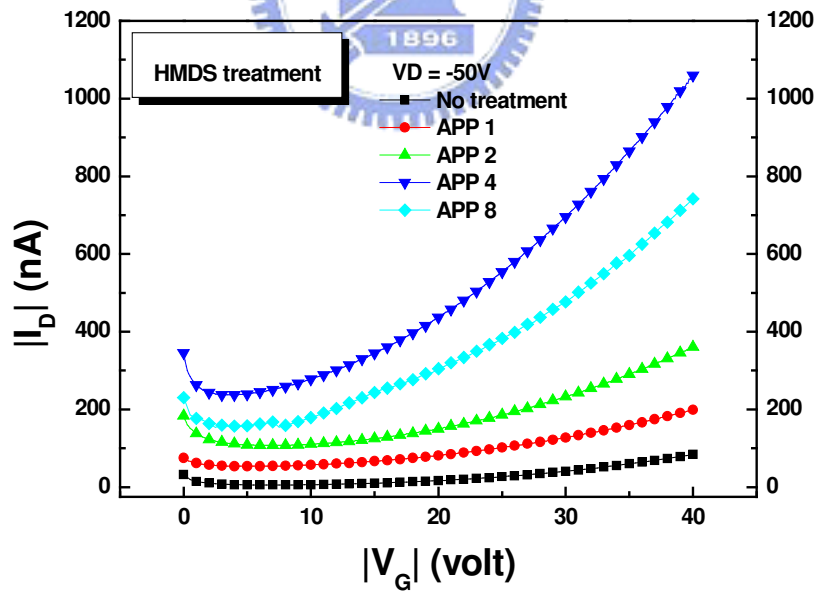


(b)

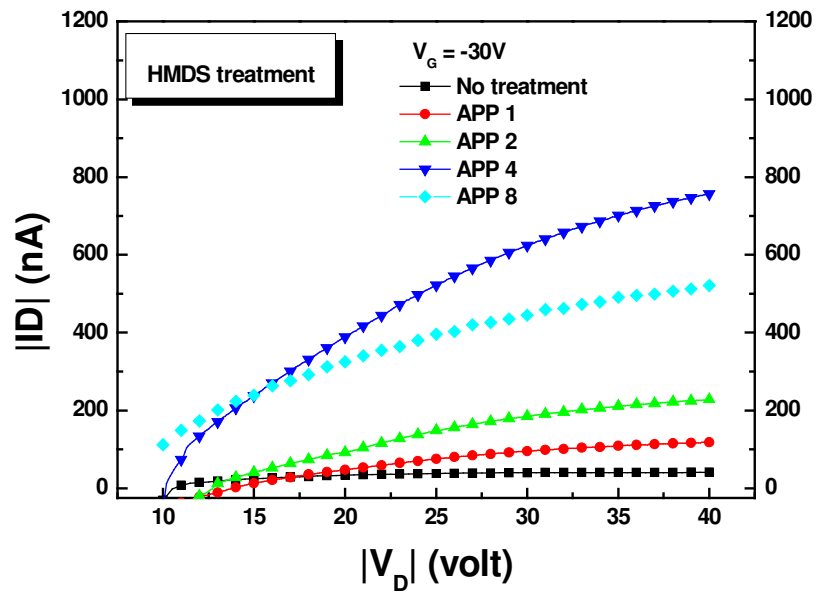
Figure 3-11: Surface treatment of APPT HMDS 8 for OTFT (a) I_D - V_G curve, (b) I_D - V_D curve ($W/L = 2000 \text{ um}/500 \text{ um}$)



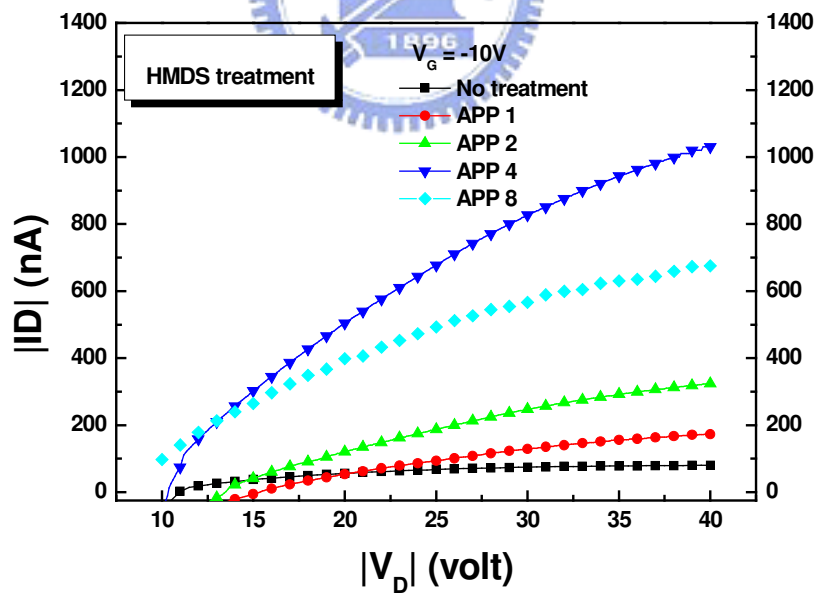
(a)



(b)



(c)



(d)

Figure 3-12: The comparison of (a), (b) I_D - V_G and (c), (d) I_D - V_D with different scanning times by APPT.

Table 3-3: Electrical parameters of the OTFTs in this study.

Surface treatment	Mobility μ_{lin} (cm^2/Vs)	Mobility μ_{sat} (cm^2/Vs)	Threshold voltage V_{th} (V)
No treatment	1.2×10^{-3}	1.9×10^{-3}	-21.7
APP 1	3.5×10^{-3}	4.3×10^{-3}	-5.3
APP 2	4.2×10^{-3}	8.0×10^{-3}	-7.8
APP 4	1.7×10^{-2}	2.6×10^{-2}	-8.3
APP 8	1.3×10^{-2}	2.0×10^{-2}	-7.7

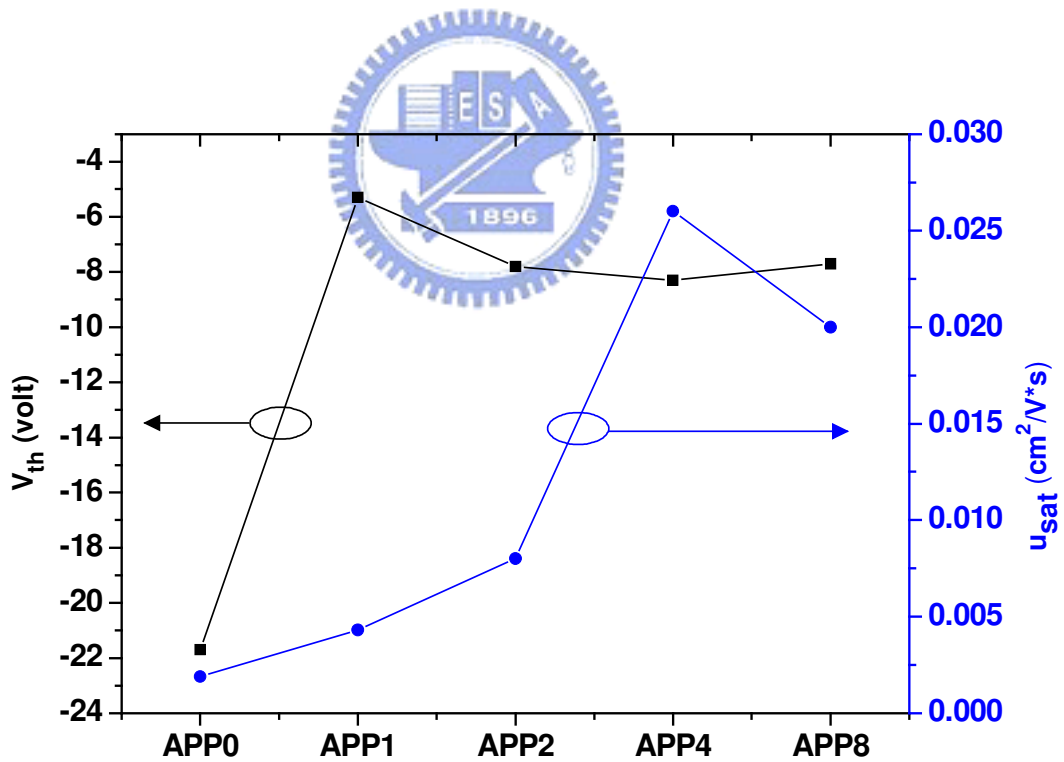


Figure 3-13: Comparison of threshold voltage and saturation mobility with different scanning times by APPT.

Table 3-4: Comparison of contact angle and surface roughness with different scanning times by APPT.

Surface treatment	Contact angle	Surface roughness (nm)	P3HT surface roughness (nm)
No treatment	< 10°	1.58	1.32
APPT-HMDS-1	68.9°	4.32	2.42
APPT-HMDS-2	76.3°	4.47	2.56
APPT-HMDS-4	90.5°	6.07	3.73
APPT-HMDS-8	90.9°	10.42	4.26

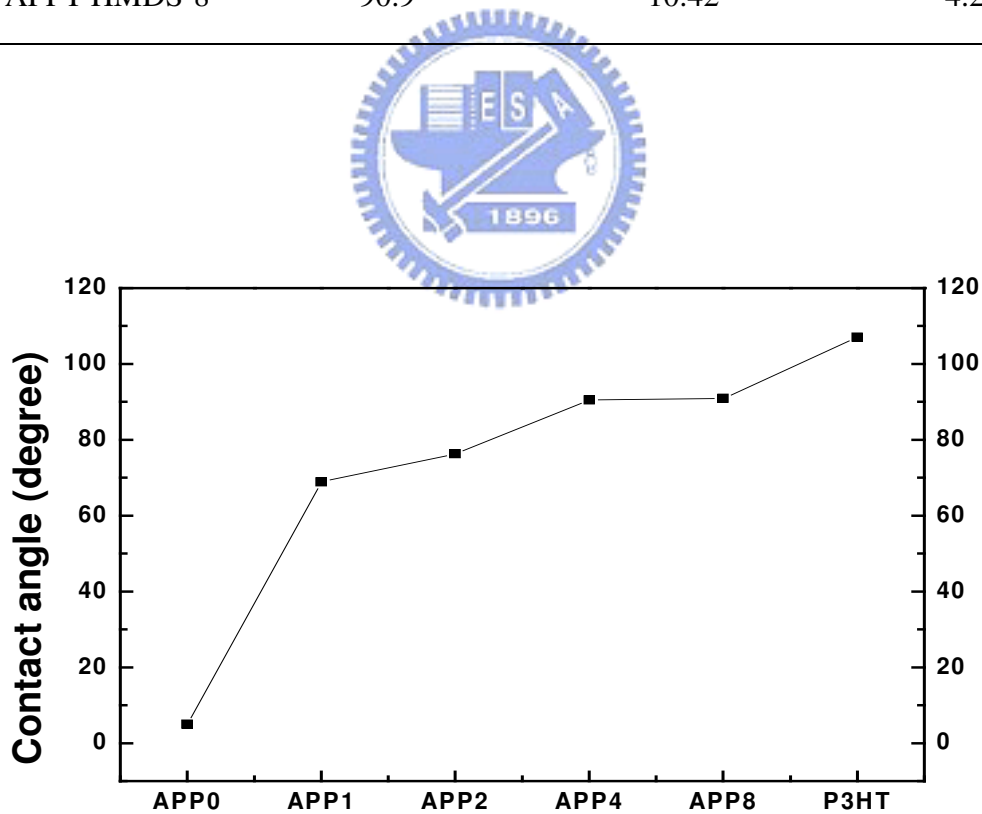


Figure 3-14: Contact angle vs. different scanning times by APPT.

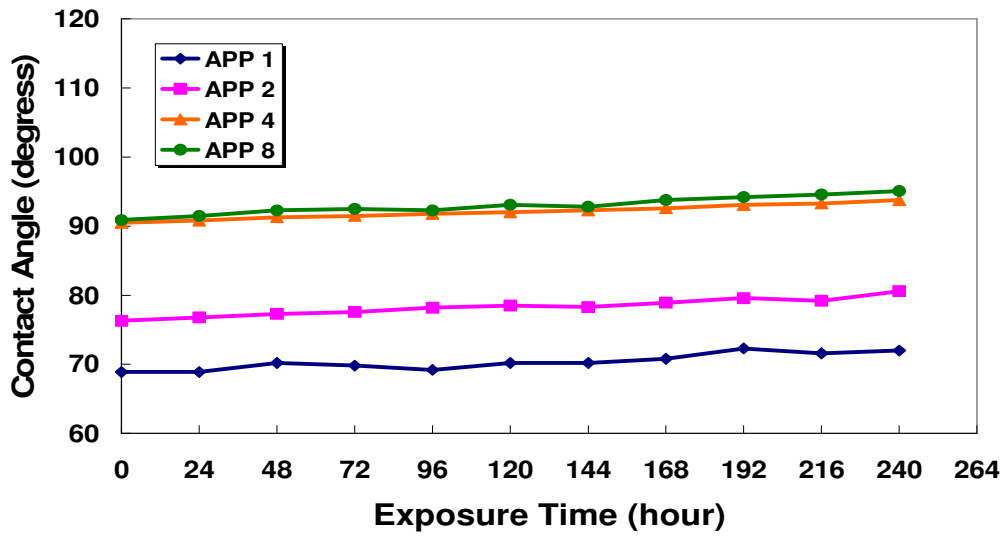


Figure 3-15: Contact angle vs. exposure time for dielectric layer with different scanning times by APPT.

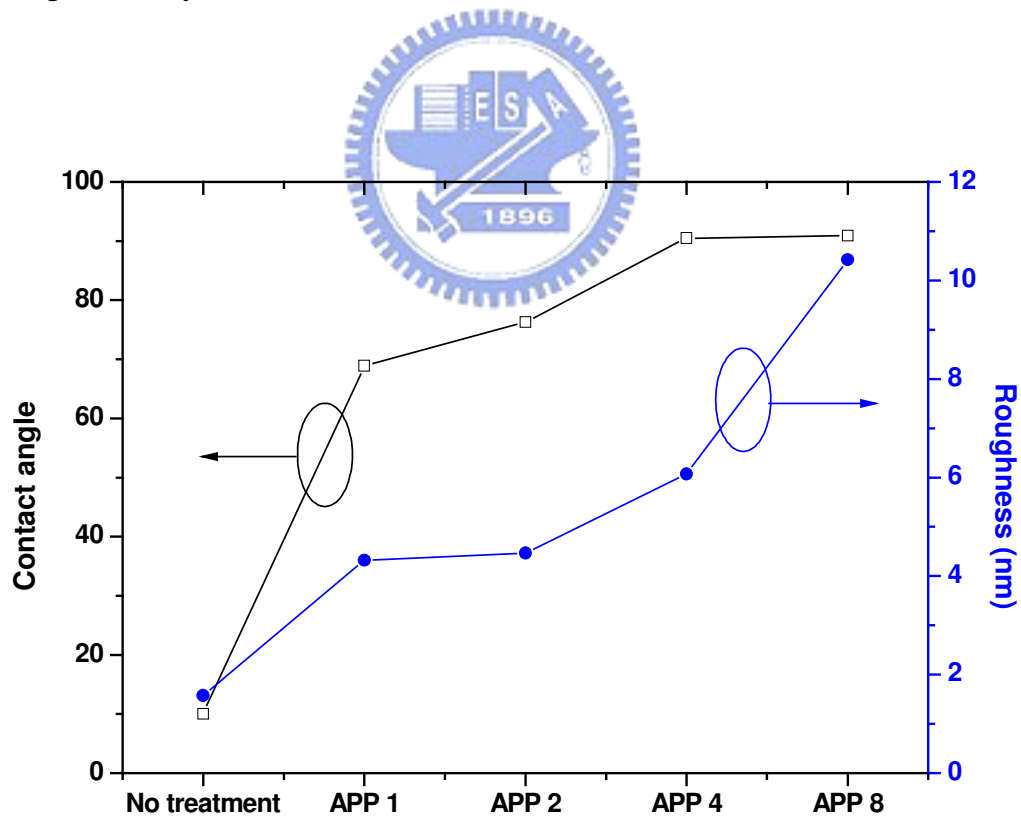


Figure 3-16: Comparison of contact angle and surface roughness with different scanning times by APPT.

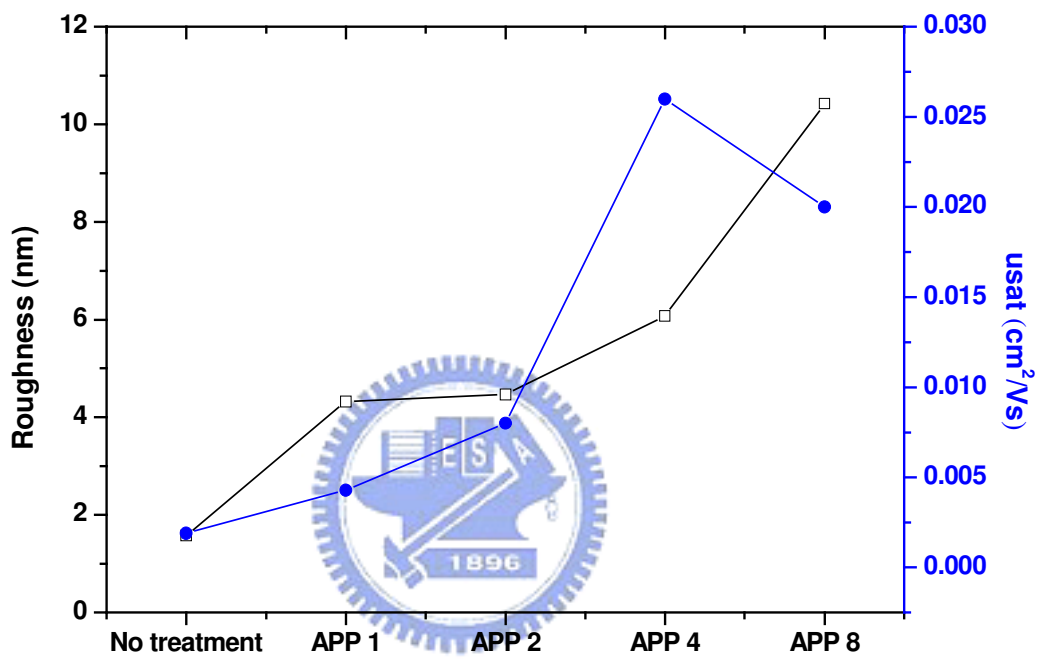
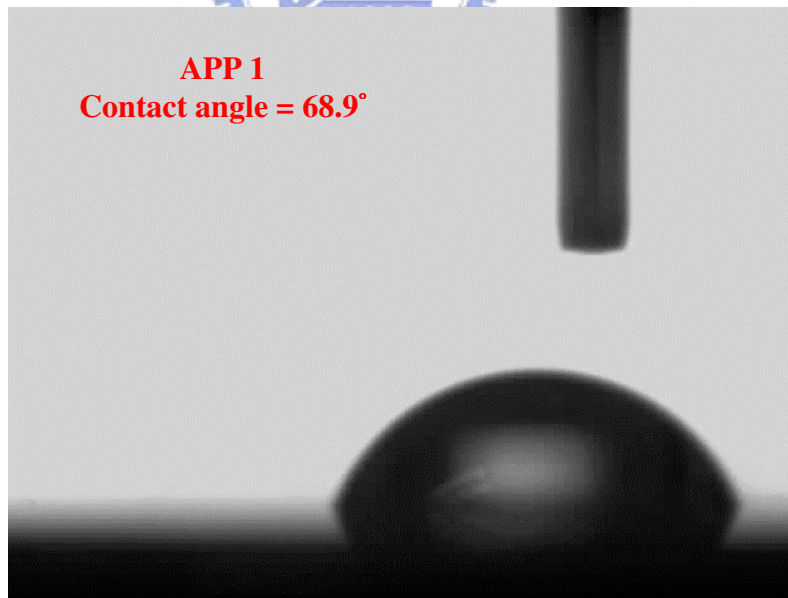
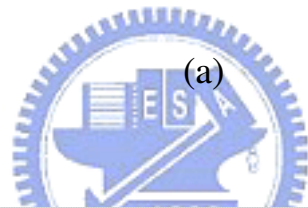
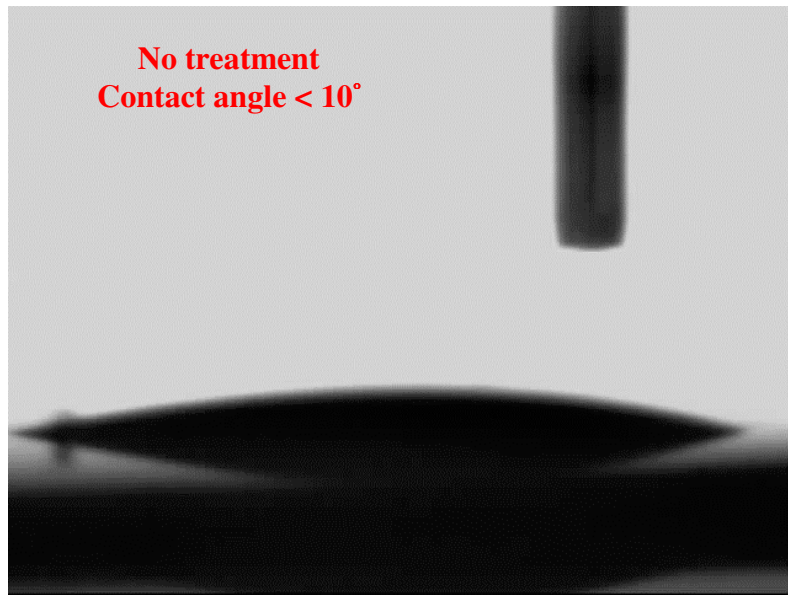
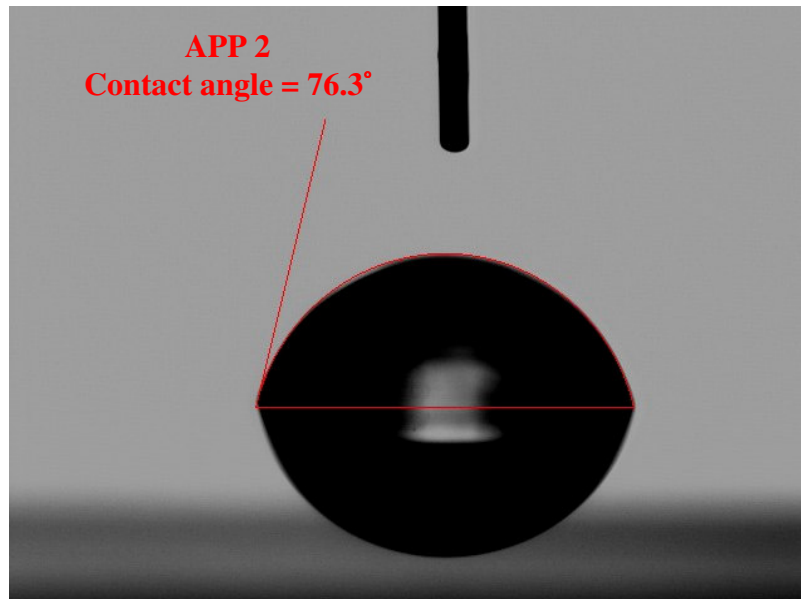


Figure 3-17: Comparison of surface roughness and mobility with different scanning times by APPT.



(b)



(d)

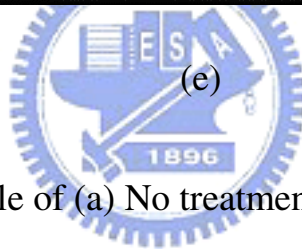
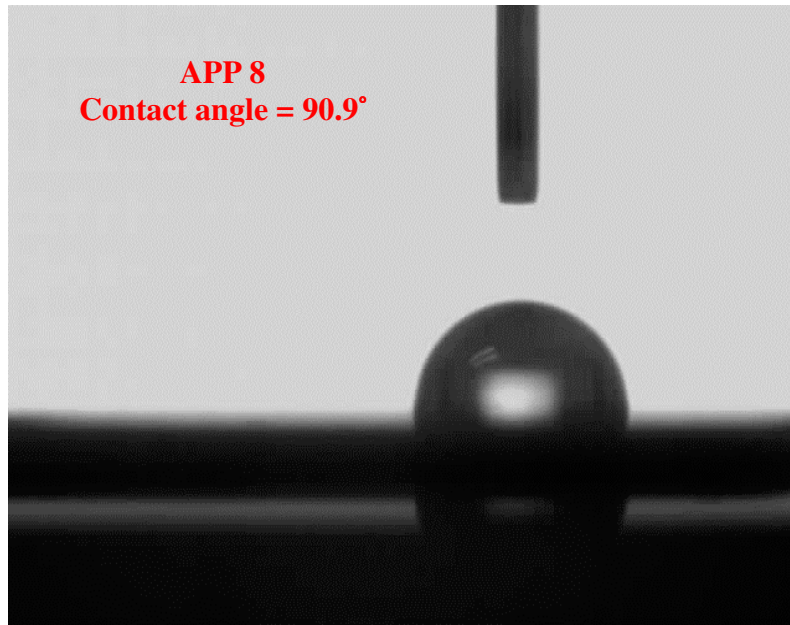
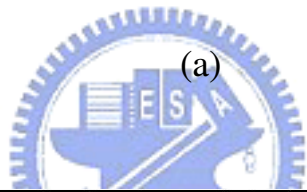
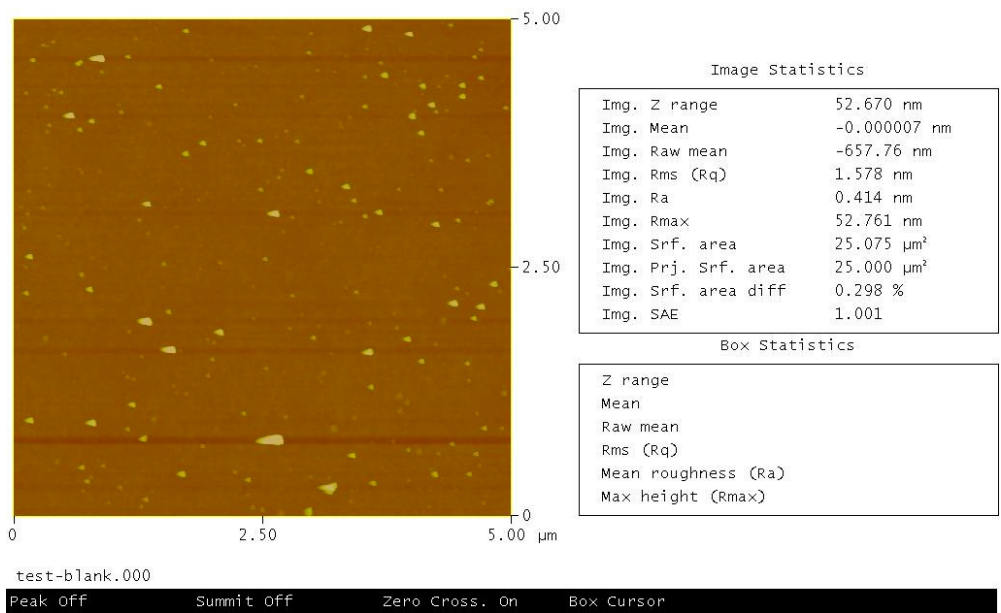


Figure 3-18: Contact angle of (a) No treatment ($<10^\circ$), (b) APP 1(68.9°), (c) APP 2 (76.3°), (d) APP 4 (90.5°), (e) APP 8 (90.9°).

Peak Surface Area Summit Zero Crossing Stopband Execute Cursor

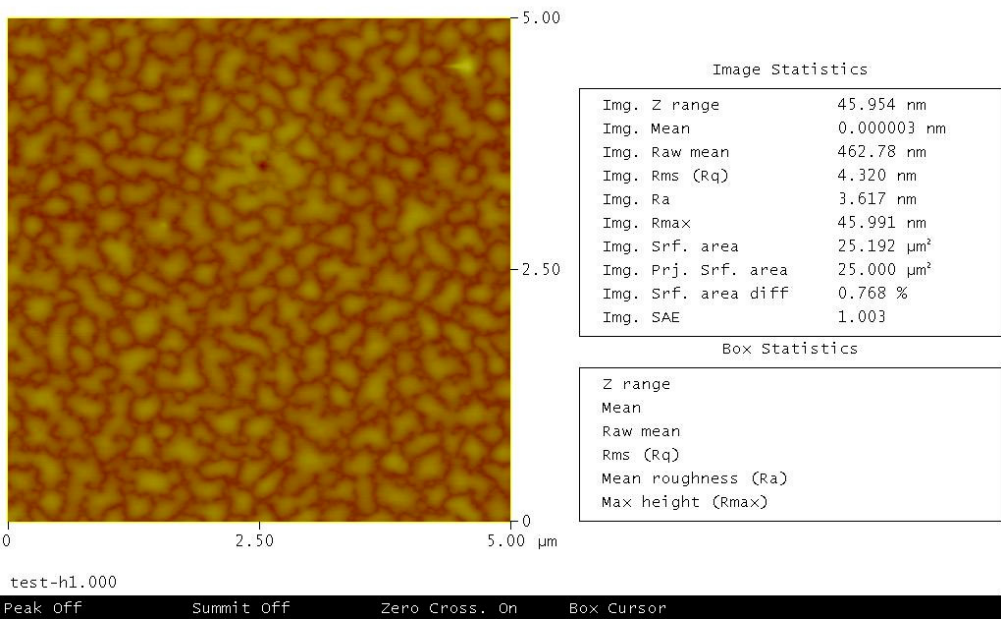
Roughness Analysis



(a)

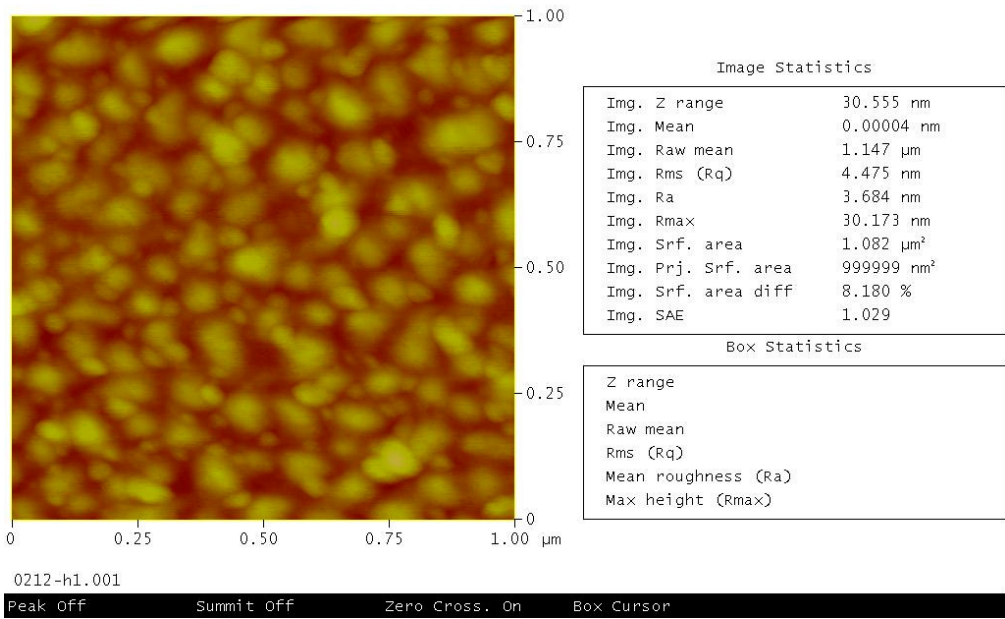
Peak Surface Area Summit Zero Crossing Stopband Execute Cursor

Roughness Analysis

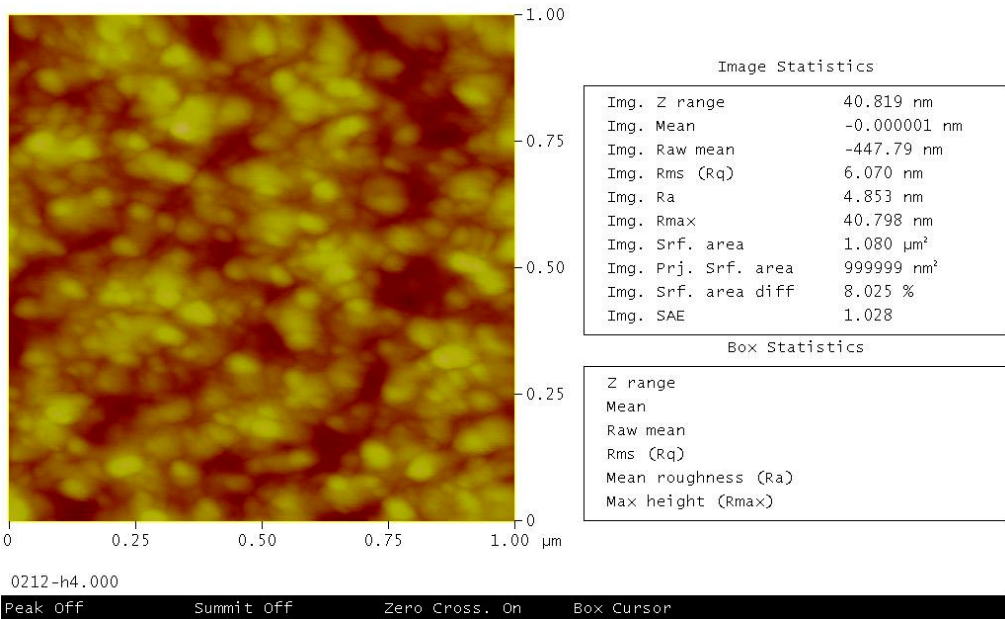


(b)

Roughness Analysis



Roughness Analysis



(d)

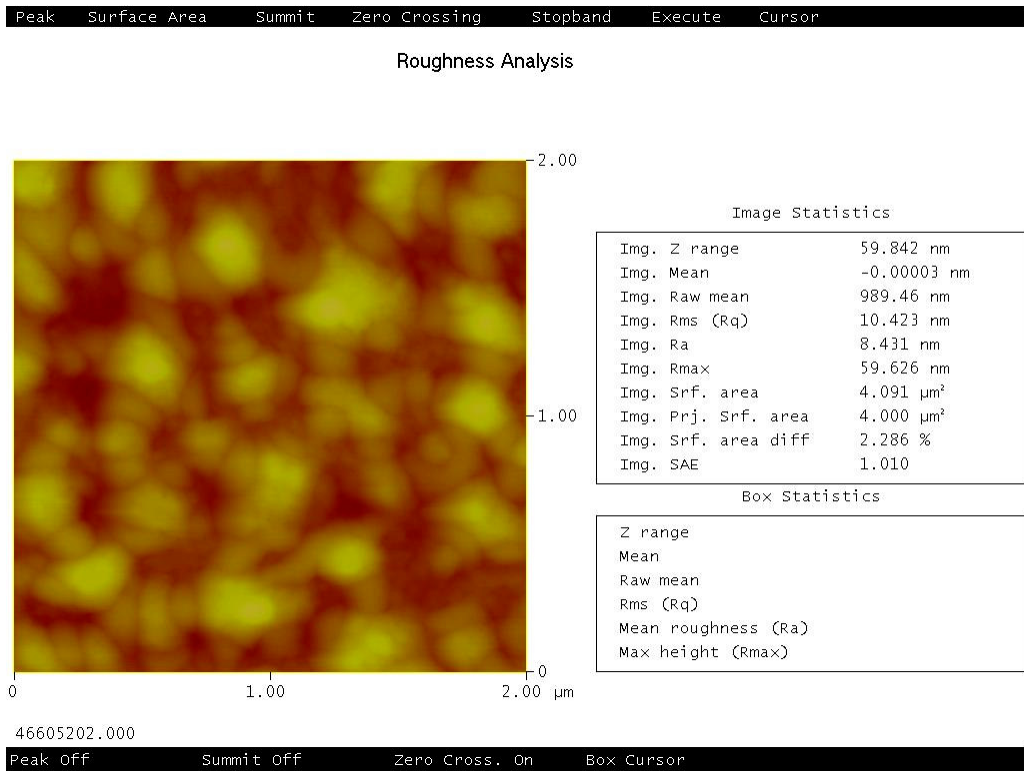
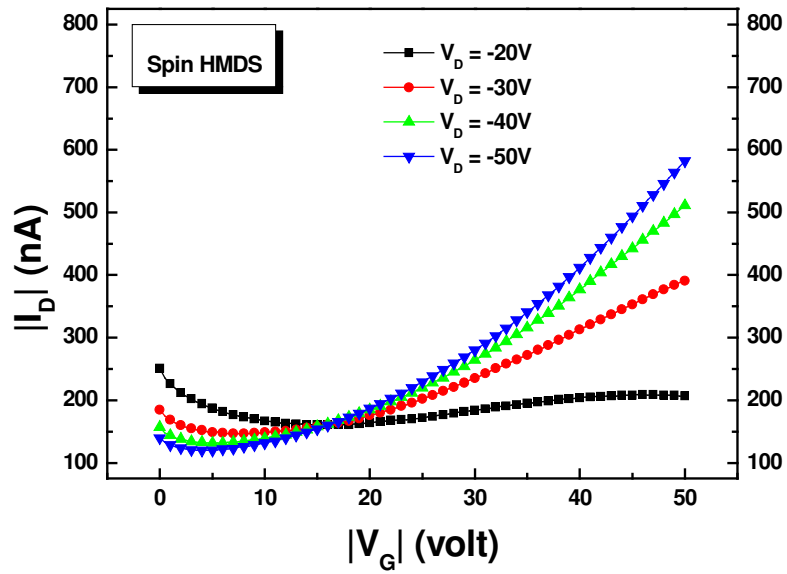
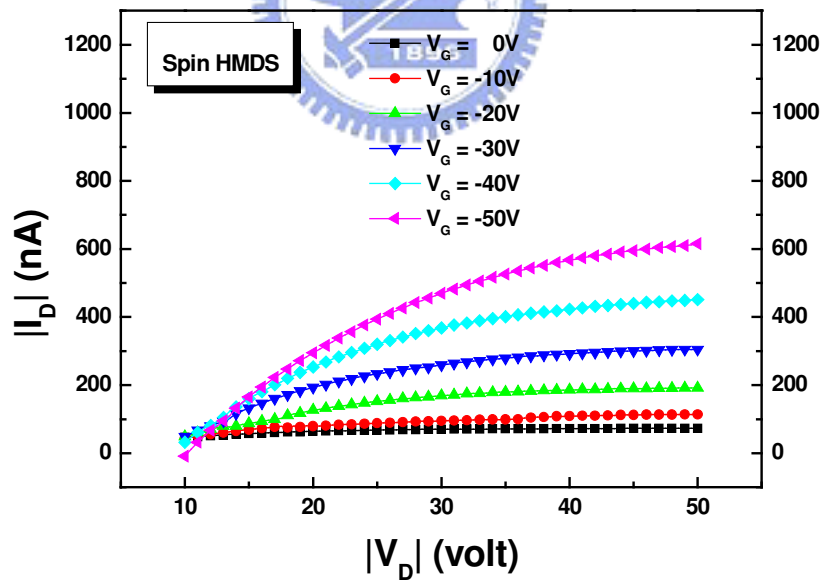


Figure 3-19: AFM photographs of (a) No treatment, (b) APP 1, (c) APP 2, (d) APP 4, (e) APP 8.



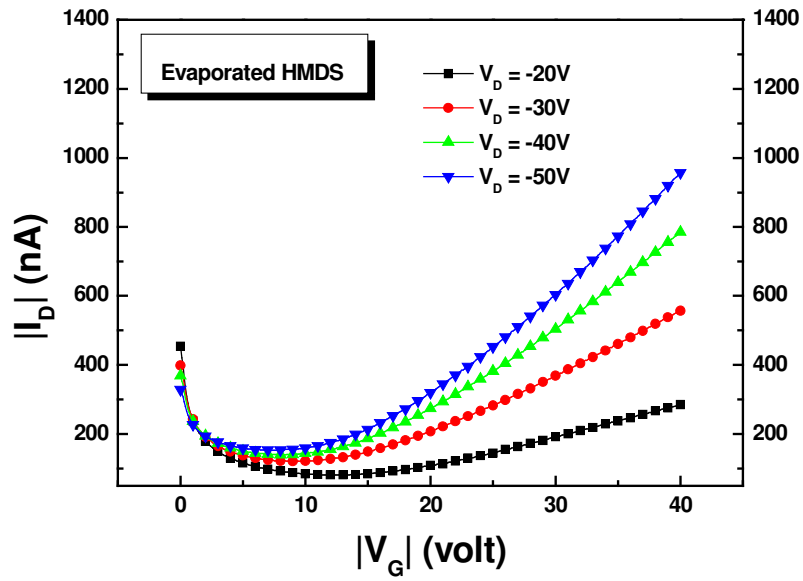
(a)



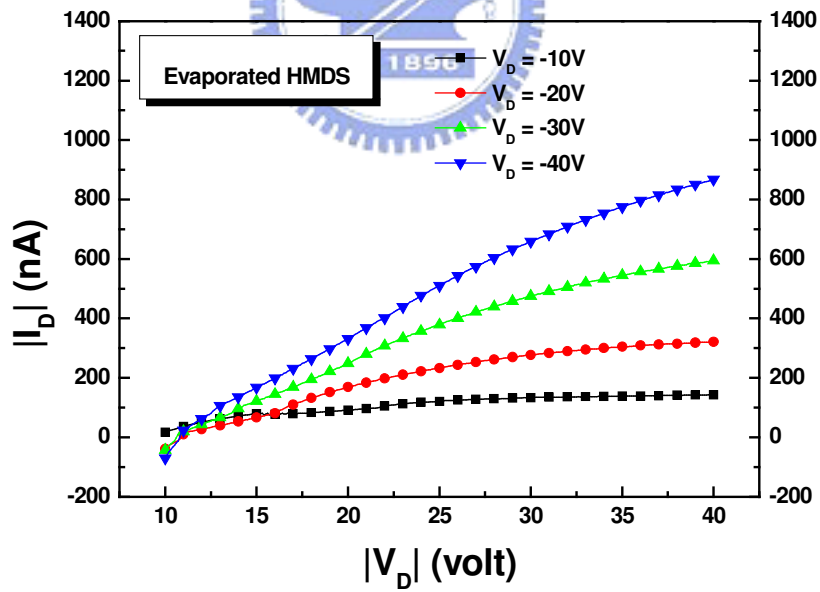
(b)

Figure 3-20: (a) I_D - V_G curve, (b) I_D - V_D curve with spin-coating HMDS

for OTFT.



(a)



(b)

Figure 3-21: (a) I_D - V_G curve, (b) I_D - V_D curve with evaporated HMDS

for OTFT.

Table 3-5 : The different methods of surface treatment.

Surface treatment	Contact angle	Surface roughness (nm)	Threshold voltage V_{th} (V)	Mobility μ_{sat} (cm^2/Vs)
No treatment	$< 10^\circ$	1.58	-21.7	1.9×10^{-3}
Spin-coating	65.5°	0.895	-9.5	7.8×10^{-3}
Evaporated	75.3°	0.890	-12.0	2.2×10^{-2}
APP 4	90.5°	6.07	-8.3	2.6×10^{-2}



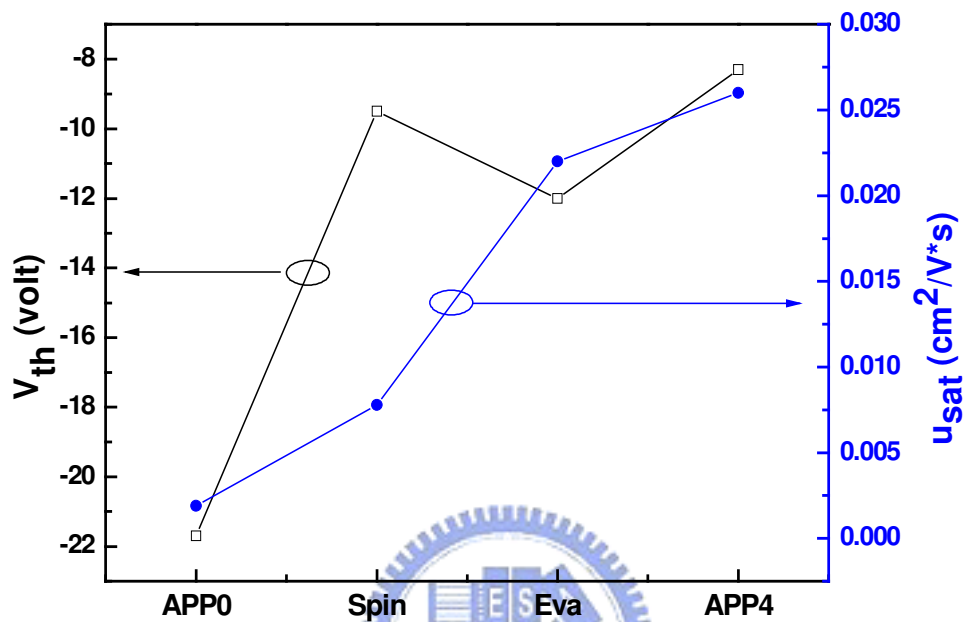
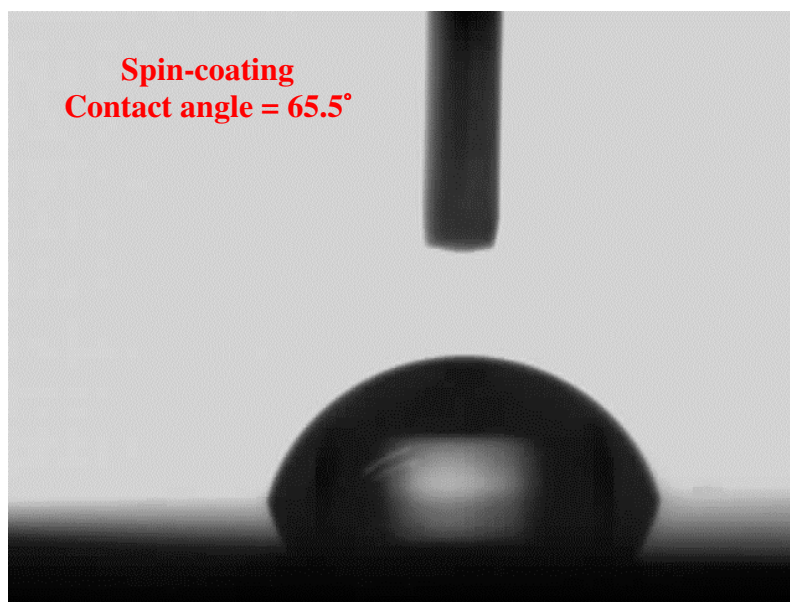
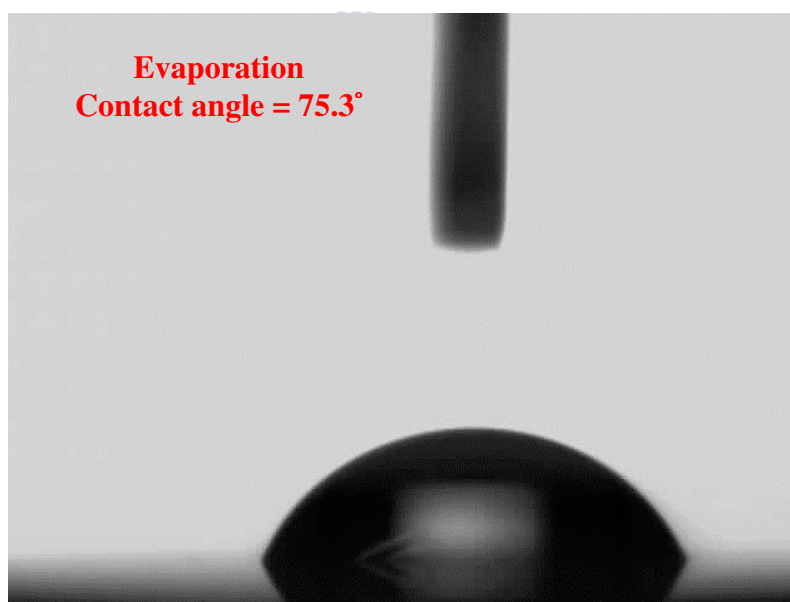


Figure 3-22: Comparison of threshold voltage and saturation mobility with different methods of surface treatment.

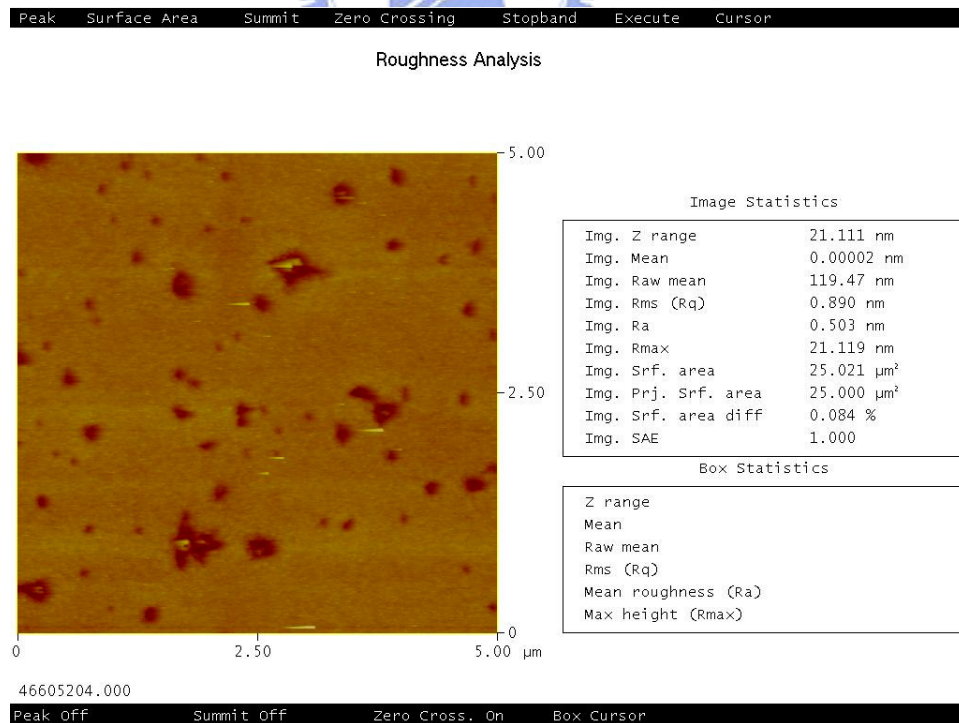
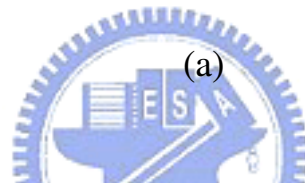
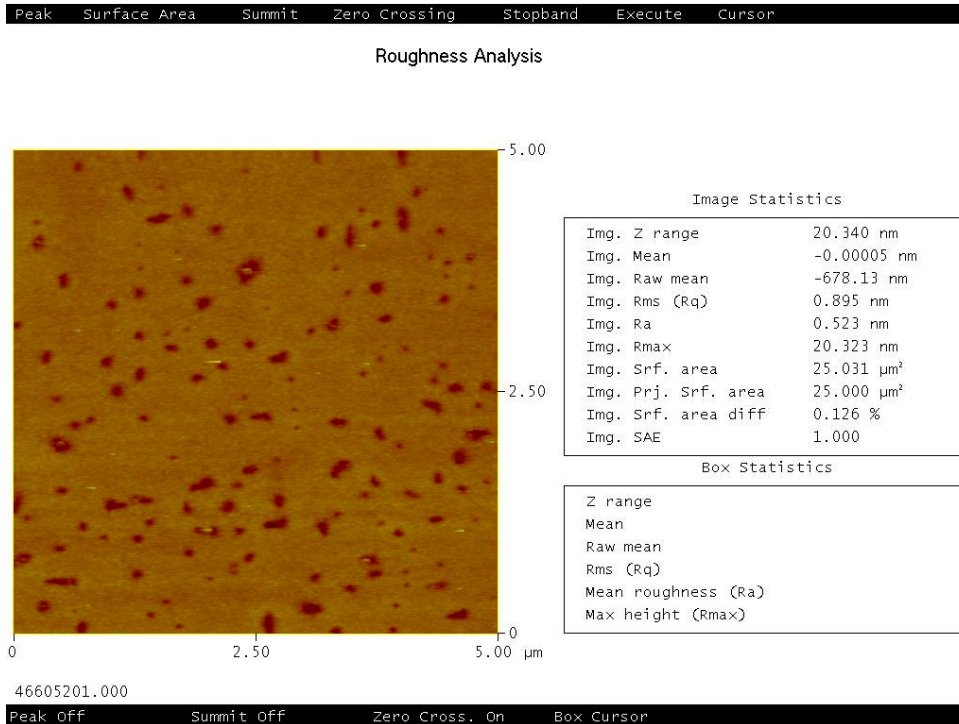


(a)



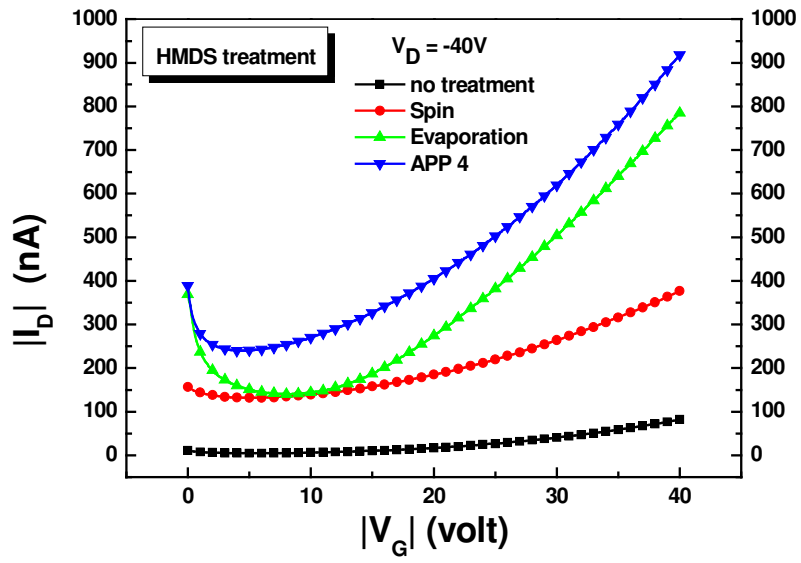
(b)

Figure 3-23: Contact angle of (a) spin-coating HMDS (65.49°), (b) Evaporated HMDS (75.28°).

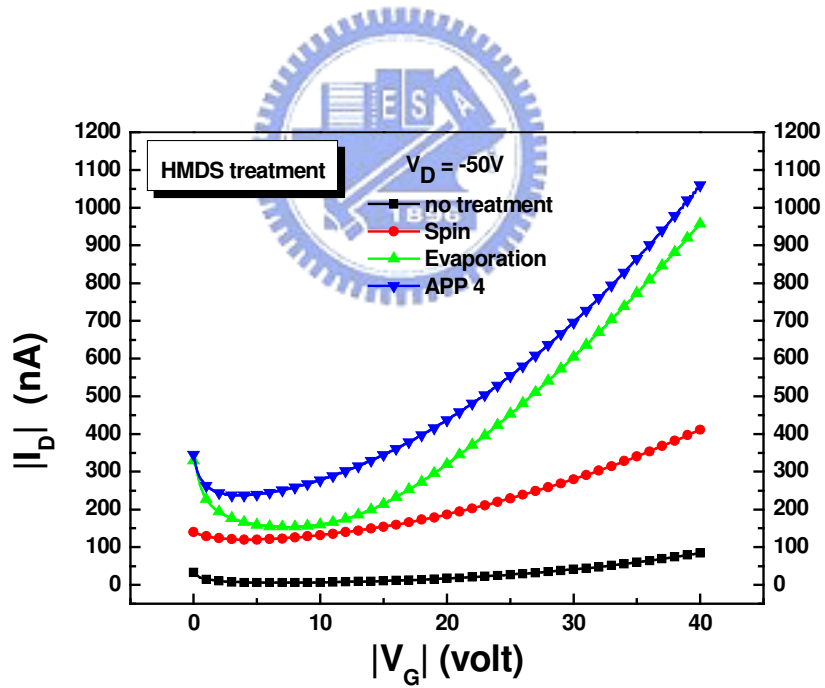


(b)

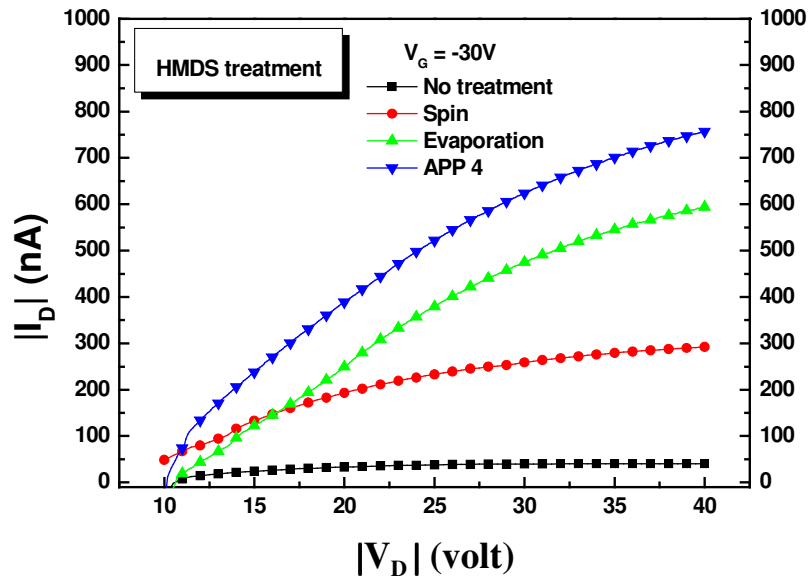
Figure 3-24: AFM photography of (a) Spin-coating, (b) Evaporated.



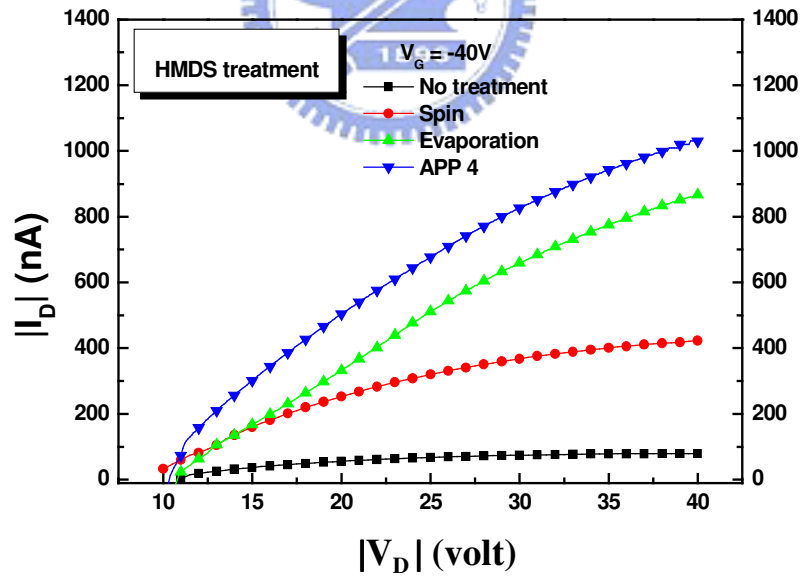
(a)



(b)



(c)



(d)

Figure 3-25: The comparison of (a), (b) I_D - V_G and (c), (d) I_D - V_D with different methods of surface treatment.

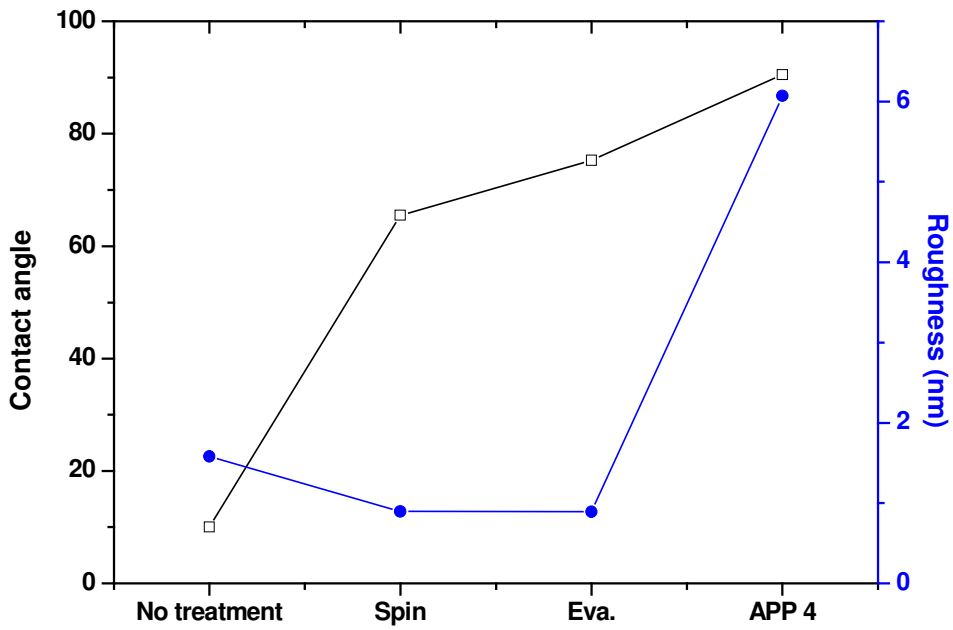


Figure 3-26: Comparison of contact angle and surface roughness with different methods of surface treatment.

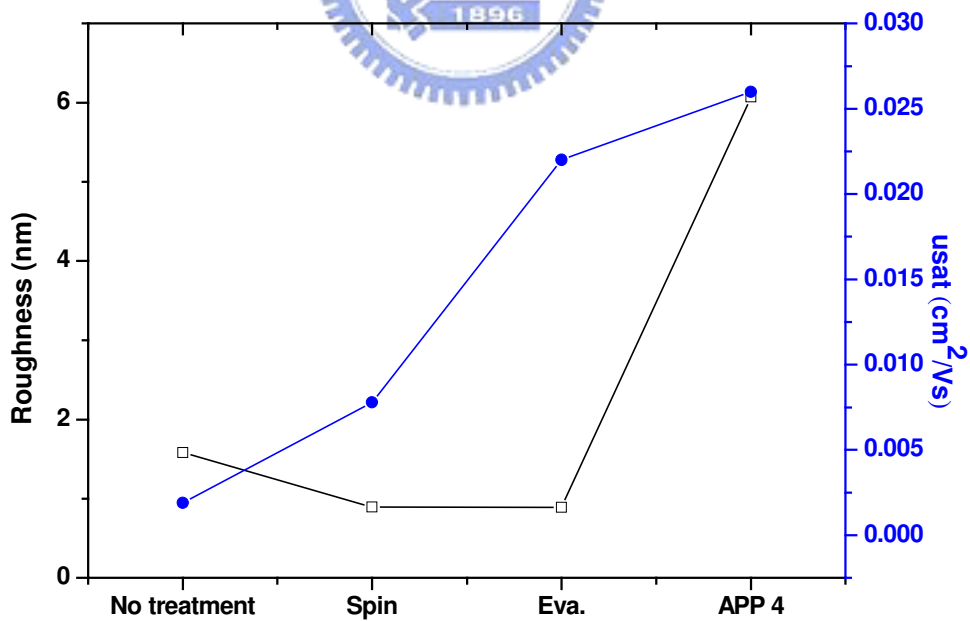


Figure 3-27: Comparison of surface roughness and mobility with different methods of surface treatment.

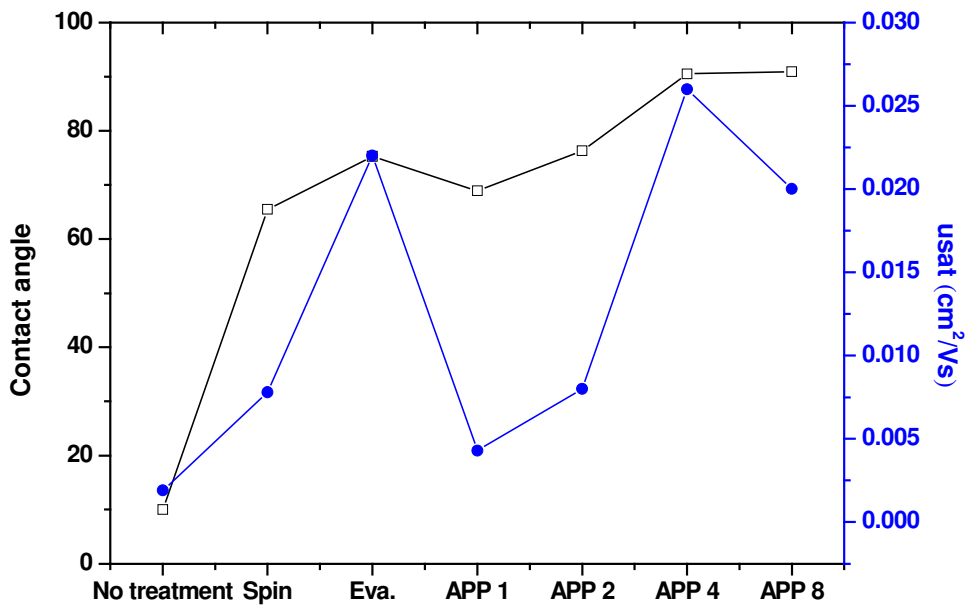


Figure 3-28: Comparison of contact angle and mobility with different methods of surface treatment and different scanning times by APPT.

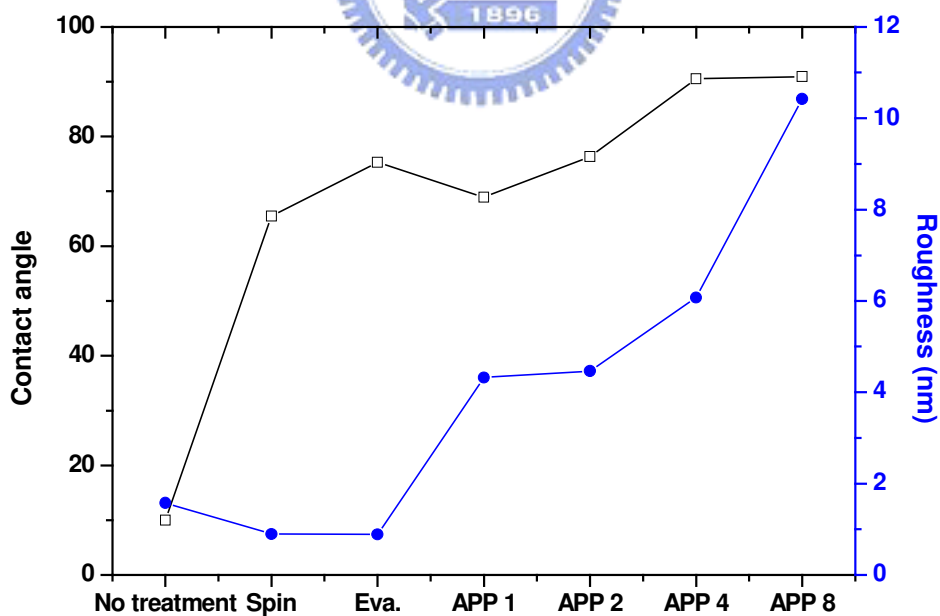


Figure 3-29: Comparison of contact angle and roughness with different methods of surface treatment and different scanning times by APPT.

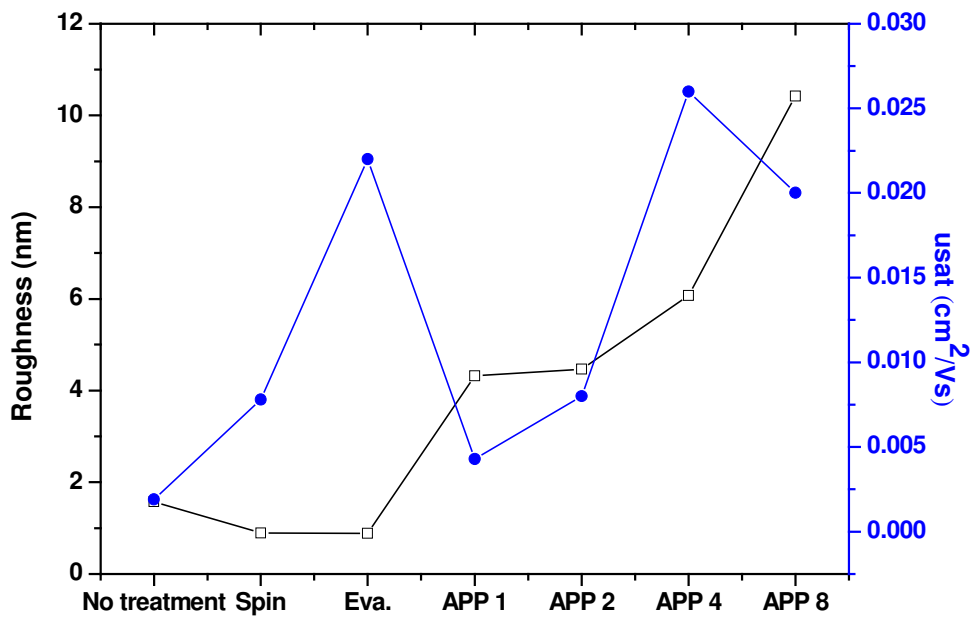


Figure 3-30: Comparison of roughness and mobility with different methods of surface treatment and different scanning times by APPT.



Chapter 4

Surface Treatment by Atmospheric-Pressure

Plasma Technology for P3HT Alignment

4.1 Introduction of P3HT alignment

3-Alkyl substituents can be incorporated into the poly(3-hexylthiophene) polymer in two arrangements (Fig. 2-1) - head to tail (HT) and head to head (HH). A regiorandom P3HT has both HH and HT 3-hexylthiophenes in a random pattern while a regioregular P3HT has only one 3-alkylthiophene - either HH or HT. Structure-controlled syntheses of P3HT have been recently developed, and regioregular P3HT with HT linkages of greater than 98.5% can be obtained [59,60]. Most interestingly, these polymers have been shown to have very different properties from their corresponding regiorandom polymers, such as smaller band gaps, better ordering and crystallinity in their solid state, as well as markedly improved electroconductivities.

Highly regioregular P3HT self-orient into a well-ordered lamellar structure with an edge-on orientation of the thiophene rings relative to the substrate. In samples with a high regioregularity (>91%), the preferential orientation of ordered domains is with the (100)-axis normal to the film and the (010)-axis in the plane of the film (Figs. 4-1 and 2-2). In contrast, low regioregularity (81% head-to-tail linkages) is associated with lamellae with a face-on orientation, and crystallites that are preferentially oriented along the (100)-axis in the plane and the (010)-axis normal to the film. In another work [61], Prosa *et al.* presented the different intensity distributions of the (100)

reflections that are associated with the lamella layer structure and the (010) reflections that are associated with π - π interchain stacking. Therefore, in this study, highly regioregular (98.5%) P3HT is adopted as the active layer, and the above characteristics are exploited to provide P3HT alignment.

4.2 The methods to provide P3HT alignment

4.2.1 Crystallization behavior of P3HT

Isothermal crystallization and melting was monitored using a Seiko SSC-5200 differential scanning calorimeter (DSC), and the temperature was calibrated using indium. About 5 mg of the polymer (P3HT) sample was weighed very accurately. It was pre-heated at 70°C, 90°C, 110°C, 130°C and 150°C for 3 min and then cooled to room temperature at a rate of 20°C/min. The sample was subsequently reheated to 300°C (Run 1), cooled to room temperature and then reheated to 300°C (Run 2) to study its melting behavior. The heating rate and the cooling rate were 20°C/min. All measurements were made in a nitrogen atmosphere, and each sample was used only once to mitigate any effect of thermal degradation after treatment at high temperature. The thermogravimetric analysis (TGA) indicated that the thermal degradation temperature of P3HT was approximately 500°C (Fig. 4-2).

Figures 4-3 ~ 4-7 plot the melting temperature (T_m) and crystallization enthalpy (ΔH) of P3HT for various pre-heating temperatures. These data were collated in in Figs. 4-8 (Heat Run 1) and 4-9 (Heat Run 2) and Table 4-1. The melting temperature did not vary in Run 1 or Run 2, but the enthalpy in Run 1 increased with the pre-heating temperature up to 130°C. The greater enthalpy of

crystallization indicated a higher degree of crystallinity - because the higher temperature gave the molecular chain enough kinetic energy to increase the overall crystallinity of P3HT. However, an excessive temperature caused the molecular chain to move too fast, reducing the strength of its orientation. Hence, the P3HT baking condition herein was set to 130°C for 3 min. The enthalpy in Run 2 did not markedly fluctuate, because the P3HT became amorphous after Run 1 at up to 300°C. The crystallization effect of pre-heating disappeared, and the enthalpy in Run 2 was almost the same in various pre-heating temperatures.

4.2.2 XRD and UV-vis for highly oriented crystals of P3HT

X-ray analysis indicates that the polymer films were composed of microcrystalline domains that were embedded in an amorphous matrix, and inside these microcrystalline regions, the polymers π stack in one direction such that UV-vis absorption spectra reveal π - π absorption, and lamella of the interlocking side chains in the other direction [62,63]. In another investigation [64], XRD data and UV-vis absorption spectra suggest that the molecules are oriented such that their long axis is almost normal to the film, and the π - π stacking direction is parallel to the substrate. XRD [65,66] and UV-vis absorption [67,68] have been adopted in many studies to identify the P3HT crystal.

When the P3HT is deposited on the SiO₂ surface, interchain stacking occurs in the molecular chain, so the molecules are ordered in a two-dimensional lamella structure [23]. If the molecular structure of P3HT exhibits high regioregularity (which is the percentage of stereoregular head-to-tail attachments of the hexyl side chains to the 3-position of the thiophene rings),

then this lamellar structure will have the edge-on orientation, its (100)-axis will be normal to the film and the (010)-axis will be in the plane of the film. Previous research has verified that good ordering is a basic requirement of improved transistor performance (better field-effect mobility) [69,70]. Figure 4-10 shows the XRD diagrams obtained following various surface treatments, including a strong and sharp diffraction peak at 5.3° (especially after treatment with APP 4), corresponding to an intermolecular spacing of 16.36 \AA in the well-organized lamellar structure, which value is consistent with the literature. The intensity of the diffraction at the same diffraction angle follows the order APP 4 > Eva > Spin > No treatment. This result was consistent with the mobility of OTFT. The surface is predicted to be more hydrophobic after APP treatment, such that the P3HT has more ordered domains along the (100)-axis and the mobility of OTFT is therefore higher.

Figure 4-11 presents the UV-vis absorption spectra in the region of the π - π^* absorption regioregular P3HT. The magnitude of the absorption peak at 610nm follows the order APP 4 > APP 8 > APP 2 > APP 1 > Spin > No treatment. This result was consistent with the mobility of OTFT. The figure indicates that modifying the surface with APP 4 increases the absorption peak at 610 nm, revealing increases in chain extension and chain alignment.

In this chapter, XRD and UV-vis were adopted to demonstrate that high mobility requires an ordered structure.

4.3 Hysteresis

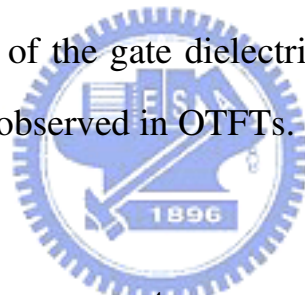
Figure 4-12 plots a typical hysteresis curve. This curve depicts the response of the polarization, P, to the externally applied electric field, E. The hysteresis

curve saturates at P_{sat} when the maximum alignment of the spontaneous polarization occurs. When the electric field is removed instantaneously after reaching P_{sat} , the electronic polarization associated with the linear capacitance component decreases to zero, and the spontaneous polarization, P_s , remains. Then, within milliseconds usually, the polarization decays to the remnant polarization, P_r . For much longer times, the polarization is observed to decay linearly with the log of time for many orders of magnitude of time [71].

The current that flows through the gate-dielectric/channel interface is widely believed to be dominant during the operation of OTFTs. Therefore, electronic conduction at the interface is expected directly to affect the TFT performance. This effect is directly related to the hysteresis behavior, which is induced by the trap sites at the interface in OTFTs. P3HT films that are deposited on the gate dielectric have many trap sites, depending on the surface state of the gate dielectric. Undoubtedly, if the gate dielectric contains trap sites inside the bulk, then these trapped charges may also induce hysteresis. The hysteresis of gate dielectrics represents a potential problem that can limit their range of applications, because this hysteresis leads to instability of the threshold voltage in OTFTs. Various studies of hysteretic behavior observed in OTFTs have been published [72,73].

However, in this work, the effects of oxide trapping are assumed to be weaker than those of interface trapping. This assumption is similar to that made in previous investigations and is supported by changes in the extent of hysteresis with the use of various surface modification protocols [74,75]. In recent reports, $-\text{OH}$ groups have been identified as the origin of the electron trapping sites that are largely responsible for the hysteretic behavior observed in OTFTs [76,77]. Since the dielectric layer (SiO_2) in this work is an $-\text{OH}$ -rich surface, the

hysteretic behavior is very serious (Fig. 4-13). Therefore, when the surface is transformed from an –OH-rich surface into a CH₃-terminated surface by HMDS surface treatment, the hysteresis behavior decreases (Figs 4-14~4-19). Furthermore, the formation of well-defined orientation of P3HT grains markedly reduces the hysteresis by reducing the number of grain boundaries, such as when the surface is treated by evaporation, APP 4 and APP 8 (Figs. 4-15, 4-18 and 4-19). Treatment of the surface by evaporation yields less hysteresis than the other methods : perhaps evaporation forms the flattest surface. In one investigation [78], the surface roughness caused strong variations in the local field with associated scattering of carriers and the possible formation of carrier traps. These results offer clear evidence that –OH groups, the orientation of P3HT and the surface roughness of the gate dielectric surface, are responsible for the hysteresis behavior that is observed in OTFTs.



4.4 Anomalous leakage current

According to the I_D - V_G plots in Fig 4-20, current increases as V_G approaches 0 V, especially following surface treatment by APP. For the APP process (Fig 4-21), the magnitude of the current as V_G approaches 0 V follows the order APP 4 > APP 8 > APP 2 > APP 1, perhaps because of an anomalous leakage current. The gate leakage current increase may have two causes - weak points [72], and the higher channel conductance of the OTFTs [79]. The poor uniformity and roughness of the surfaces are the main sources of the “weak points”, which act as local high-electric-field regions where breakdown occurs. These weak points enhance carrier injection and further increase the leakage current. As presented in Fig 4-20, surface treatment by APP increased the

leakage current, because the surface became rougher. However, although the surface of APP 8 is rougher, the leakage current is smaller than that of APP 4. APP 4 surface treatment may enlarge the crystalline domain of P3HT, causing the high channel conductance. In the future, to improve the anomalous leakage current will be studied.



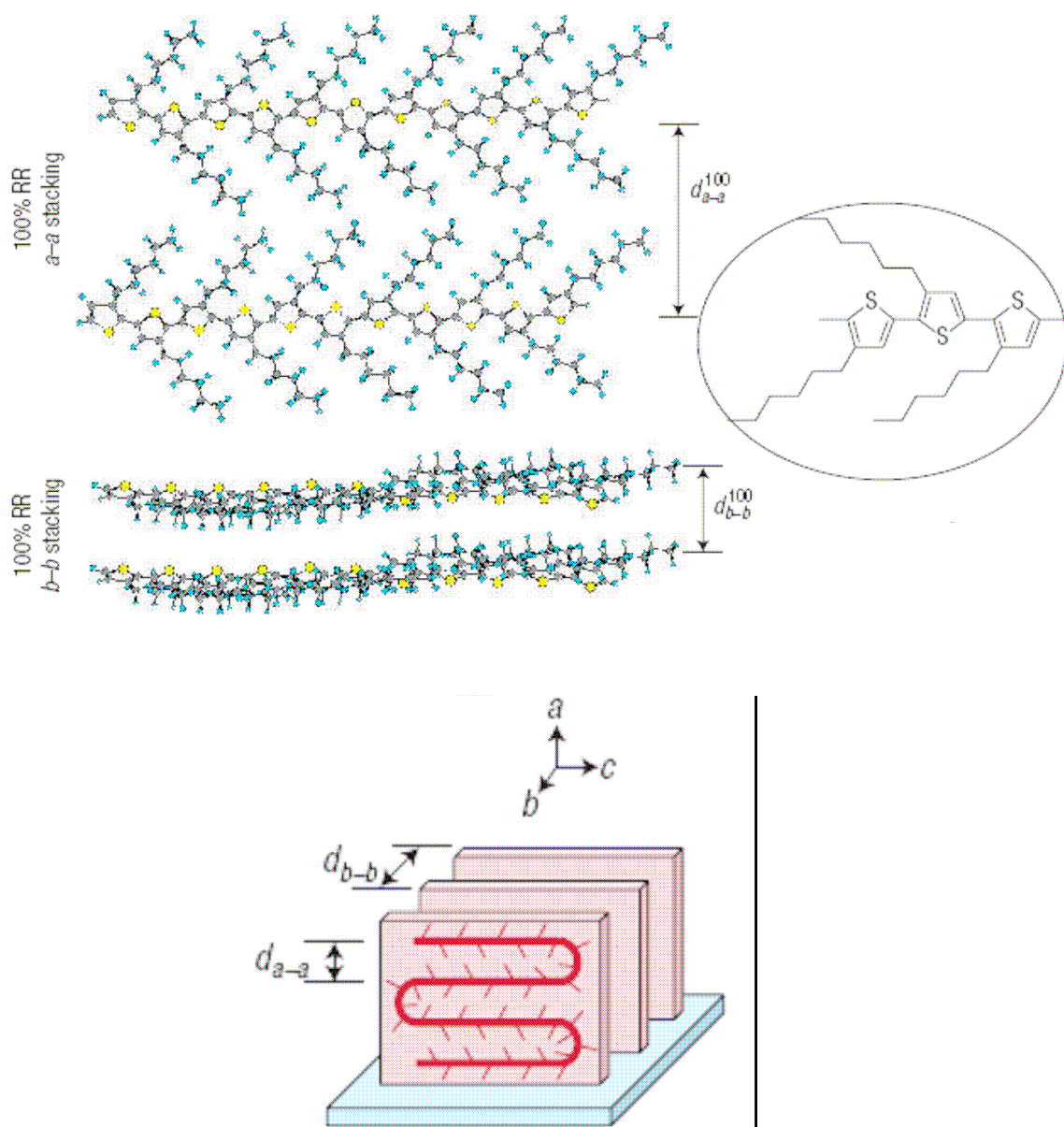


Figure 4-1: The molecular structure of P3HTs for High RR (d_{a-a}^{100} and d_{b-b}^{100} are the a -direction and b -direction chain-stacking spacings, respectively) The a -direction and b -direction are parallel and perpendicular to the thiophene ring plane, respectively (see the chemical structures within the ovals as well as the schematic illustration for lamella folding and ordering on a substrate).

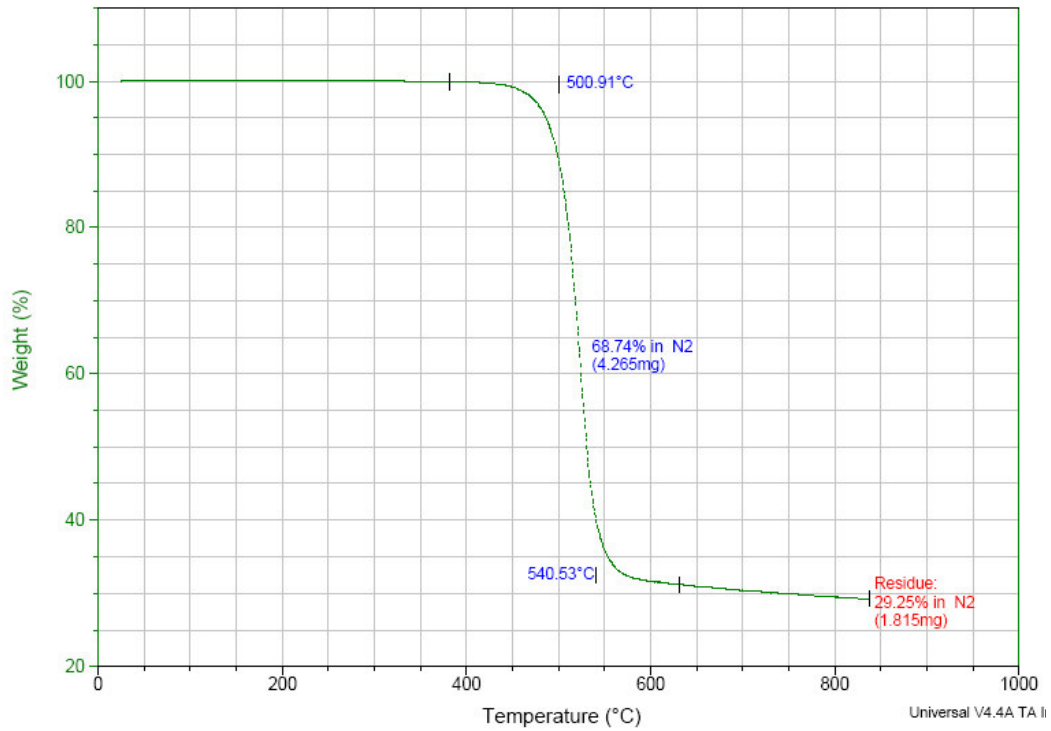


Figure 4-2: TGA thermograph of P3HT. 5 % weight loss is about 500°C.

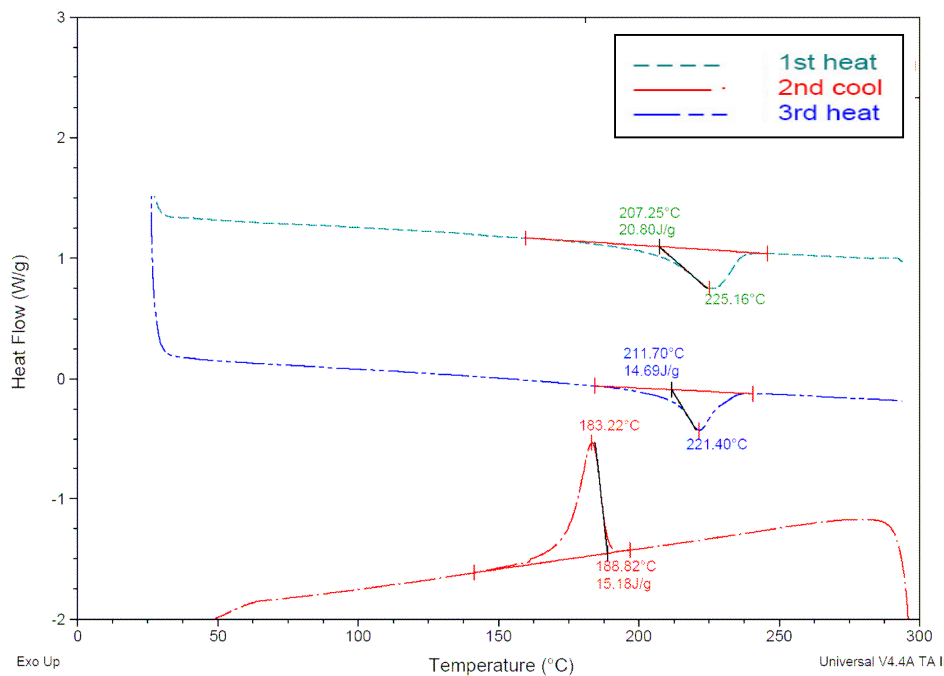


Figure 4-3: DSC thermograph of P3HT was pre-heating at the temperature of 70°C for 3 min.

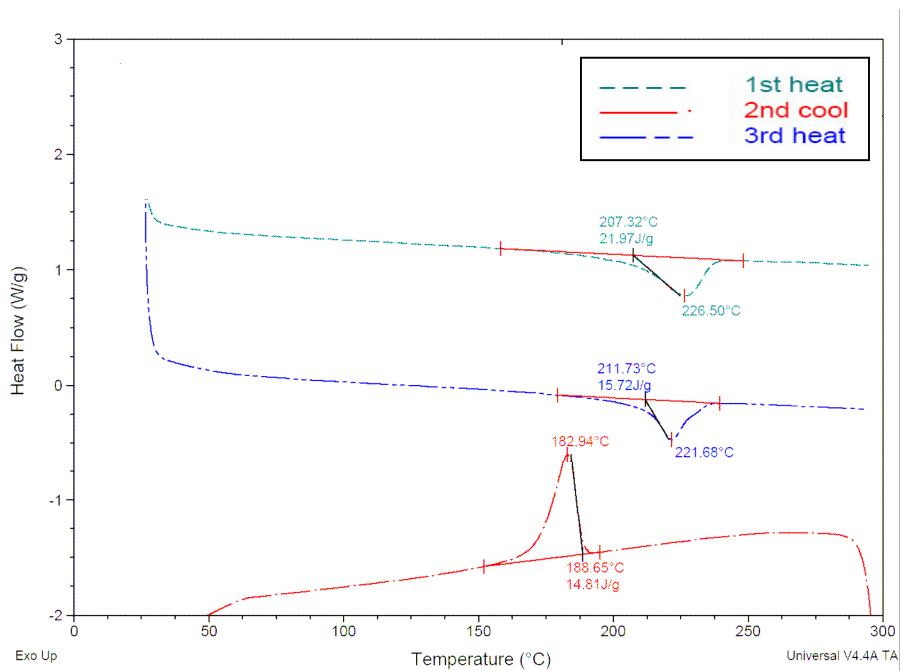


Figure 4-4: DSC thermograph of P3HT was pre-heating at the temperature of 90°C for 3 min.

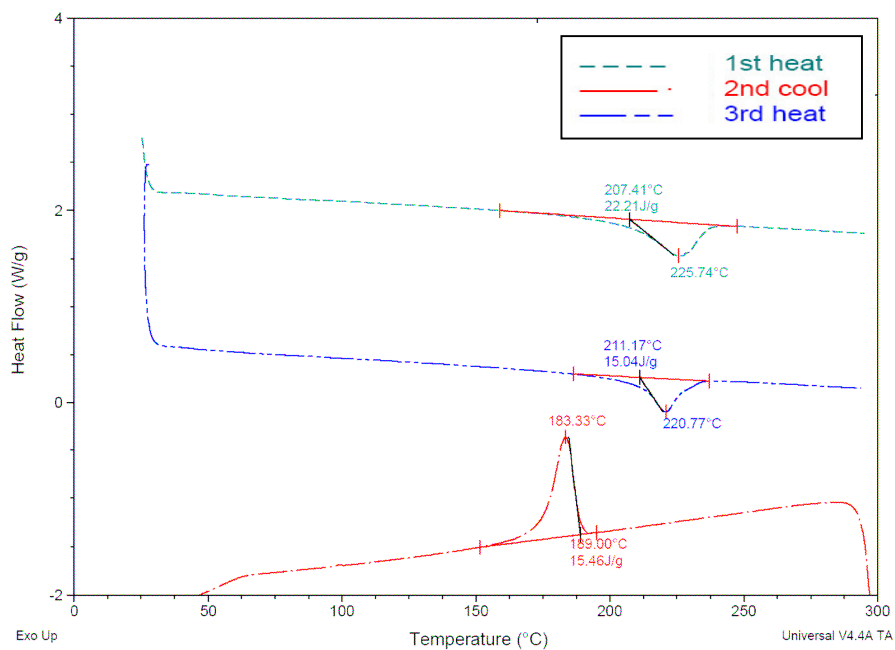


Figure 4-5: DSC thermograph of P3HT was pre-heating at the temperature of 110°C for 3 min.

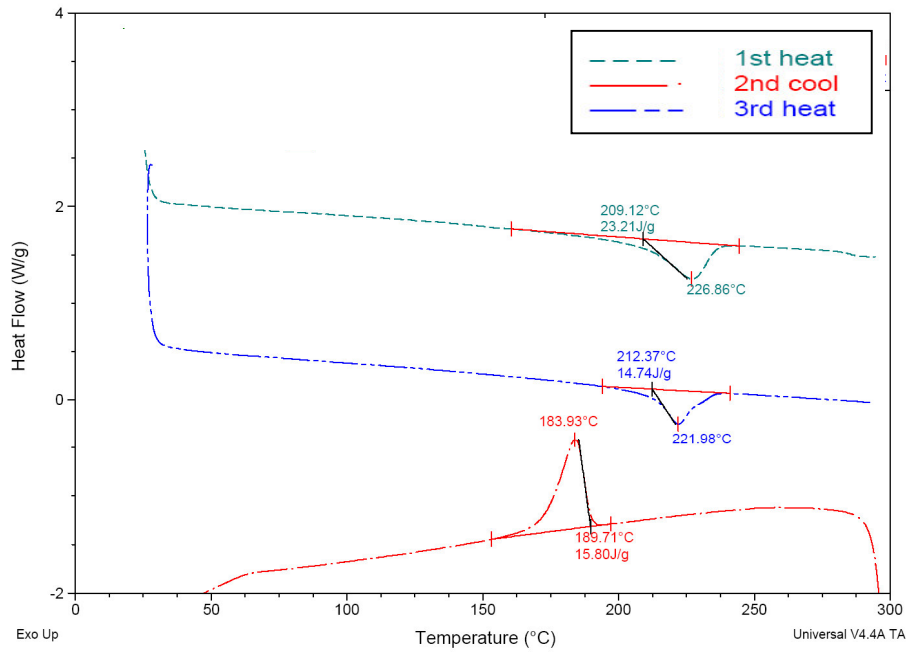


Figure 4-6: DSC thermograph of P3HT was pre-heating at the temperature of 130°C for 3 min.

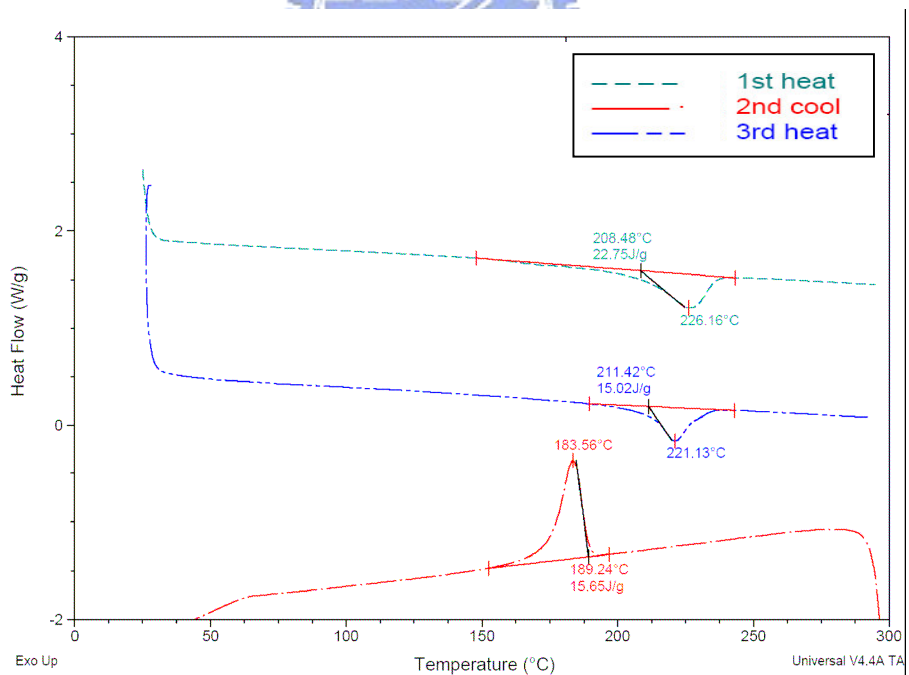


Figure 4-7: DSC thermograph of P3HT was pre-heating at the temperature of 150°C for 3 min.

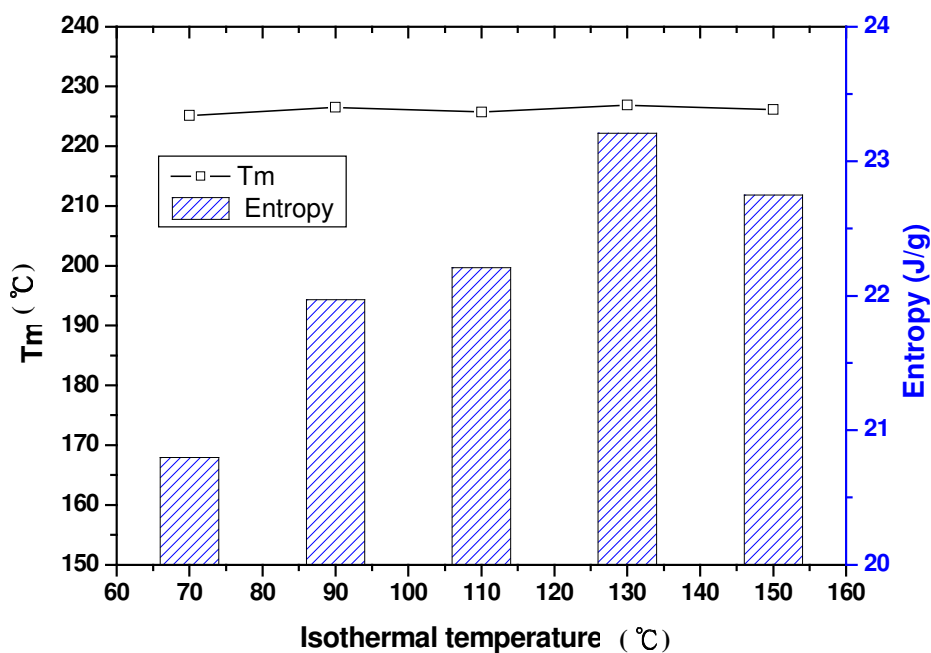


Figure 4-8: T_m and ΔH of P3HT in Run 1 with difference pre-heating temperature.

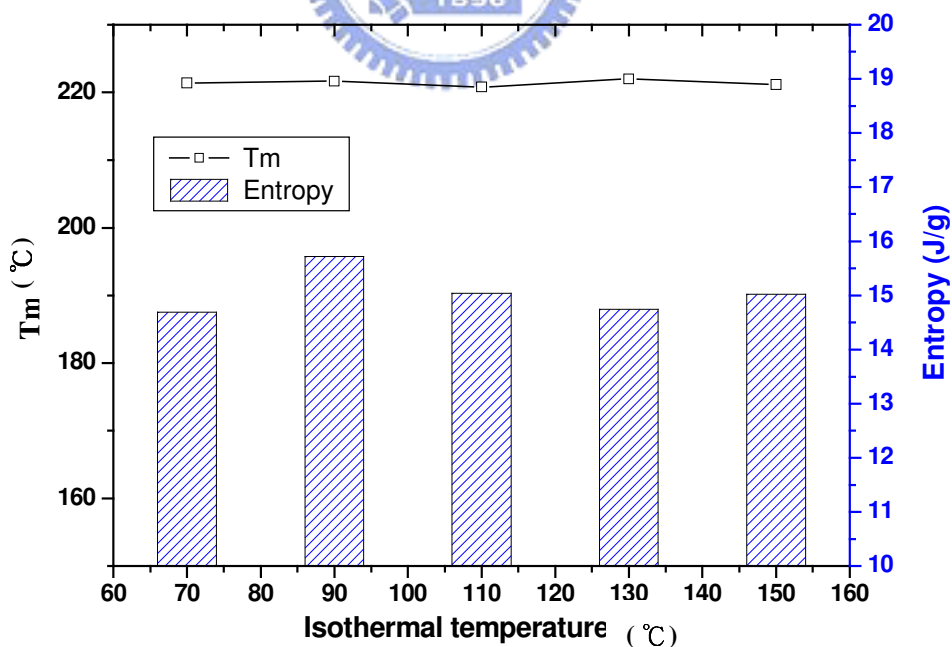


Figure 4-9: T_m and ΔH of P3HT in Run 2 with difference pre-heating temperature.

Table 4-1: T_m and ΔH of P3HT in Run 1 and Run 2 with difference pre-heating temperature.

Pre-heating temperature	Heat Run 1		Heat Run 2	
	T_m (°C)	ΔH (J/g)	T_m (°C)	ΔH (J/g)
70 °C	225.16	20.80	221.40	14.69
90 °C	226.50	21.97	221.68	15.72
110 °C	225.74	22.21	220.77	15.04
130 °C	226.86	23.21	221.98	14.74
150 °C	226.16	22.75	221.13	15.02



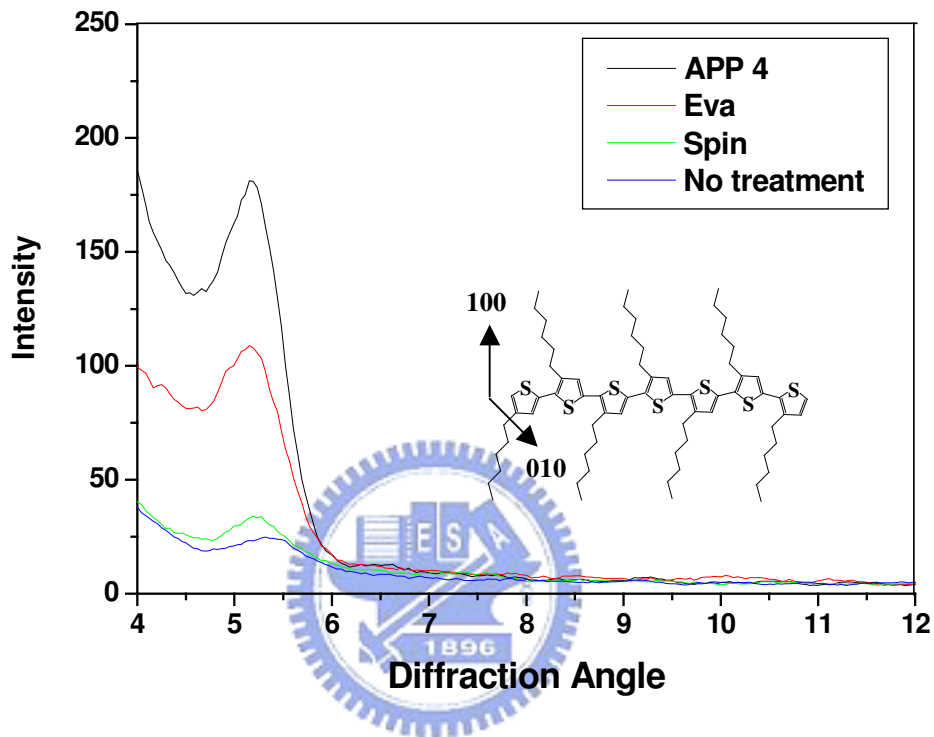


Figure 4-10: X-ray analysis of deposition of P3HT on SiO₂ dielectric layer with various surface treatments.

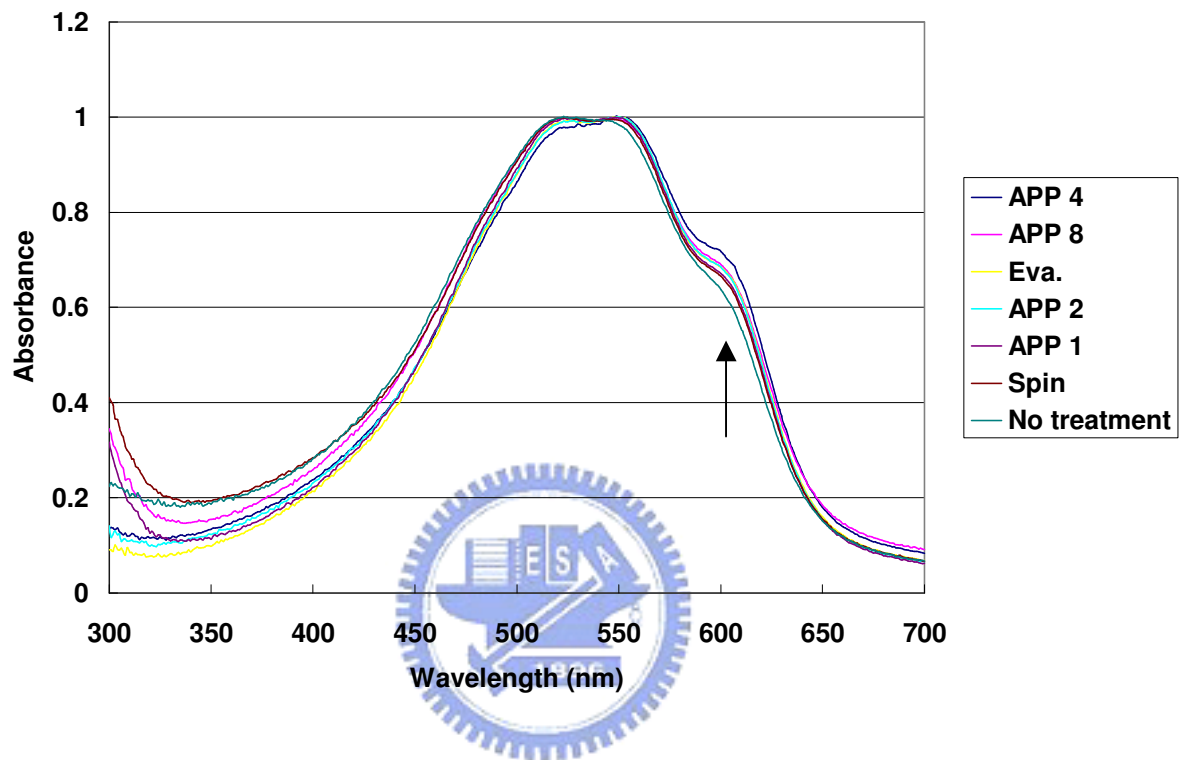


Figure 4-11: UV-vis absorption spectra of P3HT films that are deposited on SiO₂ dielectric layers following various surface treatments, normalized to the maxima of the spectra.

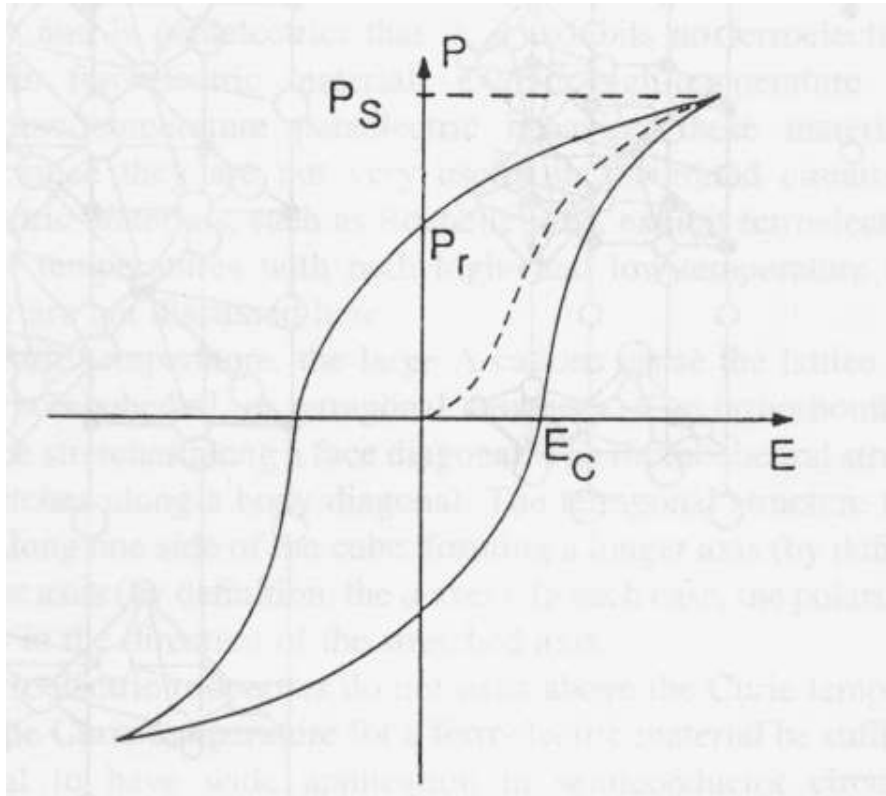


Figure 4-12: A typical hysteresis curve.

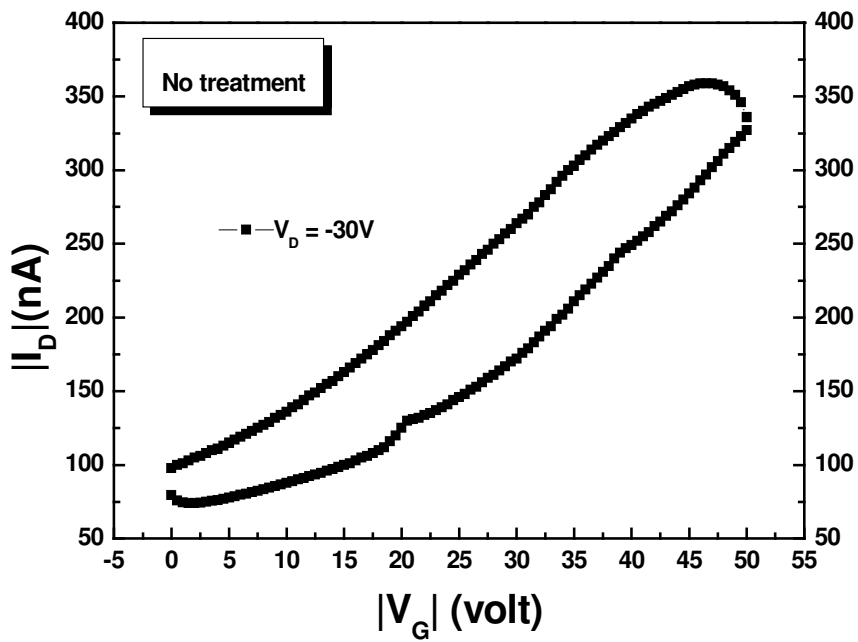


Figure 4-13: Hysteresis of P3HT OTFTs with no surface treatment.

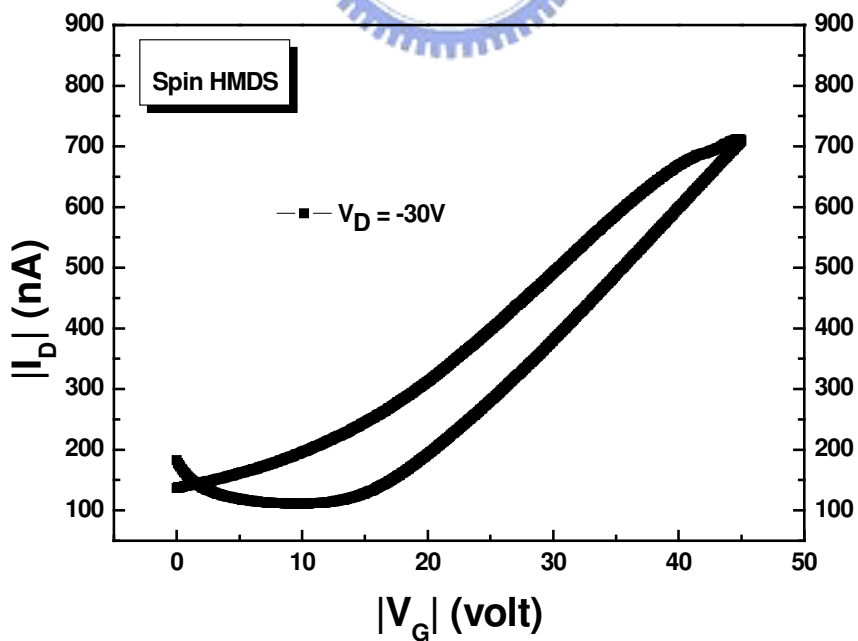


Figure 4-14: Hysteresis of P3HT OTFTs with spin-coating surface treatment.

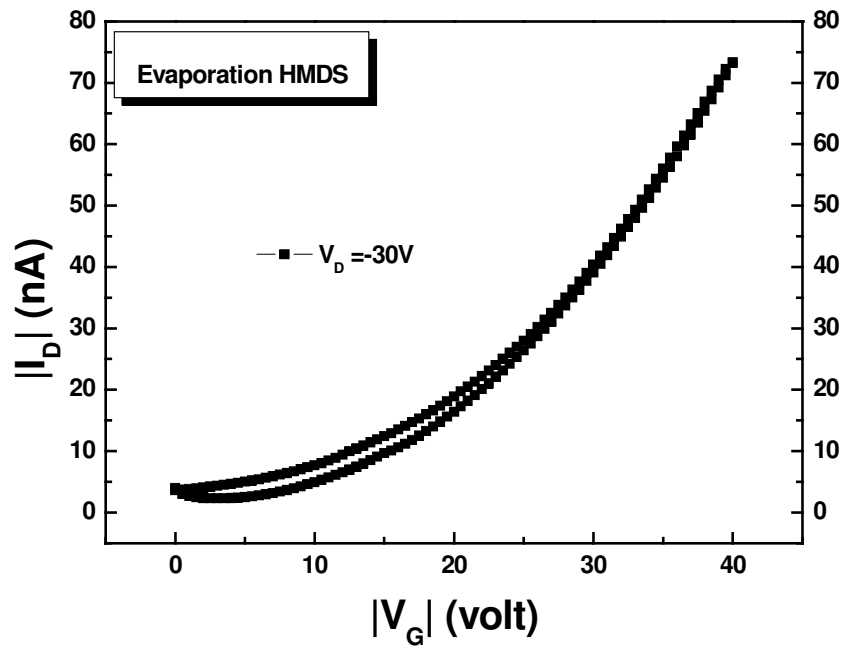


Figure 4-15: Hysteresis of P3HT OTFTs with evaporation surface treatment.

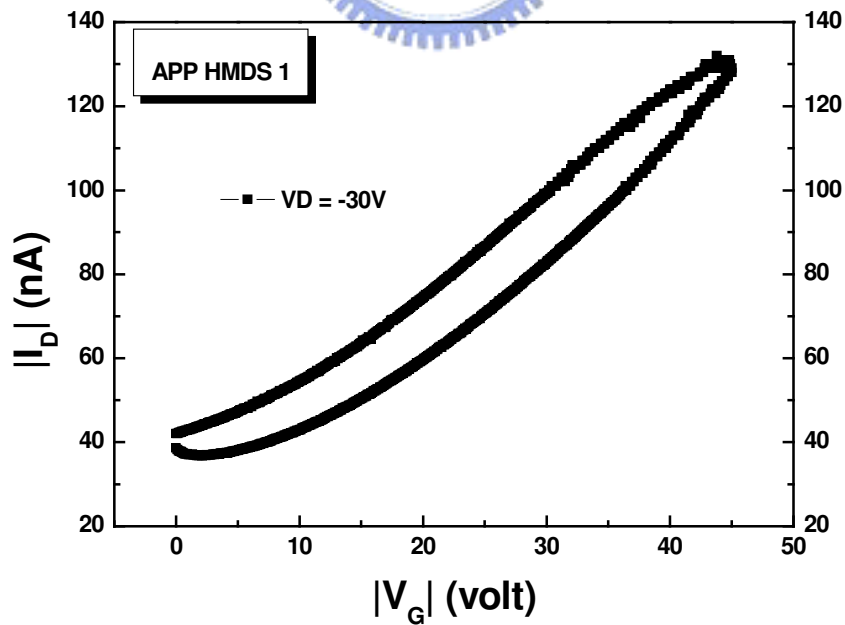


Figure 4-16: Hysteresis of P3HT OTFTs with APP 1 surface treatment.

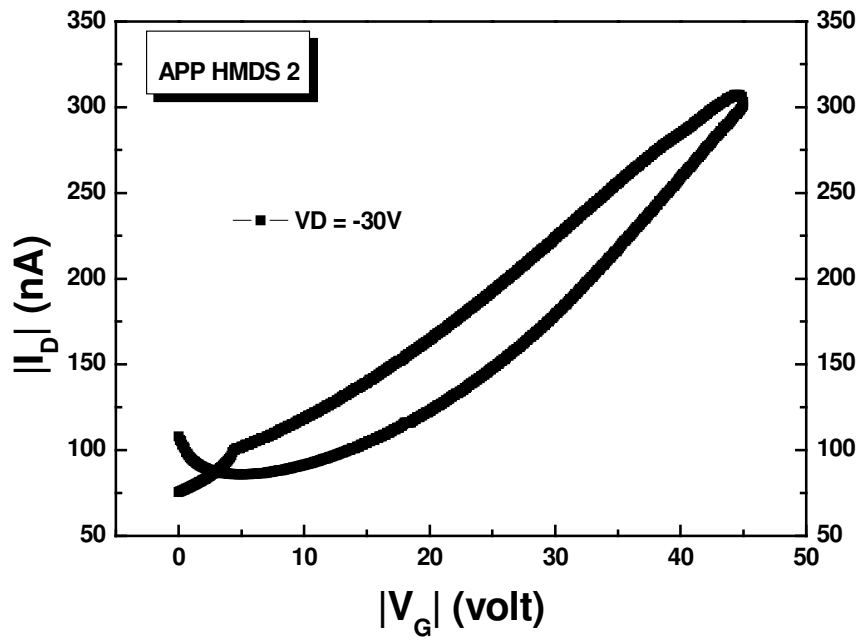


Figure 4-17: Hysteresis of P3HT OTFTs with APP 2 surface treatment.

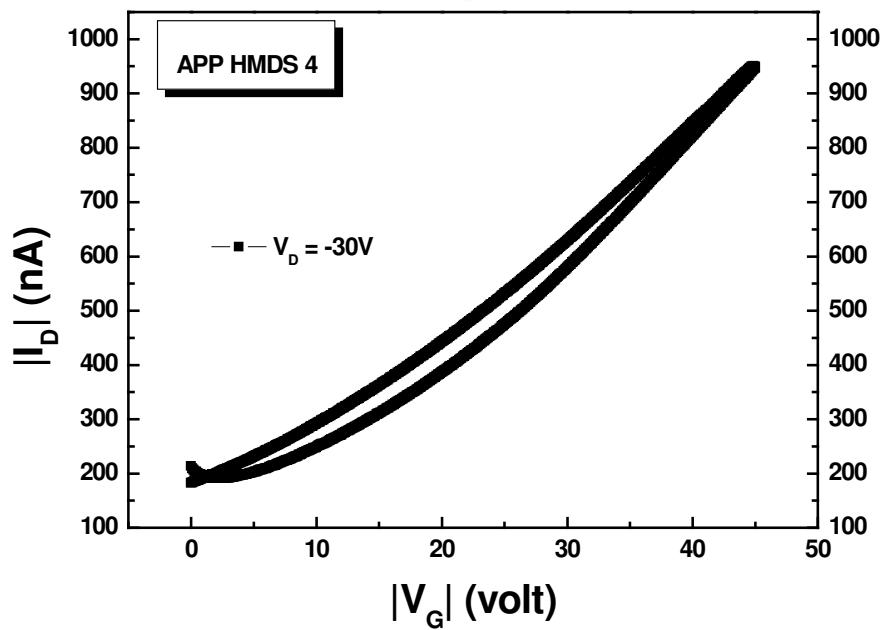


Figure 4-18: Hysteresis of P3HT OTFTs with APP 4 surface treatment.

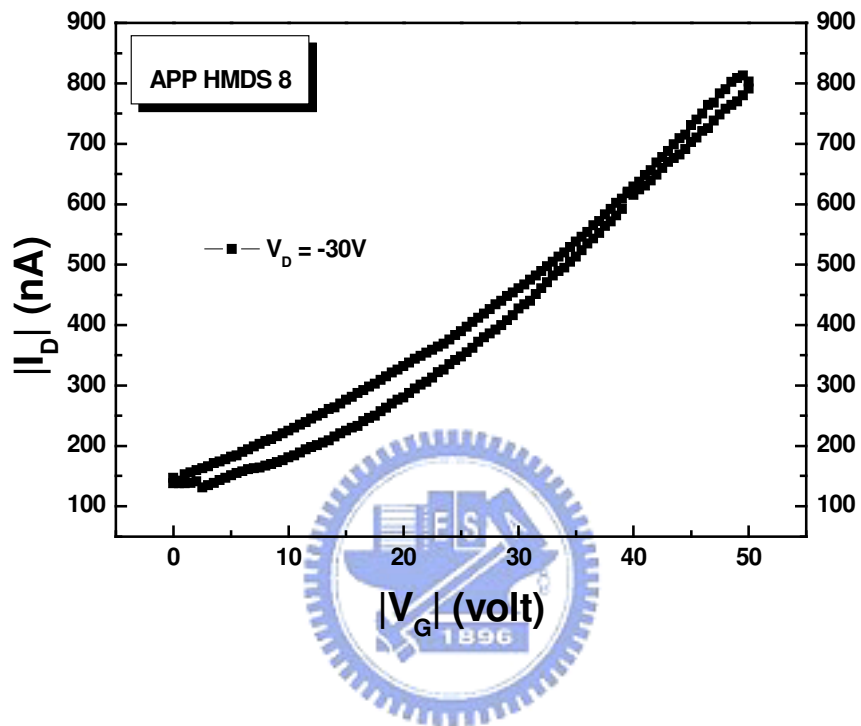


Figure 4-19: Hysteresis of P3HT OTFTs with APP 8 surface treatment.

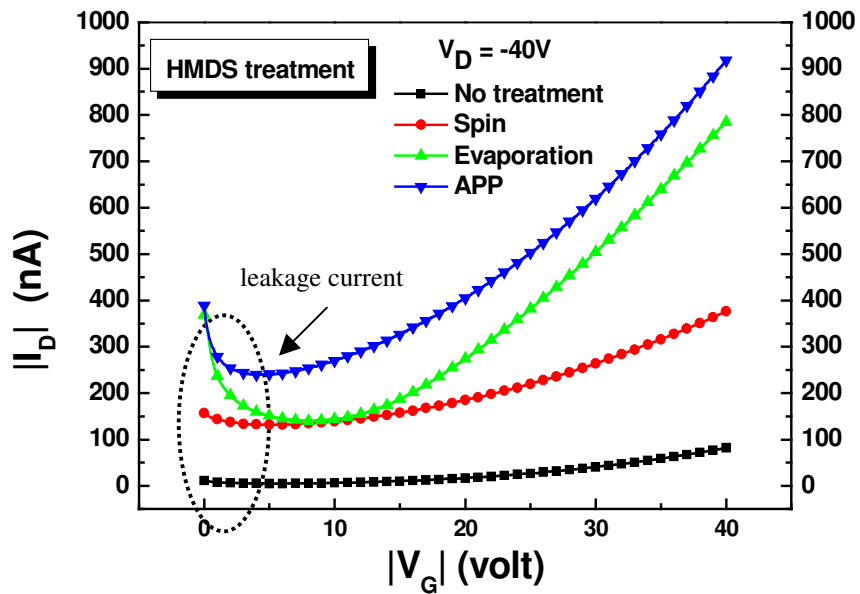


Figure 4-20: I_D versus V_G for various surface treatment processes and the gate leakage currents in V_G approaches 0 V.

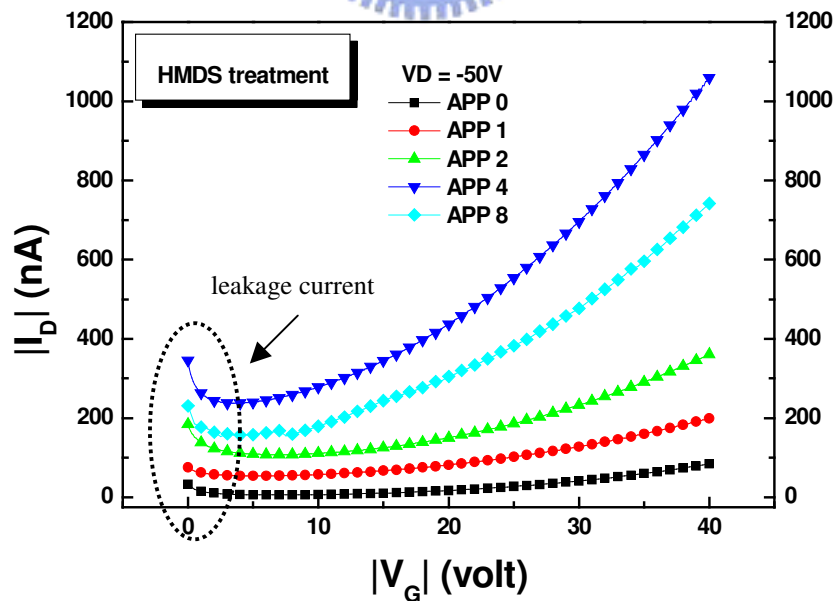


Figure 4-21: I_D versus V_G for different numbers of APP scans and the gate leakage currents in V_G approaches 0 V.

Chapter 5

Conclusions and Future Work

5.1 Conclusions

OTFT with P3HT deposited as an active layer was fabricated on SiO₂ substrate. Electrical measurements yielded typical I-V characteristics of the TFT. In this work, APPT surface treatment methods were adopted to modify parts of the device to realize OTFTs that operate at low voltages with high mobility and good electrical stability. Surface treatment was employed to transform the hydrophilic surface to a hydrophobic surface, and to passivate surface hydroxyl groups, improving the orientation, enlarging the grains of the P3HT films and increasing the field-effect mobility. The SiO₂ surface became hydrophobic upon the deposition of HMDS by APPT, and the field-effect mobility increased as the surface energy decreased. The highest mobility ($\sim 2.6 \times 10^{-2}$ cm²/Vs) was associated with APP 4. The contact angles of APP 4 and APP 8 were similar, but the field-effect mobility of APP 8 was lower than that of APP 4. APP 8 may have been too rough to cause scattering. The surface roughness of the gate dielectric is generally an important parameter that determines device performance and the morphology of the deposited organic semiconductor film. Increased roughness is associated with valleys in the channel region, which can act as carrier traps and scattering sites. The above demonstrates that the surface free energy (hydrophobic state) and surface roughness of gate dielectrics were factors that affect the performance of the OTFT. The field-effect mobility is increased with the increment of hydrophobic state, but decreases as the surface roughness increases.

Two methods of surface treatment, spin-coating HMDS and evaporated HMDS, were performed. These two methods were associated with clear improvements in the experiments. The mobility in the saturation region was 4 times higher for spin-coating HMDS ($\mu_{\text{sat}} = 7.8 \times 10^{-3} \text{ cm}^2/\text{Vs}$) and 11 times higher for evaporated HMDS ($\mu_{\text{sat}} = 2.2 \times 10^{-2} \text{ cm}^2/\text{Vs}$) than without treatment ($\mu_{\text{sat}} = 1.9 \times 10^{-2} \text{ cm}^2/\text{Vs}$). HMDS-treatment of SiO_2 reduces the threshold voltage. The magnitude of the saturation current at a given operating voltage and mobility of the OTFTs follows the order APP 4 > Evaporation > Spin-coating > No treatment. APPT is still better than the other methods of HMDS-treatment of SiO_2 in the experiment, perhaps because the APP uses chemical bonds to stack material on the SiO_2 surface, so the HMDS film becomes denser, and thus hydrophobic at the same deposited thickness, improving the performance of the OTFTs.

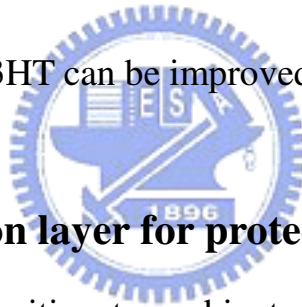
X-ray diffraction and UV-vis are adopted to provide direct evidence of highly oriented crystals at the interface between the polymer and the dielectric where the current flows in thin-film transistors. The degree of order of the lamellar structure follows the order APP 4 > Eva > Spin > No treatment, which was consistent with the mobility of OTFT, and demonstrated that high mobility requires an ordered structure. Furthermore, the formation of well-defined orientation of P3HT grains markedly reduces the hysteresis by reducing the number of grain boundaries. Surface treatment by evaporation indicated was associated with better hysteresis than other methods of surface treatment; hence $-\text{OH}$ groups, the orientation of P3HT and the surface roughness of the gate dielectric surface were responsible for the hysteresis behavior observed in OTFTs. Finally, according to the $I_{\text{D}}-V_{\text{G}}$ plots, the current increased as V_{G} approached 0 V, especially when the surface was treated by APP. An anomalous

leakage current may have been responsible for this phenomenon. The increase in the gate leakage current may have had two causes - one was weak points, and the other was the high channel conductance of the OTFTs.

This investigation has suggested an interesting direction for the preparation of high-performance OTFTs with high efficiency, involving low-temperature surface treatment by APPT. The low-temperature process and large area deposition associated with APPT surface treatment offer a great improvement in performance. Therefore, APPT has great potential for use at low-temperature and under atmospheric conditions.

5.2 Future work

The performance of P3HT can be improved as described below.



5.2.1 In-situ passivation layer for protecting the P3HT film

P3HT OTFTs are sensitive to ambient conditions. Therefore, protection from the environment by encapsulation is essential to their stability. Hence, the use of a suitable material as passivation to protect the P3HT film from environmental effects is an important topic.

5.2.2 Novel method for depositing P3HT thin films

Three methods can be used to deposit P3HT thin films: (1) spin-coating (2) dip-coating (3) drop-casting. The experiment in this work adopted the spin-coating method to deposit P3HT thin films. The best of these methods is drop-casting. Therefore, in the future drop-casting can be used in our experiment.

5.2.3 Thermal stability of P3HT OTFT

Like the device lifetime and the stability of P3HT in various ambients, thermal stability is an important topic, and for several OR numerous reasons. For example, poly(3-hexylthiophenes) devices are likely to be exposed to high elevated temperatures during fabrication. Thermal cycling studies provide essential insights into device lifetime and stability.

5.2.4 New gate insulator materials for P3HT OTFT

The parameters that dominate performance are charge carrier mobility, ON-OFF current ratio and the range of operating voltages. However, the operating voltage of P3HT OTFT that is required to produce such performance is impractically high. Although decreasing the thickness of SiO₂ reduces the operating voltage of P3HT OTFT, the leakage current increases as the thickness of SiO₂ decreases and influences the performance of P3HT OTFT. Therefore, high-dielectric gate insulator materials can be adopted to improve this.

References

- [1] C. J. Drury, C. M. Mutsaers, C. M. Hart, M. Matters and D. M. de Leeuw, *Appl. Phys. Lett.* **73** (1998) 108.
- [2] M. G. Kane, J. Campi, M. S. Hammond, F. P. Cuomo, B. Greening, C. D. Sheraw, J. A. Nichols, D. J. Gundlach, J. R. Huang, C. C. Kuo, L. Jia, L. H. Klauk and T. N. Jackson, *IEEE Electron Device Lett.* **2** (2001) 534.
- [3] W. Fix, A. Ullmann, J. Ficker and Clemens, *Appl. Phys. Lett.* **81** (2002) 1735.
- [4] C. D. Sheraw, L. Zhou, J. R. Huang, D. J. Gundlach, T. N. Jackson, M. G. Kane, I. G. Hill, M. S. Hammond, J. Campi, B. K. Greening, J. Francl and J. West, *Appl. Phys. Lett.* **80** (2002) 1088.
- [5] Y. Fujisaki, Y. Inoue, H. Sato, T. Kurita, S. Tokito and H. Fujikake, *Proc. Int. Display Workshop (2003) (IDW'03)*, p.291.
- [6] Y. Inoue, Y. Fujisaki, T. Suzuki, S. Tokito, T. Kurita, M. Mizukami, N. Hirohata, T. Tada and S. Yagyu, *Proc. Int. Display Workshop (2004) (IDW'04)*, p. 355.
- [7] Y. Taur and T. H. Ning, *Fundamentals of Modern VLSI Devices*, Cambridge University Press, New York, (1998), p.11.
- [8] H. E. Katz, Z. Bao and S. L. Gilat, *Acc. Chem. Res.* **34** (2001) 359.
- [9] Y. Y. Lin, D. J. Gundlach, S. F. Nelson and T. N. Jackson, *IEEE Electron Device Lett.* **18** (1997) 606.
- [10] F. J. Mayer zu Heringdorf, M. C. Reuter and R. M. Tromp, *Nature* **412** (2001) 517.
- [11] D. J. Gundlach, H. Klauk, C. D. Cheraw, C. C. Kuo, J. R. Huang and T. N. Jackson, *Electron Devices Meet, 1999, IEDM Tech. Dig., Washington, D.C., (1999)*, p.111.

- [12] G. Horowitz, J. Mater. Res. **19** (2004) 1946.
- [13] H. Sirringhaus, P. J. Brown, R. H. Friend, and M. M. Nielsen, Nature **401** (1999) 685.
- [14] M. Halik, H. Klauk, G. Schmid, and W. Weber, Adv. Mater. **15** (2003) 917.
- [15] F. Garnier, R. Hajlaoui, A. Elkassmi, G. Horowitz, and F. Provasoli, Chem. Mater. **10** (1998) 3334.
- [16] H. E. Katz, W. Li, and A. J. Lovinger, Synth. Metal. **102** (1999) 897.
- [17] Chrisos D. Dimitrakopoulos, and D. J. Masearo, IBM J. RES. & DEV. 45(1), (2001), p.11.
- [18] Z. Bao, A. Dodabalapur, and A. J. Lovinger, Appl. Phys. Lett. **69** (1996) 23.
- [19] C. D. Dimitrakopoulos, and R. L. Malenfant, Adv. Mater. **14** (2002) 99.
- [20] Sirringhaus, Henning, and Tessler, Science **280** (1998) 1741.
- [21] Sirringhaus, H. Brown, P. J. Friend, R. H. Nielsen, M. M. Bechgaard, and K. Langeveld-Voss, Synth. Metals **111** (2003) 129.
- [22] Guangming Wang, Jmaes Swensen, Daniel Moses, and Alan J. Heeger, Nanotechnology **93** (2003) 6137.
- [23] H. Sirringhaus, P. J. Brown, R. H. Friend, M. M. Nielsen, K. Bechgaard, B. M. W. Langeveld-Voss, A. J. H. Spiering, R. A. J. Janssen, E. W. Meijer, P. Herwig, and D. M. de Leeuw, Nature 401 (1999) 685.
- [24] G. Horowitz, Adv. Mater. **10** (1998) 365.
- [25] W. R. Salaneck, and S. Stafstrom, Cambridge University Press, Cambridge 1996.

- [26] T. Holstein, *Ann. Phys.* **8** (1959) 343.
- [27] P. G. Le Comber, W. E. Spear, *Phys. Rev. Lett.* **25** (1970) 509.
- [28] Chrisos D. Dimitralopoulos, and Parick R. Malenfant, *Adv. Mater.* **14** (2002) 16.
- [29] A. Assadi, C. Svensson, M. Willander, and O. Inganas, *Appi. Phys. Lett.* **53** (1988) 18.
- [30] Howard E. Katz, Joyce G. Laquindanum, and Andrew J. Lovinger, *Chem, Mater.* **10** (1998) 633.
- [31] Giles Lloyd, Munira Raja, Ian Sellers, Naser Sedghi, Raffaella Di Lucrezia, Simon Higgins, and Bill Eceleston, *Microelectronic Engineering* **59** (2001) 323.
- [32] Cheng Yang, P. Orfino, and Steven Holdcroft, *Marcomolecules* **29** (1996) 20.
- [33] Amundson, Karlr, Sapjeta, B. Joyce, Lovinger, Andrew J., and Bao, Zhenan, *Nature* **414** (2002) 143.
- [34] Hagen Llauk, Gunter Schmid, Wolfgang Radlik, Werner Weber, Lisong Zhou, Chris D. Sheraw, Jonathan A. Nichols, and Thomas Jackson, *Solid-State Electronics* **47** (2003) 297.
- [35] Graciela B. Blanchet, C. R. Fincher, and Micheal Lefenfeld, *Appl. Phys. Lett.* **84** (2004) 2.
- [36] Giles Lloyd, Munira Raja, Ian Sellers, Naser Sedghi, Raffaella Di Lucrezia, Simon Higgins, and Bill Eccleston, *Microelectronic Engineering* **59** (2001) 323.
- [37] Kanan Puntambekar, Jinping Dong, Greg Haugstad, and C. Daniel Frisbie *Adv. Funct. Mater.* **16** (2006) 879.
- [38] Y. Chen, I. Shin, and S. Xiao, *Journal of Applied Physics* **96** (2004) 31.

- [39] A. R. Brown, C. P. Tarrent, and D.M. de Leeuw, *Synthetic Metals* **88** (1997) 37.
- [40] J. Veres, S. Ogier, G. Lloyd, and D. Leeuw, *Chem. Mater.* **16** (2004) 4543.
- [41] A. Facchetti, M. H. Yoon, and T. J. Marks, *Adv. Mater.* **17** (2005) 1705.
- [42] Y. Sun, Y. Liu, and D. Zhu, *J. Mater. Chem.* **15** (2005) 53.
- [43] D. G. Oteyza, E. Barrena, J. Osso, and H. Dosch, *Appl. Phys. Lett.* **87** (2005) 183504.
- [44] I. Yagi, K. Tsukagoshi, and Y. Aoyagi, *Appl. Phys. Lett.* **86** (2005) 103502.
- [45] S. Kobayashi, T. Nishikawa, T. Takenobu, S. Mori, T. Shimoda, T. Mitani, H. Shimotani, N. Yoshimoto, S. Ogawa, and Y. Iwasa: *Nat. Mater.* **3** (2004) 317.
- [46] P. Too, S. Ahmed, B. J. Sealy, and R. Gwilliam: *Appl. Phys. Lett.* **80** (2002) 3745.
- [47] H. J. Ahn, S. J. Rho, K. C. Kim, J. B. Kim, B. H. Hwang, C. J. Park, and H. K. Baik: *Jpn. J. Appl. Phys.* **44** (2005) 4092.
- [48] R. H. Tredgold, Cambridge University Press, 1994.
- [49] A. Ulman, Academic press, New York, 1991.
- [50] R.F. Gould (Ed.), *Proceeding of the 144th Meeting of the American Chemical Society*, Vol.43, Washington, DC, 1964.
- [51] R.J. Good, in: K.L. Mimal (Ed.), *Contact angle, Wettability and Adhesion*, USP, The Netherlands, 1993, pp. 3–36.
- [52] H. Klauk, D. J. Gundlach, J. A. Nichols, C. D. Sheraw, M. Bonse, and T.

- N. Jackson, *Solid State Technol.* **43** (2000) 63.
- [53] H. Sirringhaus, N. Tessler, and R. H. Friend, *Science* **280** (1998) 1741.
- [54] H. Sirringhaus, N. Tessler, and R. H. Friend, *Synth. Met.* **102**, (1999) 85.
- [55] S. C. Lim, S. H. Kim, J. H. Lee, M. K. Kim, D. J. Kim, and T. Z., *Synth. Met.* **148** (2005) 75.
- [56] N. Karl in *Organic Electronic Materials*, Springer Series in Material Science, Vol. 41, edited by R. Farchioni and G. Grosso ~Springer, Berlin (2001).
- [57] R. J., M. D., M. L., and M.F. Toney, *Nature Materials* **5** (2006).
- [58] M. Hallk, H. Klauk, U. Zschieschang, G. Schmlid, C. Dehm, M. Schutz, S. Malsch, F. Effenberger, M. Brunnbauer, and F. Stellacci, *Nature*, **431** (2004) 963.
- [59] T. A. Chen, X. Wu, and R. D. Rieke, *J. Am. Chem. Soc.* **117** (1995) 233.
- [60] R. D. McCullough, R. D. Lowe, M. Jayaraman, and D. L. Anderson, *J. Org. Chem.* **58** (1993) 904 .
- [61] Prosa, T. J., Winokur, M. J., Moulton, J., Smith, P. Heeger, and A. J., *Macromolecules* **25** (1992) 4364.
- [62] T. A. Chen, X. M. Wu, and R. D. Rieke, *J. Am. Chem. Soc.* **117** (1995) 233.
- [63] E. J. Samuelsen and J. Mardalen, in *Handbook of Organic Conductive Polymers*, edited by H. S. Nalwa ~Wiley, Weinheim, 1997, Vol. 3, *Conductive Polymers: Spectroscopy and Physical Properties*, pp. 100–106.
- [64] P. J. Brown, D. S. Thomas, and J. S. Wilson, *Physical Review* **B67** (2003) 064203.

- [65] Z. Bao, A. Dodabalapur, and A. J. Lovinger, *Appl. Phys. Lett.* **69** (1996) 4108.
- [66] Y. Sun, Y. Ma, Y. Liu, Z. Wang, and Y. Wang, *Adv. Funct. Materials* **16** (2006) 426.
- [67] Y. Kim, S. Cook, and S. M. Tuladhar, *Journal of Applied Physics* **93** (2003) 6137.
- [68] G. Wang, J. Swensen, D. Moses, and A. J. Heeger, *Nat. Mater.*, **5** (2006) 197.
- [69] R. J. Kline, M. D. McGehee, and M. F. Toney, *Nat. Mater.*, **5** (2006) 222.
- [70] D. Knipp, R. A. Street, and A. R. Volkel, *Appl. Phys. Lett.*, **82** (2003) 3907.
- [71] C. Y. Chang, “**ULSI Devices**”, Wiley, New York, 2000.
- [72] C. S. Kim, S. J. Jo, S. W. Lee, and S. J. Lee, *Adv. Funct. Mater.* **17** (2007) 958.
- [73] S. Y. Park, M. Park, and H. H. Lee, *Appl. Phys. Lett.* **85** (2004) 2283.
- [74] E. M. Muller, and J. A. Marohn, *Adv. Mater.* **17** (2005) 1410.
- [75] A. Salleo, F. Endicott, and R. A. Street, *Appl. Phys. Lett.* **86** (2005) 263505.
- [76] W. Kim, A. Javey, O. Vermesh, Q. Wang, Y. Li, and H. Dai, *Nano Lett.* **3** (2003) 193.
- [77] D. K. Schroder, *Semiconductor Material and Device Characterization*, 2nd ed., Wiley, New York 1998.
- [78] G. Wang, D. Moses, and A. J. Heeger, *J. Appl. Phys.* **95** (2004) 316.
- [79] H. Jia, G. K. Pant, E. K. Gross, R. M. Wallace, and B. E. Gnade, *Organic*

Electronics 7 (2006) 16.

